It's a Trap!
Unravelling Reversible Charge Trapping in Nanocrystals Through Single Particle and Ensemble Studies

Patrick James Whitham

A dissertation
submitted in partial fulfillment of the
requirements for the degree of

Doctor of Philosophy

University of Washington

2016

Reading Committee:

Philip Reid, Chair

Daniel Gamelin, Chair

Brandi Cossairt

Dennis Heinekey

Program Authorized to Offer Degree:
Chemistry

University of Washington

Abstract

It's a Trap!
Unravelling Reversible Charge Trapping in Nanocrystals Through Single Particle and Ensemble Studies

Patrick James Whitham

Co-Chairs of the Supervisory Committee:
Professor Philip Reid
Department of Chemistry

Professor Daniel Gamelin
Department of Chemistry

Copper containing semiconductors such as copper-doped ZnS and $CuInS_2$ are classic phosphors materials that have had wide general use for decades. The photophysical processes of these bulk materials have been well studied. Recent application of these materials on the nanoscale has led to unique properties that are not exhibited in the bulk regime. Several properties, such as the large Stokes shift, tunable emission energy, and broad emission bandwidths have increased the general interest in copper containing nanomaterials. This thesis will reveal several remarkable photophysical aspects of these phosphors through studies of the ensemble, single particle, and time resolved luminescence to better understand new aspects of these materials that emerge on the nanoscale. Most notably, the homogeneous bandwidths, fluorescence blinking, and delayed luminescence were measured. The mechanistic implications of these properties and broader impact on the understanding of nanocrystal photophysics will be explained.

TABLE OF CONTENTS

Page

List of Figures v

List of Tables viii

Chapter 1: Introduction 1

1.1 Overview 1

1.2 Single Particle Spectroscopy 3

1.3 Single Particle Spectroscopy of doped Nanocrystals 4

1.3.1 Tellurium doped CdSe 5

1.3.2 Mn^{2+} doped nanocrystals 6

1.3.3 Copper doped nanocrystals 7

1.3.4 Impurity like emission from nanocrystals 11

1.4 Delayed Photoluminescence in Nanocrystals 12

1.5 Summary 14

1.6 Bibliography 15

Chapter 2: Photoluminescence Blinking and Reversible Electron Trapping in Copper-Doped CdSe Nanocrystals 18

2.1 Abstract 19

2.2 Introduction 20

2.3 Single-Particle Photoluminescence Spectra 21
2.4 Blinking Dynamics 24
2.5 Delayed Luminescence 27
2.6 Mechanistic Implications 29
2.7 Summary 33
2.8 Methods 34
2.8.1 Synthesis of Cu^{+}:CdSe Nanocrystals 34
2.8.2 Photoluminescence 35
2.8.3 Luminescence Lifetimes 35
2.8.4 Single-Particle Blinking 35
2.8.5 Single-Particle Photoluminescence Spectra 36
2.9 Supporting Information 37
2.10 Author Information 44
2.11 Acknowledgment 44
2.12 Bibliography 45

Chapter 3: Single-Particle Photoluminescence Spectra, Blinking, and Delayed Luminescence of Colloidal $CuInS_2$ Nanocrystals 48
3.1 Abstract 49
3.2 Introduction 50
3.3 Results and Analysis 52
3.3.1 Photoluminescence Spectra and Blinking 52
3.3.2 Delayed Photoluminescence 55

3.3.3 Photoluminescence Excitation Power Dependence 57
3.4 Summary 63
3.5 Methods 63
3.5.1 Synthesis of $CuInS_2$/CdS Nanocrystals 63
3.5.2 Photoluminescence 64
3.5.3 Delayed Luminescence 65
3.5.4 Luminescence Excitation Power Dependence 65
3.5.5 Single-Particle Luminescence 66
3.6 Supporting Information 67
3.7 Author Information 74
3.8 Acknowledgments 74
3.9 Bibliography 75

Chapter 4: Tunneling in the Delayed Luminescence of Colloidal CdSe, Cu^+-Doped CdSe, and $CuInS_2$ Semiconductor Nanocrystals, and Relationship to Blinking 78
4.1 Abstract 79
4.2 Introduction 80
4.3 Experimental 82
4.3.1 Synthesis of $CuInS_2$ nanocrystals 82
4.3.2 Synthesis of CdSe and Cu^+:CdSe nanocrystals 82
4.3.3 General Characterization 83
4.3.4 Spectroscopic Characterization 83

4.3.5 Temperature-dependent PL Lifetimes 84
4.3.6 Magnetic Circularly Polarized Luminescence 84
4.3.7 Time-Resolved PL Spectra 85
4.4 Results and Analysis 85
4.4.1 Absorption and Photoluminescence Spectra 85
4.4.2 Luminescence Decay 87
4.4.3 Prompt and Delayed Luminescence Spectra and Magneto-Luminescence 89
4.4.4 Temperature Dependence of Delayed Luminescence 93
4.4.5 Kinetic Model 96
4.5 Discussion 100
4.6 Summary 104
4.7 Supporting Information 105
4.8 Author Information 111
4.9 Acknowledgments 111
4.10 Bibliography 112

Appendix A: Acronyms and Symbols 116

Appendix B: Microscope Components for PL Blinking 117

Appendix C: Microscope Components for SP Spectra 118

List of Figures

1.1 Energy level diagram of nanocrystals and copper defect level 8

1.2 Copper emission bandwidth 10

2.1 Ensemble and single-particle luminescence spectra of Cu^+:CdSe and undoped CdSe 22

2.2 Photoluminescence intermittency traces of Cu^+ doped and undoped CdSe, and CDFs of "on" and "off" statistics for Cu^+ and excitonic emission 26

2.3 Proposed mechanism for blinking and delayed luminescence in Cu^+:CdSe 28

2.4 Delayed luminescence lifetimes of Cu^+:CdSe 31

2.5 Absorption and magnetic circular dichroism (MCD) spectra of Cu^+:CdSe nanocrystals 39

2.6 Electron paramagnetic resonance (EPR) spectrum of Cu^+:CdSe nanocrystals 40

2.7 Lifetime fitting of Cu^+ luminescence 41

2.8 Gated luminescence spectra of Cu^+:CdSe nanocrystals 42

2.9 Delayed Luminescence of Cu^+:CdSe and CdSe nanocrystals 43

3.1 Ensemble luminescence spectra, single-particle luminescence spectra, and blinking trace of $CuInS_2$/CdSe NCs 53

3.2 Luminescence decay and blinking "off" histogram of $CuInS_2$ nanocrystals 56

3.3 Photoluminescence power dependence of $CuInS_2$/CdS nanocrystals . 59

3.4 Relationship between delayed luminescence and PL blinking 62

3.5 Transmission electron microscopy (TEM) of $CuInS_2$/CdS nanocrystals 68

3.6 X-ray diffraction of $CuInS_2$/CdS nanocrystals 69

3.7 Single-particle peak energy and bandwidths of $CuInS_2$ nanocrystals . 70

3.8 Single-particle photoluminescence background spectrum 71

3.9 Power-dependent photoluminescence spectra of $CuInS_2$ nanocrystals . 72

3.10 Normalized power-dependent photoluminescence spectra of $CuInS_2$ nanocrystals 72

3.11 "On" blinking statistics of $CuInS_2$ nanocrystals 73

3.12 Effect of time binning and histogramming 74

3.13 Effect of the number of histogram points 74

4.1 Photoluminescence and absorption spectra of CdSe, Cu^+:CdSe, and $CuInS_2$ NCs 86

4.2 PL decays at 20 K for CdSe, Cu^+:CdSe, and $CuInS_2$ NCs 88

4.3 Spectra of the prompt and delayed luminescence of Cu^+:CdSe, and $CuInS_2$ nanocrystals at 5 K 90

4.4 Magnetic circularly polarized luminescence of Cu^+:CdSe, and $CuInS_2$ NCs 92

4.5 Temperature dependent luminescence decay of CdSe, Cu^+:CdSe, and $CuInS_2$ NCs 95

4.6 Temperature dependent luminescence decay fits for Cu^+:CdSe 99

4.7 Model for charge trapping and detrapping 102

4.8 X-ray diffraction (XRD) of $CuInS_2$ nanocrystals showing the chalcopyrite phase 106

4.9 Magneto-photoluminescence decay traces 107

4.10 Absorption and PL of Cu^{+}:CdSe NCs 108

4.11 Gated Spectra of CdSe NCs 109

B.1 Microscope components for measuring photoluminescence blinking . . 117

C.1 Microscope components for measuring single particle spectra 118

List of Tables

2.1 KS Test 38

2.2 Qds per CDF 38

4.1 Parameters used for modeling Cu^{+}:CdSe nanocrystal temperature-dependent luminescence decay data 110

ACKNOWLEDGMENTS

I would like to express my gratitude to my advisers Professors Phil Reid and Daniel Gamelin. Thank you for the guidance and assistance over the past several years. Both of you have been good advisers and have pushed me academically and scientifically. To my committee members Professors Brandi Cossairt, Mike Heinekey, and Christine Luscombe, thank you all for your feedback and advice.

To all of my coworkers, thank you for your continual help and ideas. Dr. Kathryn Knowles, you have helped me greatly over the past several years providing me with immense scientific guidance. Dr. Arianna Marchioro, working with you has been great pleasure. Rarely have our equipment and experiments worked as intended, but it has been great to work with you to troubleshoot these problems and eventually to produce successful results. Dr. Chelsea Hess, I greatly enjoyed being your coworker, I always valued your advice and opinion. Dr. Angela Rudolph, I enjoyed working with you; you are one of the kindest people I've ever known.

To my friends, you have helped keep my life balanced given all of the pressures of grad school. I can't say enough about how great it has been to spend time with all of you. You have helped make Seattle my home.

Finally, to my family. I wouldn't be where I am today without your continuing love and support.

Chapter 1

INTRODUCTION

1.1 Overview

Doped semiconductor materials are a classic group of phosphors that have been widely used in commercial applications for decades.[1,2] The properties of these bulk materials have been well characterized and their photophysics have been widely studied. Recent adaptation of these classic phosphors to the nanoscale has led to new and interesting properties that are not as well characterized. Recent investigations of the photophysics of these nanomaterials has been undertaken employing a broad range of methods, and investigating these materials employing both ensemble and single particle spectroscopic techniques. Luminescence studies have led to two interesting phenomena that occur in both undoped and doped nanocrystals, *i.e.* delayed luminescence and photoluminescence intermittency (PI), commonly referred to as blinking. Studies of doped, undoped and dopant-like nanocrystals have provided new insights that appear broadly applicable to all colloidal semiconductor nanocrystals. This introduction outlines the general background of the field of single particle spectroscopy with particular interest towards studies of dopant PL in nanocrystals, observations of PL blinking in doped nanocrystals and the relationship with delayed luminescence that has been aided by the study of dopant blinking.

Impurity doped semiconductor phosphors have been commercially important materials for the past 100 years.[1,3,4] Crystals such as ZnS doped with manganese, silver, or copper have been used in electroluminescence devices for monochromatic displays in automobiles, watches, oscilloscopes, and other technical devices.[1,3,5,6] ZnS and ZnSe doped with silver or tellurium have been used as scintillator materials for alpha par-

ticle detectors and recently in combination with ^{6}LiF salts and $^{10}B_2O_3$ glasses for neutron detection.[4] Insertion of dopant ions such as Mn^{2+}, Cu^{+}, Ag^{+}, Te^{2-} can introduce new electro-optical properties to the host materials, for example additional optical transitions and visible luminescence, allowing some tunability to the emission spectrum of the material.

Semiconductor nanocrystals have been studied for the last 30 years, with the "nanoscaling" of phosphors having many interesting applications. For nanocrystals smaller than the Bohr exciton radius of the semiconductor material, the band gap and optical transitions can be tuned by changing the size of the particle. This has led to exciting new applications due to the color tunability of both absorbance and luminescence across the entire visible spectrum. Recently CdSe nanocrystals have been incorporated into LED TVs due to their high color purity.

There has also been significant interest in luminescence from impurity doped semiconductor nanocrystals. These materials can wildly differ from their undoped counterparts depending on the nature of the dopant. Impurity dopants can introduce new electronic transitions that are lower in energy than the intrinsic band gap of the host material, thus providing broader color tunability to a wider band gap material, such as in the case of ZnSe. ZnSe is a relatively wide bandgap material whose PL is tunable from the near UV to deep blue, and introduction of a small concentration of Mn^{2+} leads to characteristic Mn^{2+} PL near 580 nm while the band edge absorbance remains in the near UV to deep blue. These materials have been proposed for solar harvesting applications such as luminescence solar concentrators, where wide separation between absorption and emission are necessary to prevent reabsorption losses.[7] Another example is Cu^{+} doping of ZnSe or CdSe that allows for broad and tunable emission across a larger portion of the visible spectrum. These have been proposed for solar concentrators,[8] LEDs,[9] and *in vivo* cellular imaging.[10] Other materials include lanthanide doped semiconductors where the rare earth ion is sensitized by the host nanocrystal are an area of significant interest; however, the PL quantum yield

of these materials have been very low.[11]

Signatures of impurity doping include changes in absorption, PL spectra, introduction of new magnetic and electronic properties, or quenching of PL. The work presented in this dissertation will focus on changes in PL. PL provides a very sensitive method of investigating impurity dopants by observing changes in the PL spectrum. This can consist of quenching of intrinsic excitonic transitions that are common to II-VI semiconductors, emergence of new electronic transitions, changes in excited state lifetimes, and changes in light polarization. Blinking in doped nanocrystals is useful due to the interesting electronic properties that an impurity atom can impart on the host nanocrystal. Several materials have been of interest for impurity doping of nanocrystals, for investigation by single particle spectroscopy, the nanocrystals must inherently have a luminescent transition. This can significantly limit the number of dopant materials used. Common ions that have been investigated for impurity doping include Te^{2-}, Mn^{2+}, and Cu^{+}.

1.2 Single Particle Spectroscopy

Single particle spectroscopy involves the study of the spectral properties of single particles that are isolated either spatially or energetically from a larger ensemble of the same material. This can be a useful approach for observing phenomena that are obscured by ensemble effects. Luminescence is one of the most sensitive probes for single particles. The focus of this introduction will be on two major categories of single particle luminescence: time-resolved luminescence and spectrally resolved luminescence.

Time resolved measurements of single particles have revealed the rather interesting phenomenon of photoluminescence intermittency or blinking. First observed by Moerner and coworkers in the early 1990's, under continuous excitation the emission from the pentacene in a para-terphenyl matrix was found to be non-continuous.[12] Blinking is characterized by the appearingly random switching of a single luminophore

between emissive and a non-emissive states. This phenomenon has been observed in a broad range of materials including molecular chromophores,[13] nanocrystals,[14] and fluorescent proteins.[15]

The dynamics of fluorescence intermittency is often quite complex, with changes in emissive intensity occurring on the microsecond to seconds timescale for many systems.[16] The causes of blinking can be quite diverse depending on the luminophore and its local environment. Spectral diffusion,[17] charge transfer,[18] and conformational flexibility[19] among others have been proposed for various systems. Understanding fluorescence blinking can be very useful in determining nonradiative processes that reduce photoluminescence quantum efficiencies and that can lead to nonreversible photodarkening. Blinking can also provide insight into the electronic and chemical nature of the chromophore and its local environment.

Spectrally resolved luminescence can also be a powerful method for studying single emitters by revealing homogeneous bandwidths. Ensemble bandwidths are often affected by inhomogeneous broadening. In nanocrystals this broadening is typically the result of particle size inhomogeneity, but can also be related to the mechanism of emission.

1.3 Single Particle Spectroscopy of doped Nanocrystals

Blinking in colloidal semiconductor nanocrystals almost universally displays highly distributed kinetics. The cause of blinking in these materials has been an area of great interest due to their proposed applications. Significant work has been done to understand blinking, exploit it and to eliminate it.[14,20–23] Eliminating blinking has proven difficult, but not impossible, with several synthetic methods that can decrease blinking through the growth of wider band gap shell layers.[20] Other groups have attempted to exploit the intermittent nature of single particle luminescence to achieve super-resolution imaging.[23] Finally many groups have studied the blinking itself to understand its kinetics and its causes.[14,16,22,24,25]

Most studies of blinking in nanocrystals has been confined to a small group of materials, namely II-VI semiconductors such as ZnSe, ZnS, CdSe and CdS. CdSe in particular has been the material of choice for the great majority of all single particle studies. Doped nanocrystals have gained interest for their unique PL properties lately, but there are few studies by single particle spectroscopy. There are some rather important properties that can be obtained from single particle measurements. The PL homogeneous bandwidths can give insights into the nature of the emissive transitions, and the blinking can reveal interesting information about nonradiative processes in the nanocrystals. These properties can provide better insights into the electronic structures of the host nanocrystal, giving a better understanding of radiative and nonradiative excited state decay pathways of the host or new understanding about the dopant ion itself. They can also impart new photophysical properties to the host crystal through new electronic transitions. This is small but growing area of investigation that has emerged over the past 10 years. The list of doped materials studied by fluorescence blinking is quite short: tellurium-, manganese-, and copper-doped II-VI semiconductors. Luminescence of single lanthanides ions in insulator nanocrystals have been reported, however these measurements involve direct excitation of the ion and not of the host material so are beyond the scope of this introduction.

1.3.1 Tellurium doped CdSe

The first report of single particle spectroscopy of a doped nanocrystal was published in 2002 on the single particle spectra of tellurium-doped CdSe.[26] Tellurium doped nanocrystals showed a distinct wavelength redshift. The band widths of undoped and tellurium doped CdSe were identical at room temperature with spectral widths reported of 500-1000 cm^{-1}. Occasional irreversible spectral blue shifts of up to 800 cm^{-1} (100 meV) of the Te:CdSe single particle spectra were observed. These were attributed to ejection of tellurium ions from the lattice.

1.3.2 Mn^{2+} doped nanocrystals

Mn^{2+} doped nanocrystals are perhaps the most widely studied doped nanocrystal by single particle spectroscopy. Mn^{2+} PL emission is characterized by a broad PL band centered at $\sim 2 - 2.2$ eV (550 – 620 nm) depending on the host lattice. Not all Mn^{2+} doped systems exhibit characteristic Mn^{2+} PL. Smaller bandgap materials, such as large CdSe NCs, retain excitonic emission because the lowest excited state of the Mn^{2+} is above the bandgap of the NC. Single particle studies have been performed on these as well but they explore magneto-optical interactions that are not the focus of this dissertation. The mechanism of Mn^{2+} PL has been widely studied in bulk systems[27] and the nanocrystal PL is generally understood to occur by a the same mechanism.[28] Following photoexcitation of the host nanocrystal, there is a fast energy transfer from the excited state of the host nanocrystal to a Mn^{2+} ion. This fast energy transfer time allows for complete suppression of the intrinsic excitonic transition in the low excitation limit. Radiative relaxation of the Mn^{2+} in tetrahedral environments is slow due to the formally spin forbiddenness of the transition from the $^4T_1$ lowest excited state to the $^6A_1$ ground state with reported lifetimes of hundreds of microseconds to milliseconds.[29] Despite the very long lived nature of this excited state, the relaxation pathway is thought to be purely radiative.[29]

Despite the high QYs, the very long lifetime of the Mn^{2+} is a significant drawback to its study at the single particle level due to the low number of photons that may be observed per unit time. Nonetheless several groups have reported measurements of single particle blinking and single particle PL spectra of Mn^{2+} in doped NCs.[30,31] There are several drawbacks to these studies, one report used sub-bandgap excitation source, rendering excitation of the host lattice impossible.[31] The emission they observe is consistent with Mn^{2+} PL, so it is likely the result of direct excitation of the lowest Mn^{2+} excited state. A second report of Mn^{2+} blinking in doped CdS/ZnS NCs had a small undoped subset of nanocrystals that showed band edge excitonic PL and low

energy surface trap emission. They attempted to chromatically separate the emission of the Mn^{2+}, band edge emission and surface-defect PL and reported suppressed blinking for Mn^{2+} emitting nanocrystals.[30] This is an interesting result but needs further study to confirm these results largely due to the low emission rate of the Mn^{2+} and overlapping bands of the Mn^{2+} and surface defect emission. A third report of Mn^{2+} single particle spectroscopy studied samples of Mn^{2+} doped Zn-Cd-S alloyed nanocrystals. The authors report tunable Mn^{2+} emission with a homogeneous band width of 70 meV at room temperature.[32] This is significantly narrower than any emission band previously observed for Mn^{2+} emission. No definitive evidence of Mn^{2+} inclusion into the nanocrystals is presented, which makes contradiction of the broadly accepted understanding of the origins and lack of tunability of Mn^{2+} emission rather surprising. Other reports of Mn^{2+} PL in doped NCs show that the emission is largely unaffected by particle size and composition.[28,29,33]

1.3.3 Copper doped nanocrystals

Copper-doped colloidal semiconductor nanocrystals have received significant attention in recent years. Colloidal copper-doped nanocrystals exhibit both size and composition tunable PL. The copper-based PL mechanism has previously been a point of contention in the literature but is now generally thought to be the result of recombination of a delocalized conduction band electron with a copper localized hole. This interpretation implies the oxidation state of copper in doped nanocrystals is +1 in the ground state. Hole-localization transiently produces Cu^{2+} *via* charge transfer which is reduced to Cu^{+} upon radiative recombination with a delocalized electron.[3] In bulk systems, Cu^{+} PL is a donor-acceptor pair type mechanism that requires electron localization at a donor site, in nanocrystal systems this is not necessarily invoked since the absence of a donor produces the characteristic emission. Furthermore, the copper luminescence is tunable with changes in the conduction band energy of the nanocrystal as seen in Figure 1.1. The Cu level is usually understood to largely unaffected

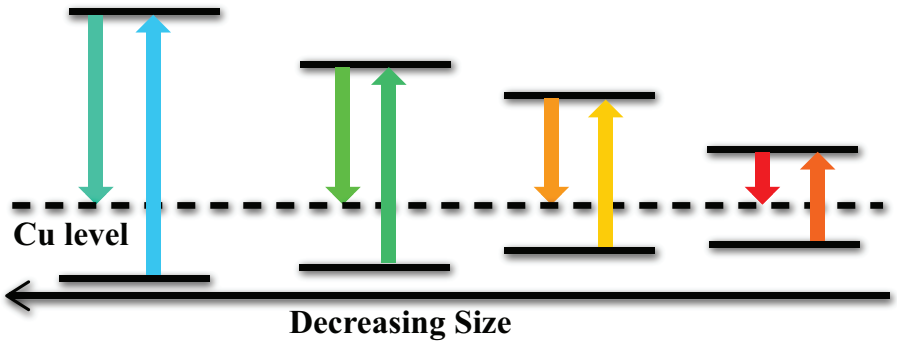

Figure 1.1: Energy level diagram showing the effect of quantum confinement on the absorption and emission of copper-doped NCs. The absorption is affected by confinement of both the conduction band and valence band while the PL scales only with the size dependence of the conduction band and the copper defect level is largely unaffected. Adapted from: Knowles, K. E.; Hartstein, K. H.; Kilburn, T. B.; Marchioro, A.; Nelson, H. D.; Whitham, P. J.; Gamelin, D. R., *Chem. Rev.* **2016**, *Article ASAP.*, Copyright (2016) American Chemical Society. Originally adapted from Grandhi, G. K.; Tomar, R.; Viswanatha, R., *ACS Nano* **2012**, 6, 9751-63., Copyright (2012) American Chemical Society.

by changes in nanocrystal composition.[3,34] The delocalized electron in the conduction band has significant wavefunction overlap with the localized hole on copper allowing for conduction band to copper radiative recombination.

Copper doped nanocrystals have been the subject of a handful of single particle studies. Luminescence of Cu^{+}, Al^{3+}:ZnS nanostructures has been measured, revealing broad single nanostructure PL bandwidths of $\sim$ 350 meV at room temperature (Figure 1.2A).[35] Low temperature studies of these nanostructures revealed a narrowing of these bandwidths to $\sim$ 275 meV.[35] A similar result was observed by our group that showed broad single particle copper bandwidths of $\sim$ 325 meV at room temperature that are only slightly narrower than ensemble bandwidths Figure 1.2B, this is result is discussed in greater detail in chapter 2 of this dissertation. Fluorescence line narrowing experiments on an ensemble of copper-doped ZnSe/CdSe came to a similar conclusion that the homogeneous bandwidth of copper-doped semiconductor nanocrystals is intrinsically very broad (Figure 1.2C).[36]

A more detailed description of the broad luminescence will be presented in more detail in chapter 2, but the broad luminescence is thought to be the result of nuclear distortions in the vicinity of copper with the change in oxidation state. Further experiments detailed in chapter 2 explore the blinking characteristics of Cu^{+}:CdSe nanocrystals and compare the results with an undoped subset of nanocrystals within the ensemble. While an undoped subset of nanocrystals is not typically an ideal situation, in this case it proved to be quite valuable. The undoped subset allowed for direct comparisons within the sample prepared under the exact same experimental conditions. The copper dopant acted as an engineered hole-trap which allowed us to determine differences between the kinetics of the electron and hole charge carriers.

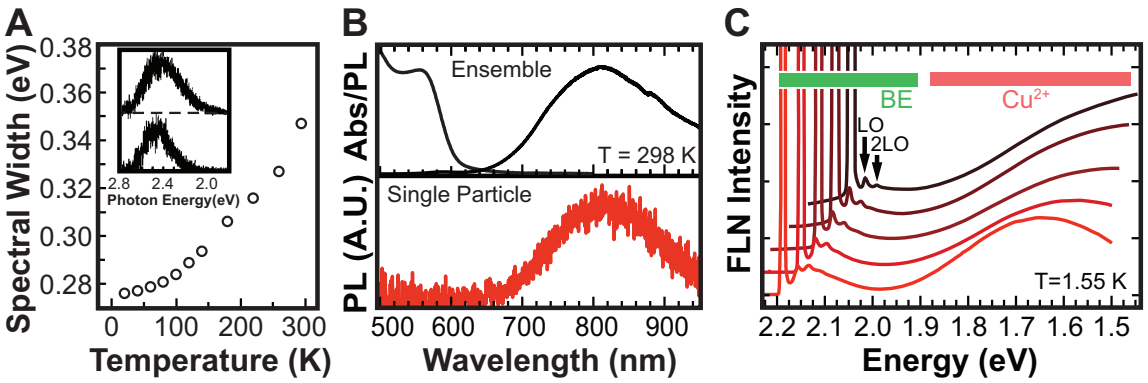

Figure 1.2: Cu PL bandwidths measured in nanostructures, single particles and ensembles. (A) Cu emission in nanostructured Cu:ZnSe, (B) Ensemble and single particle spectra in Cu^{+}:CdSe, (C) fluorescence line narrowing measurement of Cu-doped core/shell ZnSe/CdSe NCs. These experiments confirm the broad luminescence linewidth is intrinsic to copper emission, nanocrystal size has only a modest effect on the distribution of copper emission. Reprinted with permission from: Knowles, K. E.; Hartstein, K. H.; Kilburn, T. B.; Marchioro, A.; Nelson, H. D.; Whitham, P. J.; Gamelin, D. R., *Chem. Rev.* **2016**, *Article ASAP.*, Copyright (2016) American Chemical Society. Original figures adapted from: (A) Ishizumi, A.; White, C. W.; Kanemitsu, Y., *App. Phys. Lett.* **2004**, 84, 2397., with permission from AIP Publishing.; (B) Whitham, P. J.; Knowles, K. E.; Reid, P. J.; Gamelin, D. R., *Nano Lett.* **2015**, 15, 4045., Copyright (2015) American Chemical Society; (C) Brovelli, S.; Galland, C.; Viswanatha, R.; Klimov, V. I., *Nano Lett.* **2012**, 12, 4372., Copyright (2012) American Chemical Society.

1.3.4 Impurity like emission from nanocrystals

Recent studies of the PL of $CuInS_2$ NCs have suggested that the emission mechanism in these NCs is similar to the mechanism of Cu^+ doped NCs.[37] The emission of $CuInS_2$ NCs does not resemble the well-studied bulk emission of $CuInS_2$ crystals, which in itself strongly suggests a different emission mechanism. The emission of $CuInS_2$ NCs consists of a single broad band $\sim$ 300-400 meV at fwhm whereas bulk $CuInS_2$ crystals produce several distinct emission bands that are significantly narrower in energy. $CuInS_2$ bulk crystals exhibit near band edge emission while the NCs display a larger Stokes shift and no band edge emission. The emission of $CuInS_2$ nanocrystals is also tunable with changing nanocrystal size.

Recent studies have suggested that PL from $CuInS_2$ is likely the result of a self-trapped exciton mechanism.[37] This mechanism can account for the observed Stokes shifts and broad bandwidths in $CuInS_2$ and the observed similarities to Cu^+-doped systems. The broad PL bandwidths are explained by strong excited-state vibronic coupling which is similar to the large lattice distortions around individual Cu^+ ions following hole localization in copper-doped systems. The first report of blinking in $CuInS_2$ was in 2012 on $CuInS_2$/ZnS NCs where wide field fluorescence microscopy measurements. This study was able to detect fluorescence blinking from single and small clusters of NCs[38] and reported a polarization dependence in the emission of these emitters. While mainly a proof of concept this raises the possibility of some rather interesting studies on the luminescence of $CuInS_2$ NCs. A second study of non-blinking single particles of Zn-In-Cu-S alloyed NCs was reported in 2015.[39] It does not appear that complete suppression was observed in the entire sample but rather in a few nanocrystals with reduction in blinking with respect to other NCs. Our group published a report on blinking and single particle spectra of $CuInS_2$ NCs that is presented in chapter 3. The purpose of our studies was gain further understanding of the radiative and nonradiative processes of $CuInS_2$ NCs. Measurements of the single

particle bandwidths are useful in understanding the mechanism of emission. Broad intrinsic bandwidths that were obtained in the studies in chapter 3 are consistent with our self-trapped exciton interpretation of the $CuInS_2$ mechanism. Further studies presented in chapter 3 add further evidence to the relationship between delayed PL and blinking that has been proposed by several groups,[40–42] including our own.

Recently, a report on blinking in $AgInS_2$ was published. This is interesting because there are many similarities in band shape, Stokes shifts and lifetimes between $CuInS_2$ and $AgInS_2$.[38]

1.4 Delayed Photoluminescence in Nanocrystals

Recently several authors have reported observations of luminescence from nanocrystals occurring on timescales significantly longer than the intrinsic luminescence lifetime of the studied materials.[24,40–43] This long lived delayed luminescence has been observed in CdSe,[40–42] copper-doped CdSe[24] and $CuInS_2$[43] and it appears to be a universal feature of colloidal semiconductor NCs. It is attributed to the formation of a metastable charge separated excited state that can eventually re-form the emissive excited state. The emissive states are identical in both situations, but delayed luminescence occurs on a timescale much longer than the lifetime of the intrinsic prompt PL.

This delayed emission exhibits rather complex decay kinetics that cannot be described by simple exponential decay kinetics. Instead, delayed emission shows dispersed kinetics that are broadly distributed over multiple orders of magnitude in time. The observed timescales of delayed PL extend from microseconds to seconds depending on temperature and the nature of the material.

In 2008 a link was first proposed between delayed luminescence observed in ensemble measurements and blinking in single nanocrystals.[42] This was attributed to similar power law like behavior that was observed in blinking measurements and delayed PL of CdSe NCs. However the time scales were highly separated between ensemble life-

time measurements on the order of microseconds and fluorescence blinking observed on the order of seconds.

The general theory postulated for blinking attributes the distributed decay kinetics to charge carrier trapping in a metastable charge separated state that slowly detraps to re-form the emissive excited state which allows for recovery of emission. This mechanistic understanding should also hold true for delayed luminescence.

Experiments by our lab[24] and detailed in chapter 2 of CdSe and Cu^+:CdSe have made a similar correlation between delayed PL and blinking as observed by Sher *et al.*[42] We were able to measure luminescence decay from CdSe out to 5 ms and for Cu^+:CdSe out to 1.6 seconds at 20 K. It is rather remarkable that a material such as Cu^+:CdSe with an intrinsic lifetime of 100 - 500 ns is still emitting photons 1.6 seconds after excitation—over 6 orders of magnitude in time beyond the intrinsic luminescence lifetime. This observation showed strikingly that delayed luminescence and blinking can occur on overlapping timescales. However these measurements were performed at 20 K whereas the blinking measurements were measured at room temperature. As the sample temperature increases, the prompt lifetime decreases and the number of delayed emission photons measured also decreases leading in this case to no observed delayed PL photons on an overlapping timescale with blinking measurements. Experiments and modeling reported by Rabouw *et al.* presented a similar correlation between delayed luminescence and blinking in CdSe showing that these phenomena have very similar distributed kinetics.[40] This report was unique in that it fit both blinking and delayed PL measurements with the same model—providing further evidence that the two phenomena are related. A successive report by Rabouw *et al.* in 2016 showed that CdSe nano-platelets also exhibit similar delayed PL.[41]

Ensemble and single particle measurements carried out by our lab on $CuInS_2$/CdS NCs demonstrated that these two phenomena overlap on a broad experimental time window. Ensemble excitation power dependence measurements showed that the delayed luminescence saturated at low emission intensities. This is consistent with a

meta-stable charge separated state causing delayed luminescence and is consistent with current theories of the origins of blinking, a further accounting of these measurements are presented in chapter 3. Further studies of the temperature dependence of luminescence decay in CdSe, Cu^{+}:CdSe and $CuInS_2$ have expanded on the model presented by Rabouw *et al.* in 2015. These will be discussed in further detail in chapter 4.

1.5 Summary

The subsequent chapters of this dissertation will present the results of work I have performed towards understanding the origins of blinking and its relationship to delayed luminescence. What is interesting about the observations of delayed PL is that it is occurring over several classes of materials from undoped, to doped, to ternary I-III-VI systems, and suggests a general phenomenon. The studies correlating the observation of delayed PL to blinking, adds credence to the argument that delayed PL and blinking originate from the same phenomenon observed in two radically different ways.

1.6 Bibliography

[1] Yen, W.M., Shionoya, S., & Yamamoto, H.(Eds.) (2006). *Phosphor Handbook.* Boca Raton: CRC Press.

[2] Smet, P.F., Moreels, I., Hens, Z., & Poelman, D. (2010). *Materials* **3**, 2834–2883.

[3] Knowles, K.E., Hartstein, K.H., Kilburn, T.B., Marchioro, A., Nelson, H.D., Whitham, P.J., & Gamelin, D.R. (2016). *Chemical Reviews*, Article ASAP.

[4] McCloy, J.S., Bliss, M., Miller, B., Wang, Z., & Stave, S. (2015). *Journal of Luminescence* **157**, 416–423.

[5] Kajiwara, K., Hida, T., & Tanaka, K. (2003). *Journal of Vacuum Science & Technology B: Microelectronics and Nanometer Structures* **21**, 515.

[6] Sajan, P., Vinod, R., & Bushiri, M.J. (2015). *Journal of Luminescence* **158**, 110–115.

[7] Erickson, C.S., Bradshaw, L.R., McDowall, S., Gilbertson, J.D., Gamelin, D.R., & Patrick, D.L. (2014). *ACS Nano* **8**, 3461–7.

[8] Bradshaw, L.R., Knowles, K.E., McDowall, S., & Gamelin, D.R. (2015). *Nano Letters* **15**, 1315–23.

[9] Chen, B., Zhong, H., Wang, M., Liu, R., & Zou, B. (2013). *Nanoscale* **5**, 3514–9.

[10] Xu, S., Wang, C., Wang, Z., Zhang, H., Yang, J., Xu, Q., Shao, H., Li, R., Lei, W., & Cui, Y. (2011). *Nanotechnology* **22**, 275605.

[11] Martin-Rodriguez, R., Geitenbeek, R., & Meijerink, A. (2013). *Journal of the American Chemical Society* **135**, 13668–71.

[12] Basche, T., Moerner, W.E., Orrit, M., & Talon, H. (1992). *Physical Review Letters* **69**, 1516–1519.

[13] Riley, E.A., Hess, C.M., Pioquinto, J.R., Kaminsky, W., Kahr, B., & Reid, P.J. (2013). *The Journal of Physical Chemistry B* **117**, 4313–24.

[14] Nirmal, M., Dabbousi, B.O., Bawendi, M.G., Macklin, J.J., Trautman, J.K., Harris, T.D., & Brus, L.E. (1996). *Nature* **383**, 802–804.

[15] Dickson, R.M., Cubitt, A.B., Tsien, R.Y., & Moerner, W.E. (1997). *Nature* **388**, 355–358.

[16] Kuno, M., Fromm, D.P., Hamann, H.F., Gallagher, A., & Nesbitt, D.J. (2001). *The Journal of Chemical Physics* **115**, 1028–1040.

[17] Empedocles, S.A. & Bawendi, M.G. (1999). *The Journal of Physical Chemistry B* **103**, 1826–1830.

[18] Krauss, T.D. & Peterson, J.J. (2012). *Nature Materials* **11**, 14–16.

[19] Osad'ko, I.S. & Fedyanin, V.V. (2011). *Physical Review A* **83**.

[20] Chen, Y., Vela, J., Htoon, H., Casson, J.L., Werder, D.J., Bussian, D.A., Klimov, V.I., & Hollingsworth, J.A. (2008). *Journal of the American Chemical Society* **130**, 5026–7.

[21] Kuno, M., Fromm, D.P., Hamann, H.F., Gallagher, A., & Nesbitt, D.J. (2000). *The Journal of Chemical Physics* **112**, 3117.

[22] Shimizu, K.T., Neuhauser, R.G., Leatherdale, C.A., Empedocles, S.A., Woo, W.K., & Bawendi, M.G. (2001). *Physical Review B* **63**.

[23] Wang, Y., Fruhwirth, G., Cai, E., Ng, T., & Selvin, P.R. (2013). *Nano Letters* **13**, 5233–41.

[24] Whitham, P.J., Knowles, K.E., Reid, P.J., & Gamelin, D.R. (2015). *Nano Letters* **15**, 4045–4051.

[25] Zhao, J., Nair, G., Fisher, B.R., & Bawendi, M.G. (2010). *Physical Review Letters* **104**, 157403.

[26] Murase, N. (2003). *Chemical Physics Letters* **368**, 76–81.

[27] Beaulac, R., Ochsenbein, S.T., & Gamelin, D.R. (2010). *Colloidal Transition-Metal-Doped Quantum Dots*, Chapter 11, pp. 397–453. New York: Taylor & Francis.

[28] Suyver, J.F., Kelly, J.J., & Meijerink, A. (2003). *Journal of Luminescence* **104**, 187–196.

[29] Beaulac, R., Archer, P.I., Ochsenbein, S.T., & Gamelin, D.R. (2008). *Advanced Functional Materials* **18**, 3873–3891.

[30] Ishizumi, A. & Kanemitsu, Y. (2009). *Journal of the Physical Society of Japan* **78**, 083705.

[31] Zhang, Y., Gan, C., Muhammad, J., Battaglia, D., Peng, X., & Xiao, M. (2008). *The Journal of Physical Chemistry C* **112**, 20200–20205.

[32] Hazarika, A., Layek, A., De, S., Nag, A., Debnath, S., Mahadevan, P., Chowdhury, A., & Sarma, D.D. (2013). *Physical Review Letters* **110**, 267401.

[33] Bradshaw, L.R., Hauser, A., McLaurin, E.J., & Gamelin, D.R. (2012). *The Journal of Physical Chemistry C* **116**, 9300–9310.

[34] Grandhi, G.K., Tomar, R., & Viswanatha, R. (2012). *ACS Nano* **6**, 9751–63.

[35] Ishizumi, A., White, C.W., & Kanemitsu, Y. (2004). *Applied Physics Letters* **84**, 2397–2399.

[36] Brovelli, S., Galland, C., Viswanatha, R., & Klimov, V.I. (2012). *Nano Letters* **12**, 4372–4379.

[37] Knowles, K.E., Nelson, H.D., Kilburn, T.B., & Gamelin, D.R. (2015). *Journal of the American Chemical Society* **137**, 13138–13147.

[38] Cichy, B., Rich, R., Olejniczak, A., Gryczynski, Z., & Strek, W. (2016). *Nanoscale* **8**, 4151–9.

[39] Zhang, A., Dong, C., Li, L., Yin, J., Liu, H., Huang, X., & Ren, J. (2015). *Scientific Reports* **5**, 15227.

[40] Rabouw, F.T., Kamp, M., van Dijk-Moes, R.J., Gamelin, D.R., Koenderink, A.F., Meijerink, A., & Vanmaekelbergh, D. (2015). *Nano Letters* **15**, 7718–7725.

[41] Rabouw, F.T., van der Bok, J.C., Spinicelli, P., Mahler, B., Nasilowski, M., Pedetti, S., Dubertret, B., & Vanmaekelbergh, D. (2016). *Nano Letters* **16**, 2047–2053.

[42] Sher, P.H., Smith, J.M., Dalgarno, P.A., Warburton, R.J., Chen, X., Dobson, P.J., Daniels, S.M., Pickett, N.L., & O'Brien, P. (2008). *Applied Physics Letters* **92**, 101111.

[43] Whitham, P.J., Marchioro, A., Knowles, K.E., Kilburn, T.B., Reid, P.J., & Gamelin, D.R. (2016). *The Journal of Physical Chemistry C* **120**, 17136–17142.

Chapter 2

PHOTOLUMINESCENCE BLINKING AND REVERSIBLE ELECTRON TRAPPING IN COPPER-DOPED CdSe NANOCRYSTALS

Patrick J. Whitham, Kathryn E. Knowles, Philip J. Reid,* and Daniel R. Gamelin*

Department of Chemistry, University of Washington, Seattle, WA 98195-1700, USA

2.1 Abstract

Single-particle photoluminescence blinking is observed in the copper-centered deep-trap luminescence of copper-doped CdSe (Cu^+:CdSe) nanocrystals. Blinking dynamics for Cu^+:CdSe and undoped CdSe nanocrystals are analyzed to identify the effect of Cu^+, which selectively traps photogenerated holes. Analysis of the blinking data reveals that the Cu^+:CdSe and CdSe nanocrystal "off"-state dynamics are statistically identical, but the Cu^+:CdSe nanocrystal "on" state is shorter lived. Additionally, a new and pronounced temperature-dependent delayed luminescence is observed in the Cu^+:CdSe nanocrystals that persists long beyond the radiative lifetime of the luminescent excited state. This delayed luminescence is analogous to the well-known donor-acceptor pair luminescence of bulk copper-doped phosphors and is interpreted as revealing metastable charge-separated excited states formed by reversible electron trapping at the nanocrystal surfaces. A mechanistic link between this delayed luminescence and the luminescence blinking is proposed. Collectively, these data suggest that electron (rather than hole) trapping/detrapping is responsible for photoluminescence intermittency in these nanocrystals.

Keywords: *Doped nanocrystal, luminescence intermittency, delayed luminescence, copper dopant, carrier trapping, blinking*

2.2 Introduction

Copper-doped chalcogenide semiconductors have been used as commercial phosphors for nearly a century.[1,2] Their most prominent and technologically useful luminescence derives from recombination of ionized copper acceptor ions with partially localized electrons associated with aliovalent donor impurity ions, for example, Al^{3+}, Cl^{-}, or related defects.[3,4] This recombination represents one of the classic illustrations of phosphor donor/acceptor pair (DAP) recombination. The donor electron binding energy and donor-acceptor distance both play major roles in determining the luminescence decay kinetics, which in bulk can take place over timescales as long as minutes.[3,4]

In recent years, a great deal of attention has turned to copper-doped colloidal semiconductor nanocrystals. Excellent progress has been made by several groups in developing colloidal copper-doped nanocrystals as size- or composition-tunable nanophosphors.[5–13] In nanocrystals, the copper-based photoluminescence (PL) is usually interpreted as involving recombination of delocalized conduction-band-like electrons with copper-localized holes,[5,9,11] that is, $e^{-}_{CB} \rightarrow Cu^{2+}$-like charge-transfer recombination. Donors are thus not explicitly invoked in this interpretation. So far, the PL quantum yields of colloidal Cu^{+}-doped semiconductor nanocrystals (up to $\sim 50\%$[9,10,14]) are generally not as high as for Mn^{2+}-doped nanocrystals (up to $\sim 90\%$[15]), but there remains promise for further improvement. For example, quantum yields of $\sim 85\%$ have been achieved in $CuInS_2/CdS$[16] and copper-doped ZnS/In_2S_3 alloy[17] nanocrystals. Further development of colloidal copper-doped nanocrystals may open doors to their application as solution-processable color-conversion phosphors for light-emitting diodes (LEDs)[17,18] or luminescent solar concentrators,[15,19] or as soluble nanolabels for optical microscopies.[20,21]

Spectroscopic measurements at the single-particle level can reveal phenomena and electronic-structure characteristics that are obscured in ensemble measurements.

There have so far been very few single-particle measurements on colloidal doped semiconductor nanocrystals. The few reports to date have described blinking in colloidal Mn^{2+}-doped ZnSe and CdS nanocrystals,[22,23] luminescence energies and linewidths in colloidal Mn^{2+}-doped ZnS/CdS alloyed nanocrystals,[24] and the luminescence linewidths in ZnS nanostructures codoped with Cu^{+} and Al^{3+}, formed by sequential ion implantation into Al_2O_3 matrices.[25] Here, we report single-particle PL measurements of colloidal copper-doped CdSe (Cu^{+}:CdSe) nanocrystals. The different roles of electrons and holes in the copper-centered luminescence make Cu^{+}-doped nanocrystals particularly compelling for such studies because Cu^{+} can be considered a designer trap that exclusively localizes holes. We observe blinking in the copper-based luminescence that resembles the blinking of excitonic luminescence in undoped nanocrystals within the same ensemble. Statistical analysis of the blinking trajectories reveals that the average duration of nonemissive ("off") states is the same for the Cu^{+}:CdSe and undoped CdSe nanocrystals, but the average duration of emissive ("on") states is shorter for the Cu^{+}:CdSe nanocrystals. These results are interpreted to suggest that the primary mechanism by which these Cu^{+}:CdSe and CdSe nanocrystals transition from "on" to "off" is *via* trapping of conduction-band electrons (rather than valence-band holes). In addition, ensemble PL measurements reveal an extremely long-lived PL decay signal attributable to formation of metastable charge-separated states involving electrons in shallow surface traps, that is, nanocrystal analogs of the classic DAP states in bulk copper-based semiconductor phosphors, in which nanocrystal surface traps serve as the donors. Mechanistic links between this delayed luminescence and the luminescence blinking are discussed.

2.3 Single-Particle Photoluminescence Spectra

Figure 2.1 shows absorption and PL spectra of an ensemble of $d = 3.5$ nm, 0.6% Cu^{+}:CdSe nanocrystals (PL quantum yield, $\eta_{PL} = 0.25$) in toluene solution and PL spectra of representative single nanocrystals from the same solution (see Methods for

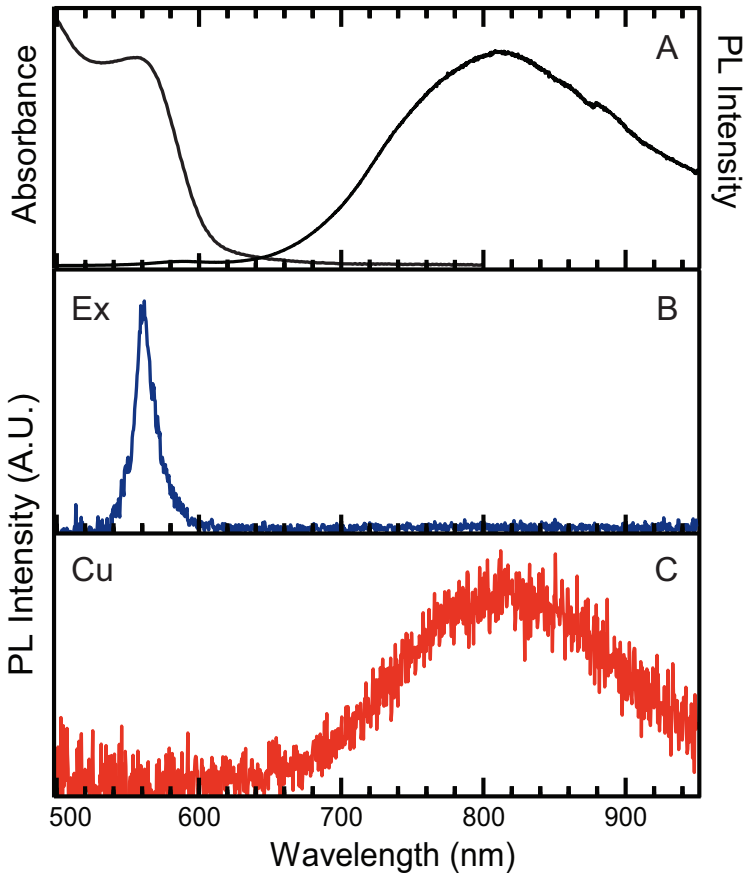

Figure 2.1: (A) Ensemble absorption and PL spectra of a toluene solution of $d = 3.5$ nm, 0.6% Cu^+:CdSe nanocrystals at room temperature($\eta_{PL} = 0.25$). (B) Single-particle spectrum of a representative undoped CdSe nanocrystal in PMMA at room temperature, showing solely excitonic emission. (C) Single-particle spectrum of a representative Cu^+-doped CdSe nanocrystal in PMMA at room temperature, showing solely copper-based emission.

experimental details). The absorption spectrum of the ensemble (Figure 2.1A) shows a peak at 557 nm that represents the average band gap of the nanocrystals. The PL spectrum of the ensemble is dominated by a broad (fwhm = 375 meV) band centered at 810 nm. This PL band is the charge-transfer transition formally involving recombination of a conduction-band electron with a photo-oxidized Cu^{+} dopant (*i.e.*, Cu^{2+}-like) characteristic of copper-doped II-VI semiconductors.

Figure 2.1, panel B shows the PL spectrum of one single nanocrystal that is representative of a minority subset of the nanocrystals in the 0.6% Cu^{+}:CdSe nanocrystal ensemble. This PL spectrum is dominated by a narrow (fwhm $\sim$ 54 meV) emission band centered at 561 nm. This spectrum is consistent with excitonic emission from a single undoped CdSe nanocrystal. Nanocrystals exhibiting only excitonic emission likely contain no Cu^{+} dopants. At 0.6% Cu^{+}, the average number of Cu^{+} dopants per nanocrystal is about 2, and a Poissonian distribution of these Cu^{+} dopants among the ensemble of nanocrystals results in $\sim$ 14% of the nanocrystals possessing no copper. Importantly, this small subset of undoped nanocrystals within this ensemble has exactly the same synthesis and processing history as the more prevalent doped nanocrystals, so they serve as excellent control samples for probing the impact of Cu^{+} doping on nanocrystal PL blinking.

Figure 2.1, panel C shows the PL spectrum of another single nanocrystal, this time representative of the majority of nanocrystals observed in these measurements. This spectrum displays a broad (fwhm $\sim$ 325 meV) band centered at 816 nm that is very similar to the ensemble luminescence in Figure 2.1, panel A and hence attributable to copper-based PL in the single nanocrystal. The line width of the copper-based PL is nearly the same in the single-particle spectrum as in the ensemble spectrum, consistent with observations from studies of Cu^{+},Al^{3+}:ZnS nanostructures[25] and from fluorescence line narrowing measurements of ensembles of copper-doped ZnSe/CdSe nanocrystals.[26] The single-particle emission occurs slightly lower in energy than the ensemble emission, indicating some inhomogeneous broadening in the ensemble spec-

trum that can be attributed to the nanocrystal size distribution and the dependence of this transition energy on nanocrystal size.[5,9,11] Because of the extremely low Cu^+ concentrations used here, inhomogeneous broadening due to Cu^+ positioning within the nanocrystal can be excluded as a major factor in this line width. Instead, this large line width is attributable to strong electron-phonon coupling associated with excited-state hole localization, including an anticipated Jahn-Teller distortion of the Cu^{2+}-like center in the luminescent excited state.[27] Notably, there is no detectable excitonic PL in the single-particle spectrum of Figure 2.1, panel C, which indicates very fast relaxation from excitonic to charge-transfer excited states in Cu^+-doped CdSe nanocrystals.

2.4 Blinking Dynamics

Figures 2.2, panels A and B show representative single-particle blinking traces from two different nanocrystals in the ensemble. The blue traces document emission from 490–635 nm and represent excitonic emission; the red traces document emission from 635–950 nm and represent copper-based charge-transfer emission. Occasionally, single particles showing emission on both channels were observed. This behavior could conceivably reflect a subset of nanocrystals with Cu^+ ions near their surfaces and hence slower hole transfer to Cu^+, but it is likely also partly an experimental artifact arising from emission bands tailing across the dichroic cutoff near 635 nm, allowing the same band to be counted by both detectors. This subset of nanocrystals is therefore not considered further. Figure 2.2, panel C plots a representative blinking trace for the copper-based emission on an expanded time axis. Overall, a total of 20 nanocrystals showing excitonic emission and 73 nanocrystals showing copper-based emission were measured in detail for subsequent analysis.

The doped and undoped nanocrystal blinking data were analyzed following the method outlined by Hess *et al.* for determining the probability that two data sets share the same underlying statistical distribution.[28] This method involves comput-

ing a cumulative distribution function (CDF) for each data set and then using the Komlogorov-Smirnov (KS) test to determine the "goodness of fit" between the two functions. CDFs are computed directly from the blinking data using eq 2.1,[29] where N is the number of events, and t_i is an event duration smaller than time t, with no additional manipulation of the data:

$$\mathrm{CDF}\,(t) = \frac{1}{N}\sum_i t_i < t \tag{2.1}$$

Plotting the data as the complementary CDF (cCDF, eq 2.2)[29] is useful for visualizing blinking data because at short times, the event probabilities are greatest:

$$\mathrm{cCDF}\,(t) = 1 - \mathrm{CDF}\,(t) \tag{2.2}$$

Figure 2.2, panels D and E present cCDFs compiling the emissive ("on") and non-emissive ("off") event durations from the blinking traces of all 73 Cu^+-doped (red) and 20 undoped (blue) CdSe nanocrystals. A hard threshold of three standard deviations above the mean background was used to distinguish between "on" and "off" events. The KS test was then applied to determine the likelihood that the excitonic- and copper-emitting nanocrystals exhibited similar kinetics.[29,30] From this test, the "off" cCDFs for the CdSe and Cu^+:CdSe nanocrystals are identical to greater than a 95% confidence interval (see Supporting Information), which means a high likelihood that the "off" to "on" transitions have the same microscopic origins in both the CdSe and Cu^+:CdSe nanocrystals. In contrast, the "on" cCDFs for the CdSe and Cu^+:CdSe nanocrystals are similar in shape but exhibit a statistically significant difference, falling well below a 95% confidence interval for the goodness of fit (see Supporting Information). Their difference is especially apparent in the linear plot of Figure 2.2, panel E. The sharper curvature in the Cu^+:CdSe "on" cCDF indicates that the Cu^+:CdSe nanocrystal "on" times are shorter, on average, than those of CdSe nanocrystals. We interpret the indistinguishable "off" statistics to imply similar carrier-detrapping processes in both Cu^+-doped and undoped nanocrystals and the

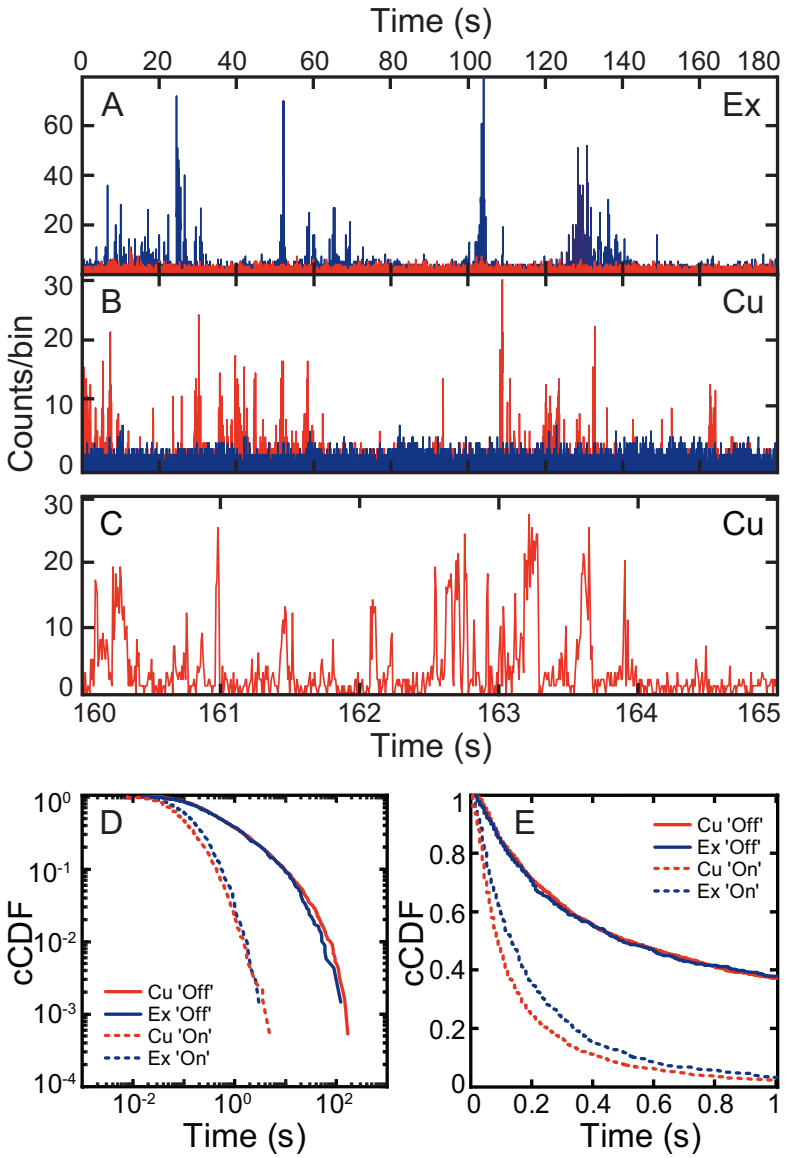

Figure 2.2: (A, B) Single-nanocrystal blinking traces documenting emission from 490 - 635 nm (blue) and from 635 - 950 nm (red) for (A) a single nanocrystal that exhibits only excitonic emission and (B) a single nanocrystal that exhibits only copper-based emission. (C) Expanded view of a blinking trace showing discrete jumps in copper-based emission. (D) Logarithmic and (E) linear plots of "on" (dashed lines) and "off" (solid lines) complementary cumulative distribution functions (cCDFs) for excitonic (blue) and copper-based (red) emission.

different "on" statistics to mean that CdSe and Cu^+:CdSe nanocrystals experience different carrier-trapping probabilities.

These data suggest that electron trapping/detrapping is primarily responsible for blinking in these nanocrystals. If hole trapping were responsible, then the CdSe nanocrystals would have shorter "on" times than the Cu^+:CdSe nanocrystals because hole trapping in CdSe does not need to compete with hole transfer to Cu^+ and hence is more probable than hole trapping in Cu^+:CdSe. Instead, undoped CdSe nanocrystals have longer "on" times than Cu^+:CdSe nanocrystals. Longer "on" times in CdSe nanocrystals are also consistent with "off" states arising from electron trapping: decay of the Cu^+:CdSe luminescence is approximately an order of magnitude slower than that of CdSe excitonic luminescence ($\tau \approx 300$ ns compared to $\sim$ 10 - 50 ns, at room temperature). The slow decay of the Cu^+:CdSe luminescent excited state, which still possesses a delocalized conduction-band electron, increases the probability of electron trapping and hence causes shorter "on" times in the blinking traces. These data thus strongly implicate electron trapping as the primary process that turns bright nanocrystals "off" in the blinking traces of both these Cu^+:CdSe and undoped CdSe nanocrystals. Potential alternative mechanisms are discussed below.

2.5 Delayed Luminescence

Figure 2.3 shows PL decay traces of Cu^+-doped nanocrystals measured at 20 and 297 K. In addition to PL decay within the first few microseconds similar to that reported in several related materials,[11,16,17,31] the data reveal a small but pronounced component of the PL decay that has an extremely long apparent time constant ($\sim$ 3.5 ms at room temperature, $\sim$ 300 ms at 20 K), extending the PL decay well beyond its radiative lifetime. A similar delayed luminescence was also observed in undoped CdSe and related core/shell nanocrystals,[32,33] but the phenomenon is much more pronounced in the luminescence of the Cu^+:CdSe nanocrystals (see Supporting Information). Such extremely slow luminescence has not been reported previously in

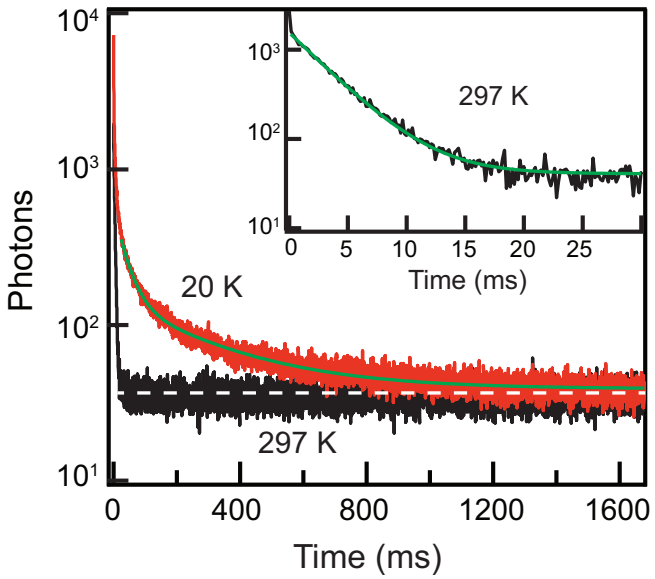

Figure 2.3: Ensemble photoluminescence decay in Cu^{+}:CdSe nanocrystals, measured at 20 K (red) and 297 K (black). The inset shows the lifetime measured at 297 K plotted over a 30 ms time window. The horizontal dashed line indicates the baseline counts. In addition to the dominant prompt decay components on the single-microsecond time scale associated with the copper charge-transfer state, a very slow component is observed that has a time constant of 3.5 ms at 297 K (green) and 300 ms at 20 K (green). This delayed luminescence is attributed to recombination following electron detrapping, and confirms the presence of long-lived electron trap states.

Cu^+-doped or copper-based nanocrystals. Importantly, the spectrum associated with the delayed luminescence is essentially identical to that measured under continuous illumination, showing only a small redshift with time (see Supporting Information). This spectral similarity indicates that the same luminescent excited state is re-formed after the temporary formation of a long-lived, dark intermediate excited state. We attribute this delayed luminescence to the formation of metastable charge-separated states *via* trapping of photoexcited carriers followed by carrier detrapping and radiative recombination. The large increase in the delayed luminescence decay time constant at low temperature demonstrates that carrier detrapping is thermally activated.

The larger amplitude of delayed luminescence in Cu^+:CdSe nanocrystals than in comparable undoped CdSe nanocrystals allows assignment of this process specifically to electron trapping/detrapping, analogous to DAP recombination in bulk Cu^+-doped phosphors and the same mechanism concluded from analysis of the blinking data described above. Delayed luminescence is favored by the slow decay of the luminescent excited state in Cu^+:CdSe nanocrystals, which gives electron trapping more time to compete with recombination.

2.6 Mechanistic Implications

Despite broad interest in Cu^+-doped colloidal semiconductor nanocrystals for spectroscopic studies and nanophosphor applications,[5–13] neither photoluminescence blinking nor delayed luminescence has been reported previously for any Cu^+-doped or copper-based colloidal semiconductor nanocrystals. The observations presented here provide new insights into the electronic structures and photophysical properties of this important class of nanocrystals. More generally, the observations here provide new insights into the interpretation of blinking and delayed luminescence in semiconductor nanocrystals, and specifically, implicate a mechanistic link between these two phenomena. Such a link has also been proposed for undoped II-VI semiconductor

nanocrystals based on similarities between luminescence power-law dynamics on the nano- to microsecond timescale and blinking power-law dynamics on even longer time scales.[32] The present results extend the understanding of these processes by specifically identifying electrons as the charge carriers responsible for these two phenomena.

Figure 2.4 summarizes the various processes in Cu^{+}:CdSe nanocrystals deduced from analysis of the photoluminescence, blinking, and delayed luminescence results. As detailed previously, the broad midgap photoluminescence of Cu^{+}-doped nanocrystals stems from photoexcitation (1) followed by rapid hole trapping at copper (2), and radiative electron-hole recombination (3). The data obtained here are consistent with this description. Both the blinking and delayed luminescence data reported here point to the existence of surface electron traps that reversibly intercept conduction-band electrons (4) to form long-lived metastable charge-separated states, analogous to donor-acceptor pair excited states in bulk Cu^{+}-doped chalcogenide phosphors.[3] The electrons spontaneously detrap on a very slow time scale that depends on temperature. Rather than Al^{3+} or Cl^{-} impurities, the donors in these nanocrystals are thus shallow electron traps on the nanocrystal surfaces.

Once an electron has been trapped the nanocrystal is dark and remains so until the electron is detrapped. Photoexcitation of a nanocrystal in this metastable charge-separated state yields only nonradiative recombination. This nonradiative recombination may occur *via* a Shockley-Read-Hall-like mechanism[34] (Figure 2.4, right panel) involving hole quenching by the reduced surface trap (6) followed by electron trapping (7) to re-form the metastable state. Fast trap-assisted Auger recombination[35,36] or the presence of low-energy Cu^{2+} excited states[3] may also contribute to nonradiative decay in the dark state of the Cu^{+}:CdSe nanocrystals. Recovery of nanocrystal emission only occurs by electron detrapping. Because the electron detrapping kinetics are largely independent of the presence of copper, the "off" state dynamics in these Cu^{+}:CdSe and CdSe nanocrystals are statistically indistinguishable, and only their "on" state dynamics differ. Overall, the data presented here provide strong evidence

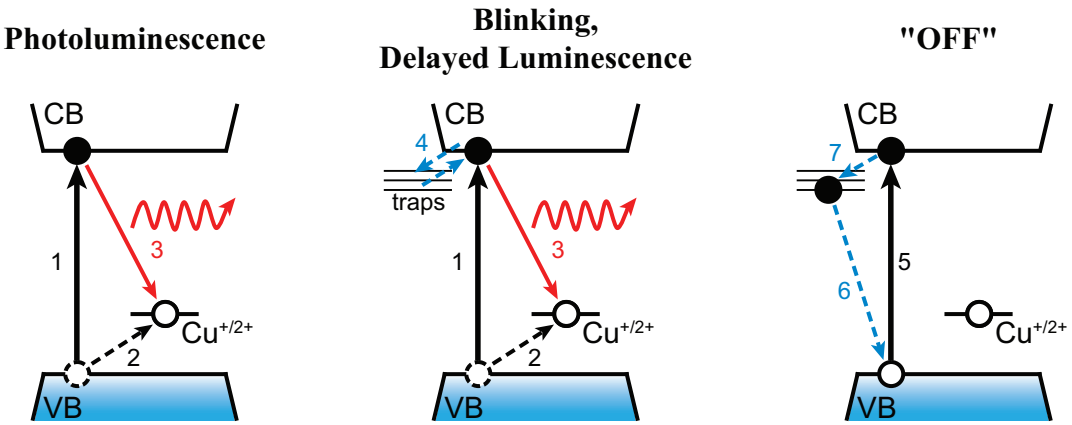

Figure 2.4: Schematic illustrations of the processes responsible for PL, luminescence blinking, delayed luminescence, and "off" states in Cu^{+}-doped CdSe nanocrystals. Solid arrows show processes involving photons, and dashed arrows show nonradiative processes. Left: Band-to-band photoexcitation (1) is followed by picosecond hole localization at copper (2). This hole subsequently recombines with the conduction-band electron to emit a photon (3). Center: The nanocrystal surfaces trap and detrap conduction-band electrons (4). Detrapping occurs on the millisecond time scale and generates delayed luminescence (3). Right: Photoexcitation of a nanocrystal already in its metastable charge-separated state (5) leads to nonradiative recombination and the nanocrystal appears dark. Nonradiative recombination may occur *via* a Shockley-Read-Hall-type mechanism involving rapid hole quenching from the reduced trap (6) followed by trap repopulation (7) to return to the original state, but other processes may also be important. The data indicate similar electron trapping/detrapping in undoped CdSe nanocrystals, and similar nonradiative decay processes may also be active in their "off" state.

that a similar electron trapping/detrapping mechanism underlies both the blinking and the delayed luminescence of the Cu^+:CdSe and CdSe nanocrystals studied here. Although the hole localizes at copper in the Cu^+:CdSe nanocrystals, the present interpretation does not speak to the location or extent of localization of the hole in the analogous "off" state of CdSe nanocrystals. Given the chemical instability of delocalized holes in CdSe nanocrystals, it can be reasonably anticipated that this hole also localizes. The present data suggest only that the blinking and delayed-luminescence kinetics are governed by electron trapping and detrapping kinetics.

One alternative interpretation of the blinking data presented here invokes Auger ionization of a hole from a biexciton as the process that forms the "off" state, followed by Auger recombination of the negative trions formed upon subsequent photoexcitation while in the dark state. The "off" state survives until nonradiative electron-hole recombination eliminates the excess electron and re-forms the "on" state. In this scenario, the distinction between electrons and holes would be less clear from the blinking data alone. In our experiments, this scenario is considered less likely than the reversible electron-trapping scenario proposed above because (a) our nanocrystals were excited using a low-power pulsed laser from which the average number of excitations per nanocrystal per pulse was limited to < 0.066 to avoid the formation of biexcitons or other multiply excited states (see Methods), and (b) the correlation between delayed luminescence and blinking proposed in ref 32 and supported by our measurements strongly implies that the photochemical processes responsible for blinking must also occur with the even lower nanocrystal excitation rates of the delayed-luminescence measurements. These considerations argue against a multiphoton Auger ionization mechanism for "off"-state formation.

Moreover, the interpretation proposed here is also broadly consistent with the results of several recent studies that have implicated surface recombination centers, rather than trion Auger recombination, as the cause of luminescence suppression in nanocrystal "off" states.[37–40] Although trion Auger recombination is too slow to ac-

count for the "off"-state PL quenching of many nanocrystals,[37–39] the trap-assisted recombination mechanism proposed in Figure 2.4 (right panel) would be consistent with experimental observations.[38] Redox-active surface traps of colloidal CdSe nanocrystals, when in specific oxidation states, can introduce nonradiative decay channels for the exciton that are much faster than trion Auger recombination.[41] In some studies, redox control of surface states has been proposed to regulate blinking itself.[40,42] For example, Galland *et al.* have proposed that electrochemical reduction of subconduction-band surface traps in CdSe/CdS nanocrystals eliminates these traps from participation in a nonradiative recombination channel similar to that illustrated in Figure 2.4 (right panel).[40] The microscopic identities and redox properties of the relevant surface traps remain unclear.

2.7 Summary

In summary, PL blinking has been examined in the luminescence of single Cu^+:CdSe and CdSe nanocrystals. Copper doping is found to perturb the blinking "on" statistics but not the blinking "off" statistics. Because copper selectively traps photogenerated holes, this result allows blinking in these nanocrystals to be associated specifically with electron trapping and detrapping. The same Cu^+:CdSe nanocrystals also show an extremely long-lived delayed luminescence signal due to reversible electron trapping/detrapping that allows luminescence long beyond the radiative recombination time of the luminescent excited state. These results complement existing nanocrystal blinking literature by providing new insights into the specific carriers involved in these processes through the use of copper dopants as well-defined traps that selectively localize holes. This study advances our understanding of the photophysical properties of colloidal Cu^+-doped semiconductor nanocrystals, with broad ramifications for applications of such doped nanocrystals as spectral-conversion or optical-imaging phosphors.

2.8 Methods

2.8.1 Synthesis of Cu^+:CdSe Nanocrystals

Copper-doped CdSe (*i.e.*, Cu^+:CdSe) nanocrystals were synthesized by a hot-injection method adapted from recent literature.[43] Briefly, cadmium acetate hydrate (0.116 g, 0.5 mmol), oleic acid (0.32 g, 1.1 mmol), and hexadecane (5 g) were degassed under vacuum at 70 °C for 1 h. The mixture was heated to 110 °C under nitrogen for 10 min, which produced a clear, colorless solution. After it was cooled to 70 °C, copper stearate (0.032 g, 0.05 mmol) was added under positive nitrogen flow, the mixture was degassed with three pump-purge cycles at 70 °C, and then the temperature was increased to 180 °C under nitrogen. Rapid injection of 0.25 mL of a 1 M solution of selenium in trioctylphosphine at 180 °C caused the mixture to change color within a few seconds from deep blue to colorless (consistent with reduction of Cu^{2+} to Cu^+) and then from colorless to orange to red (indicating nucleation and growth of CdSe nanocrystals). After 30 min at 180 °C, the mixture was cooled to room temperature. Addition of an equal volume of a $\sim$ 3:1 ethanol/acetone mixture followed by centrifugation produced dark red pellets from a colorless supernatant. The supernatant was discarded, and the pellets were washed with acetone, dried under nitrogen flow, and redispersed in toluene. Samples were characterized by UV-vis absorbance (Varian, Cary 500) and as described in the following by PL, lifetime measurements, and fluorescence microscopy. Copper concentrations were quantified using inductively coupled plasma atomic emission spectroscopy (ICP-AES). Magnetic circular dichroism and electron paramagnetic resonance measurements show no evidence of paramagnetism (see Supporting Information), consistent with copper in its monovalent oxidation state. We note that our copper precursor, copper stearate, is a Cu^{2+} complex, but the anaerobic reaction conditions and the addition of easily oxidized ligands such as trioctylphosphine can facilitate the reduction necessary for incorporation as Cu^+.

2.8.2 Photoluminescence

Solutions of nanocrystals suspended in toluene were excited using a 405 nm diode laser. The resulting PL was collected perpendicular to the excitation field, and delivered to a monochromator (Acton, SpectraPro 500i, 0.5m, 150 g/mm grating blazed at 500 nm) equipped with a LN_2 cooled CCD (Roper Scientific, LN100EB) for detection. A Hamamatsu integrating sphere quantum yield measurement system with 400 nm excitation was used to measure the PL quantum yields of toluene solutions of Cu^+:CdSe nanocrystals.

2.8.3 Luminescence Lifetimes

Samples were prepared by sandwiching drop-cast films of nanocrystals between sapphire disks. Samples were cooled to 20 K in a closed-cycle cryostat and excited using a 405 nm diode laser at a power density of ~ 0.05 W/cm^2, modulated at 0.2 Hz with the square-wave output of a function generator (SRS, DS345). Lifetimes were measured at 760 nm using a monochromator (Acton, SpectraPro 500i, 0.5m, 150 g/mm grating blazed at 500 nm) equipped with a PMT (Hamamatsu, H7422). Lifetimes were collected over a 1600 ms time window; the PMT signal was processed using a multichannel analyzer and collected with a custom LabView program. Lifetimes were determined from a multiexponential fit of the decay curves.

2.8.4 Single-Particle Blinking

Cu^+:CdSe nanocrystals were dispersed at 0.1 - 1.0 nM concentrations in solutions of 1% PMMA in toluene, then spin coated onto cleaned zinc titania glass coverslips at 1000 rpm. The samples were mounted on an xy-piezoelectric nanopositioning stage (PI, P-545.2R7) on an inverted confocal microscope (Nikon, TE2000U). Photoexcitation was accomplished using a 405 nm pulsed picosecond diode laser (PicoQuant, PDL 800-B with LDH-P-C-405B laser head) having a temporal width of 63 ps

(fwhm) and a repetition rate of 5 MHz. A 425 nm dichroic long-pass mirror (Chroma, T425LPXR) directed the excitation field to the back of a 100× oil-immersion objective (Nikon, PlanFluor, 1.4 NA) where it was focused through the glass coverslip. An average power of 90 nW was measured at the focal point of the objective. Assuming a diffraction-limited focal spot, this excitation power corresponds to an average of ~ 5 photons incident on a NC per pulse, which in turn corresponds to ~ 0.066 excitations per nanocrystal per pulse, or an average of one absorption event every 6 μs. The excitation rate is thus slow compared to the decay time of the copper luminescence ($\sim$ 300 ns). This excitation rate represents an upper bound because a diffraction-limited focal point is likely not truly achieved. Such low excitation rates are used to minimize the probability of generating multiply excited nanocrystals. Emission was collected in an epi-geometry, passed through the 425 nm dichroic long-pass mirror, and then passed through a second long-pass filter (Chroma, ET490LP) to reject scatter from the photoexcitation field. The emission was then split by a 635 nm dichroic long-pass mirror (Chroma, T635LPXR) with the transmitted and reflected fields focused onto two separate avalanche photodiode detectors (APDs) with 50 μm active areas (MPD, PDM050CTB) providing confocal resolution. Observation of single-step photobleaching events, diffraction-limited spot sizes, and a dependence of emission spots per area on nanocrystal concentration confirm measurement of single nanocrystals. Microscope and collection-electronics control were accomplished using a custom LabView program. Data were binned in 7.5 ms intervals.

2.8.5 Single-Particle Photoluminescence Spectra

Luminescence spectra of single Cu^+:CdSe nanocrystals were measured on the same polymer films used for the luminescence blinking studies and using the same microscope. The luminescence was focused onto a 100 μm pinhole to achieve confocal resolution and then delivered to a monochromator (Acton, SP2300i, 0.3 m, 150 g/mm grating blazed at 800 nm) equipped with a LN_2 cooled CCD detector (Roper Scien-

tific, 7346-0005). Spectra were collected with 300 s exposures, 5 MHz rep rate, and 90 nW average excitation power.

2.9 Supporting Information

KS test parameters used in the analysis of the blinking data, fitting parameters for the photoluminescence decays, and additional spectroscopic data. The Supporting Information is available free of charge on the ACS Publications website at DOI: 10.1021/acs.nanolett.5b01046.

KS test parameters

The following parameters were used to calculate the similarity between the CDFs. This follows the method of Riley *et al.*[29]

$$\text{D value} = max_{-\infty<t<\infty}|S_1(t) - S_2(t)|$$

The D value is used to compare two different CDFs to gauge magnitude of similarity between the CDFs.

$$\text{p value} = S_{KS}\left(\left[\sqrt{N_e} + 0.12 + 0.11/\sqrt{N_e}\right]D\right)$$

The p value is computed from the CDF of the KS distribution, this is used to quantify the differences observed between the two CDFs. A p-value greater than 0.05 indicates that there is a very high likelihood, to a 95% confidence interval, that the two CDFs are from the same distribution.

The CDF of the KS distribution, S_{KS}, is given by the expression below.

$$S_{KS}(z) = \sqrt{\frac{2\pi}{z}}\sum_{j=1}^{\infty} exp\left(\frac{-(2j-1)^2\pi^2}{8z^2}\right)$$

$$N_e = \frac{N_1 N_2}{N_1 + N_2}$$

N_e is the reduced data density, this accounts for differences in the number of data points between the two CDFs of interest.

Table 2.1: KS Test

Kolmogorov-Smirnov (KS) Test		
	On Intervals	Off Intervals
	Cu vs Ex	Cu vs Ex
p	9.85E-09	0.9222
D	0.1368	0.0244

Table 2.2: Qds per CDF

QDs per CDF	
Cu	73
Ex	20

Magnetic Circular Dichroism Spectroscopy

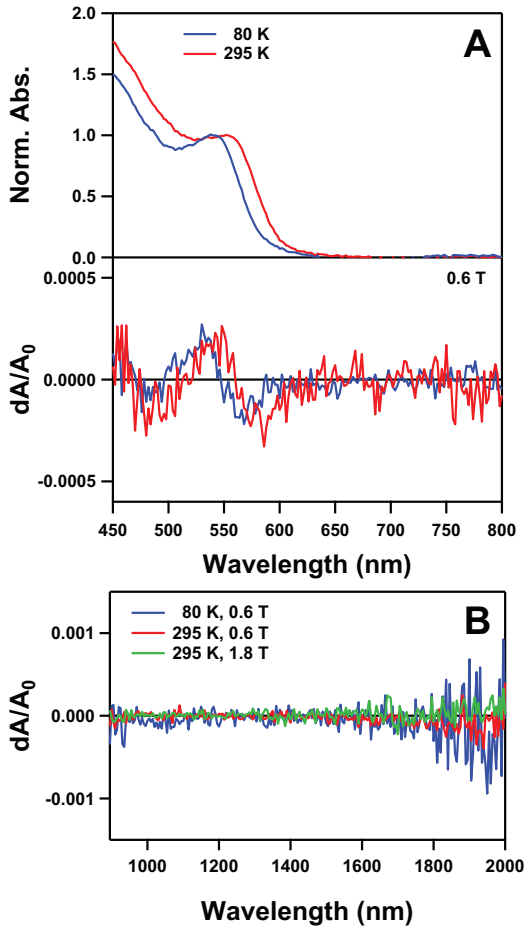

Figure 2.5: (A) Absorption (top) and magnetic circular dichroism (MCD, bottom) spectra of Cu^{+}:CdSe nanocrystals in a polylaurylmethacrylate film sandwiched between quartz discs. The film was mounted in a cryostat and measured in an electromagnet at an applied 0.6 T magnetic field in the Faraday geometry. Spectra measured at 80 K (blue) and 295 K (red). (B) Near-infrared MCD spectra taken of the sample under the same conditions as in A (blue and red), and of a toluene solution of Cu^{+}:CdSe NCs at room temperature with an applied field of 1.8 T. No MCD signal is observed from 900 - 2000 nm. The only MCD signals observed in the range from 400 - 2000 nm occur for $\lambda <$ 600 nm, corresponding to the small Zeeman splitting of the excitonic transitions of Cu^{+}:CdSe nanocrystals. The magnitude of the Zeeman splitting of the exciton is the same at 80 K and 295 K indicating there are no significant sp-d exchange interactions between the exciton and copper dopants in the ground state. This observation, combined with the absence of any signals corresponding to Cu^{2+} ligand-field transitions in the near-infrared (900 - 2000 nm), confirms that the oxidation state of the copper dopants in these nanocrystals is most likely Cu^{+}.

Electron Paramagnetic Resonance Spectroscopy

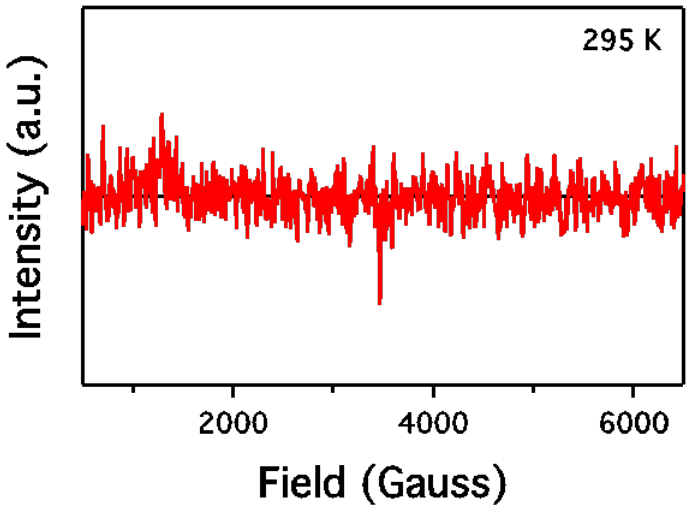

Figure 2.6: Electron paramagnetic resonance (EPR) spectrum of Cu^{+}:CdSe suspended in toluene at room temperature in a Bruker EMX continuous wave X-band EPR spectrometer. The spectrum shows no evidence for the presence of Cu^{2+} ions in the ground state.

Lifetime Fitting

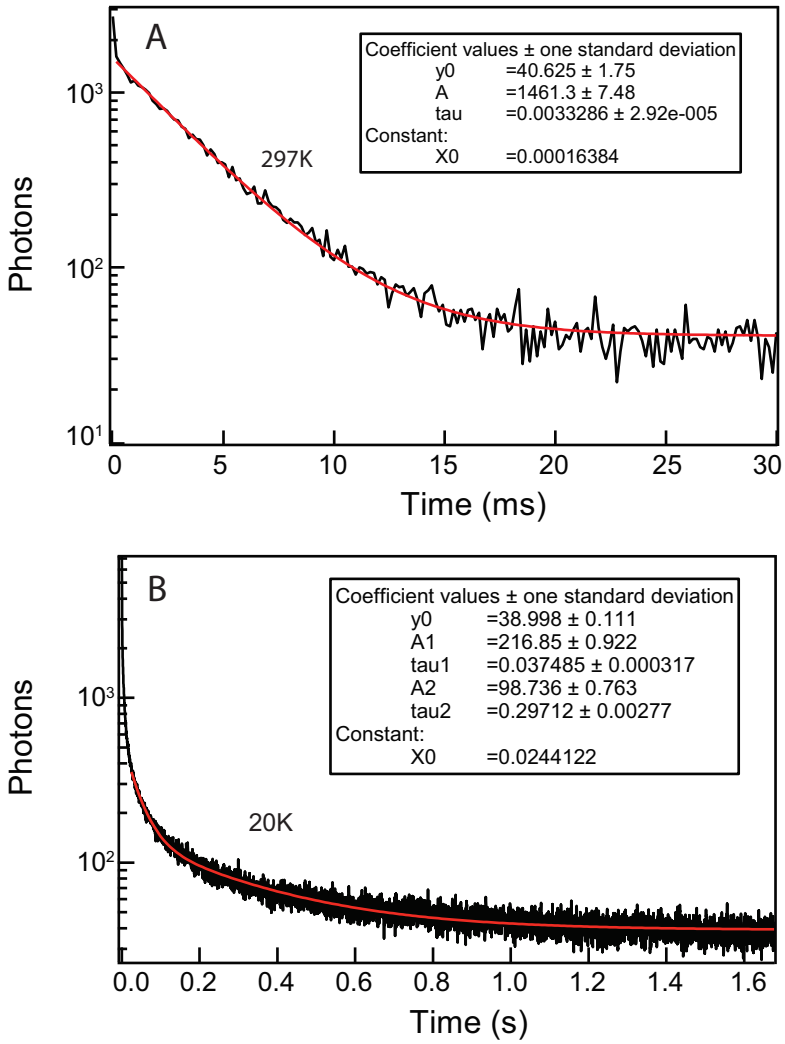

Figure 2.7: Plots of the intensity of the Cu luminescence feature versus time for the ensemble of Cu^{+}:CdSe nanocrystals measured at (A) 297 K and (B) 20 K. The long time component fits to a single exponential at 297 K with a lifetime $\tau = 3.3$ ms, and fits to a double exponential at 20 K with a long time component of $\tau = 300$ ms. The solid red lines represent these fits.

Gated Luminescence Spectra

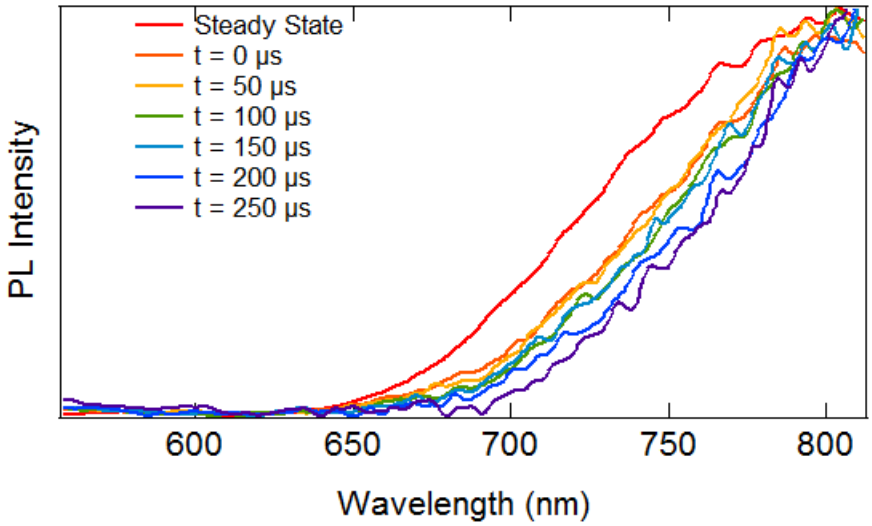

Figure 2.8: Gated luminescence spectra collected at room temperature of Cu^{+}:CdSe excitation was provided by a square wave source, steady state measurement prior to decay. The spectrum taken at longer delay times shows a slight red shift in the Cu^{+} emission maximum.

Delayed Luminescence is More Intense in Copper-Doped Nanocrystals

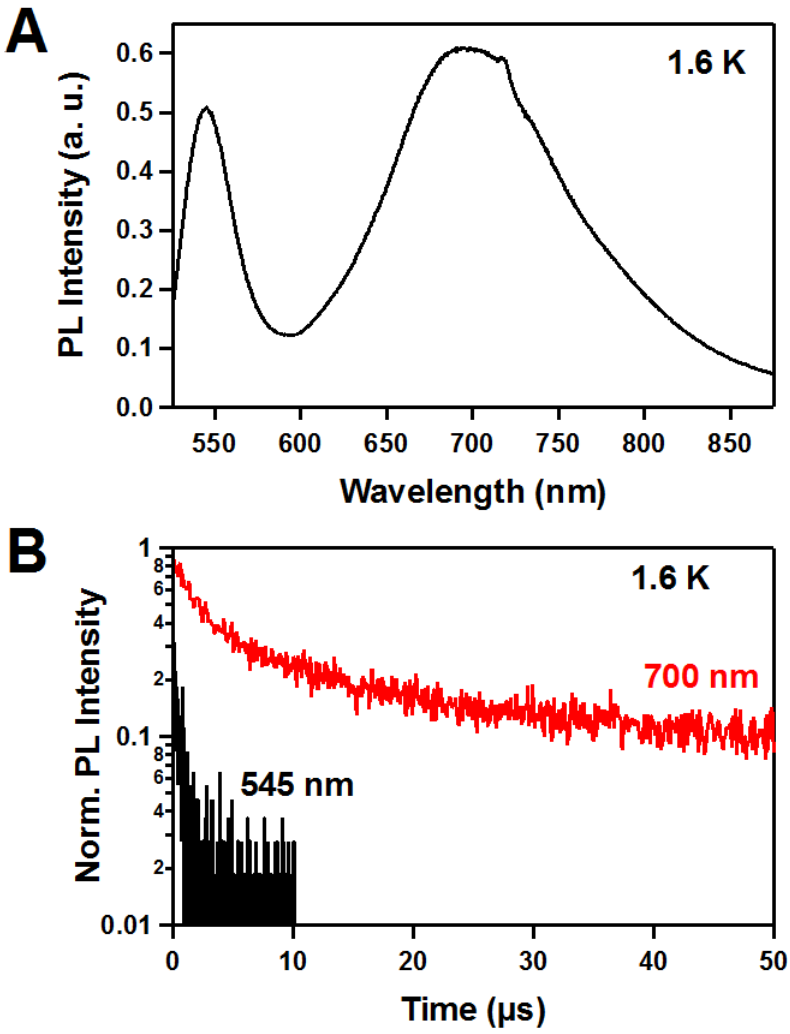

Figure 2.9: (A) Photoluminescence spectrum of an ensemble containing significant populations of both undoped CdSe (PL peak at 545 nm) and Cu^{+}:CdSe (PL peak at 700 nm) nanocrystals measured at 1.6 K. (B) PL decay traces measured at 1.6 K of the excitonic (545 nm) and Cu (700 nm) PL features of the same sample shown in (A).

2.10 Author Information

Corresponding Authors

**E-mail: gamelin@chem.washington.edu.*

**E-mail: pjreid@uw.edu.*

Notes

The authors declare no competing financial interest.

2.11 Acknowledgment

This work was supported by the National Science Foundation under CHE-1404674 (to P.J.R.) and DMR-1206221 (to D.R.G.). Financial support from the U.S. Department Of Energy, Office of Energy Efficiency and Renewable Energy (DOE EERE) Postdoctoral Research Award (to K.E.K.) is also gratefully acknowledged.

2.12 Bibliography

[1] Yen, W.M., Shionoya, S., & Yamamoto, H.(Eds.) (2006). *Phosphor Handbook.* CRC press.

[2] Smet, P.F., Moreels, I., Hens, Z., & Poelman, D. (2010). *Materials* **3**, 2834–2883.

[3] Suzuki, A. & Shionoya, S. (1971). *Journal of the Physical Society of Japan* **31**, 1455–1461.

[4] Allen, J. (1974). *Physical Review B* **9**, 1564.

[5] Suyver, J., Van der Beek, T., Wuister, S., Kelly, J., & Meijerink, A. (2001). *Applied Physics Letters* **79**, 4222–4224.

[6] Pradhan, N., Goorskey, D., Thessing, J., & Peng, X. (2005). *Journal of the American Chemical Society* **127**, 17586–17587.

[7] Pradhan, N., Battaglia, D.M., Liu, Y., & Peng, X. (2007). *Nano Letters* **7**, 312–317.

[8] Xie, R. & Peng, X. (2009). *Journal of the American Chemical Society* **131**, 10645–10651.

[9] Srivastava, B.B., Jana, S., & Pradhan, N. (2011). *Journal of the American Chemical Society* **133**, 1007–1015.

[10] Viswanatha, R., Brovelli, S., Pandey, A., Crooker, S.A., & Klimov, V.I. (2011). *Nano Letters* **11**, 4753–4758.

[11] Grandhi, G.K., Tomar, R., & Viswanatha, R. (2012). *ACS Nano* **6**, 9751–9763.

[12] Grandhi, G.K. & Viswanatha, R. (2013). *The Journal of Physical Chemistry Letters* **4**, 409–415.

[13] Zhang, J.Z., Cooper, J.K., & Gul, S. (2014). *The Journal of Physical Chemistry Letters* **5**, 3694–3700.

[14] Stouwdam, J.W. & Janssen, R.A. (2009). *Advanced Materials* **21**, 2916–2920.

[15] Bradshaw, L.R., Knowles, K.E., McDowall, S., & Gamelin, D.R. (2015). *Nano letters* **15**, 1315–1323.

[16] Li, L., Pandey, A., Werder, D.J., Khanal, B.P., Pietryga, J.M., & Klimov, V.I. (2011). *Journal of the American Chemical Society* **133**, 1176–1179.

[17] Zhang, W., Lou, Q., Ji, W., Zhao, J., & Zhong, X. (2014). *Chemistry of Materials* **26**, 1204–1212.

[18] Yuan, X., Hua, J., Zeng, R., Zhu, D., Ji, W., Jing, P., Meng, X., Zhao, J., & Li, H. (2014). *Nanotechnology* **25**, 435202.

[19] Knowles, K.E., Kilburn, T.B., Alzate, D.G., McDowall, S., & Gamelin, D.R. (2015). *Chemical Communications* **51**, 9129–9132.

[20] Li, M., Xu, C., Wu, L., Wu, P., & Hou, X. (2015). *Chemical Communications* **51**, 3552–3555.

[21] Jiang, T., Song, J., Wang, H., Ye, X., Wang, H., Zhang, W., Yang, M., Xia, R., Zhu, L., & Xu, X. (2015). *Journal of Materials Chemistry B* **3**, 2402–2410.

[22] Ishizumi, A. & Kanemitsu, Y. (2009). *Journal of the Physical Society of Japan* **78**, 083705.

[23] Zhang, Y., Gan, C., Muhammad, J., Battaglia, D., Peng, X., & Xiao, M. (2008). *The Journal of Physical Chemistry C* **112**, 20200–20205.

[24] Hazarika, A., Layek, A., De, S., Nag, A., Debnath, S., Mahadevan, P., Chowdhury, A., & Sarma, D.D. (2013). *Physical Review Letters* **110**, 267401.

[25] Ishizumi, A., White, C., & Kanemitsu, Y. (2004). *Applied Physics Letters* **84**, 2397–2399.

[26] Brovelli, S., Galland, C., Viswanatha, R., & Klimov, V.I. (2012). *Nano Letters* **12**, 4372–4379.

[27] Siddique, Z.A., Yamamoto, Y., Ohno, T., & Nozaki, K. (2003). *Inorganic Chemistry* **42**, 6366–6378.

[28] Hess, C.M., Riley, E.A., & Reid, P.J. (2014). *The Journal of Physical Chemistry B* **118**, 8905–8913.

[29] Riley, E., Hess, C., Whitham, P., & Reid, P. (2012). *The Journal of Chemical Physics* **136**, 184508.

[30] Clauset, A., Shalizi, C.R., & Newman, M.E. (2009). *SIAM Review* **51**, 661–703.

[31] Gul, S., Cooper, J.K., Glans, P.A., Guo, J., Yachandra, V.K., Yano, J., & Zhang, J.Z. (2013). *ACS Nano* **7**, 8680–8692.

[32] Sher, P., Smith, J., Dalgarno, P., Warburton, R., Chen, X., Dobson, P., Daniels, S., Pickett, N., & O'Brien, P. (2008). *Applied Physics Letters* **92**, 101111.

[33] Jones, M., Lo, S.S., & Scholes, G.D. (2009). *Proceedings of the National Academy of Sciences* **106**, 3011–3016.

[34] Shockley, W. & Read Jr, W. (1952). *Physical Review* **87**, 835.

[35] Cohn, A.W., Janßen, N., Mayer, J.M., & Gamelin, D.R. (2012). *The Journal of Physical Chemistry C* **116**, 20633–20642.

[36] Cohn, A.W., Schimpf, A.M., Gunthardt, C.E., & Gamelin, D.R. (2013). *Nano Letters* **13**, 1810–1815.

[37] Jha, P.P. & Guyot-Sionnest, P. (2009). *ACS Nano* **3**, 1011–1015.

[38] Zhao, J., Nair, G., Fisher, B.R., & Bawendi, M.G. (2010). *Physical Review Letters* **104**, 157403.

[39] Rosen, S., Schwartz, O., & Oron, D. (2010). *Physical Review Letters* **104**, 157404.

[40] Galland, C., Ghosh, Y., Steinbrück, A., Sykora, M., Hollingsworth, J.A., Klimov, V.I., & Htoon, H. (2011). *Nature* **479**, 203–207.

[41] Rinehart, J.D., Schimpf, A.M., Weaver, A.L., Cohn, A.W., & Gamelin, D.R. (2013). *Journal of the American Chemical Society* **135**, 18782–18785.

[42] Hohng, S. & Ha, T. (2004). *Journal of the American Chemical Society* **126**, 1324–1325.

[43] Tananaev, P., Dorofeev, S., Vasil'ev, R., & Kuznetsova, T. (2009). *Inorganic Materials* **45**, 347–351.

Chapter 3

SINGLE-PARTICLE PHOTOLUMINESCENCE SPECTRA, BLINKING, AND DELAYED LUMINESCENCE OF COLLOIDAL $CuInS_2$ NANOCRYSTALS

Patrick J. Whitham, Arianna Marchioro, Kathryn E. Knowles, Troy B. Kilburn, Philip J. Reid,* and Daniel R. Gamelin*

Department of Chemistry, University of Washington, Seattle, WA 98195-1700, USA

3.1 Abstract

Single-nanocrystal and ensemble photoluminescence measurements on $CuInS_2$ semiconductor nanocrystals reveal luminescence bandshapes that are broad compared to those typical of individual II-VI or related semiconductor nanocrystals. This finding is consistent with the hypothesis of strong electron-phonon coupling in the emissive excited state of these $CuInS_2$ semiconductor nanocrystals. Blinking is observed that resembles that of other semiconductor nanocrystals. Ensemble luminescence measurements also reveal the existence of a remarkably long-lived excited state in these nanocrystals that continues to emit photons over several orders of magnitude in time following the excitation pulse. The delayed luminescence overlaps in time and shows similar distributed kinetics to the blinking "off" times of the same nanocrystal sample, supporting the proposal that these two phenomena arise from the same microscopic carrier-trapping and -detrapping processes. Excitation power dependence measurements illustrate that the delayed luminescence saturates at very low emission intensities under the excitation power densities used in the single-nanocrystal measurements, consistent with this metastable charge-trapped state being the "off" state of the luminescence blinking cycle.

3.2 Introduction

$CuInE_2$ (E = S, Se, Te) nanocrystals (NCs) have recently attracted a great deal of interest as nontoxic alternatives to CdSe, PbS, and related semiconductor NCs for numerous nanophosphor applications.[1–3] The large photoluminescence (PL) Stokes shifts and long lifetimes of $CuInE_2$ NCs make them particularly attractive emitters for applications in bioimaging,[3,4] light-emitting diodes,[5] and luminescent solar concentrators.[6–8] Compared to II-VI or IV-VI semiconductor NCs such as CdSe and PbS, however, the luminescence mechanism in $CuInE_2$ NCs is not very well understood. Bulk $CuInS_2$ displays several distinct PL transitions including free-exciton emission, free-to-bound recombination, and donor-acceptor pair (DAP) recombination.[9–12] A narrow near-band-edge emission feature is observed at 1.53 eV ($\sim$ 50 meV full-width at half maximum (fwhm) at 300 K), and broader deep-trap emission is observed between 1.3 and 1.4 eV.[11,12] The free-to-bound and DAP recombination processes are generally interpreted as involving lattice vacancies or other point defects. The specific PL spectrum displayed by bulk $CuInS_2$ thus depends on the methods of crystal growth and post-growth annealing, which affect the concentrations of such defects.[13,14] The PL spectra of $CuInS_2$ NCs are dominated by a broad mid-gap feature ($\sim$ 300 – 400 meV fwhm at 300 K)[15] that exhibits a large Stokes shift of $\sim$ 250 – 500 meV and that bears little resemblance to the characteristic PL features of bulk $CuInS_2$.[16] The energy of this broad PL can be tuned by changing the NC size.[15,17–22] Various mechanisms have been proposed to explain this PL. Most proposed mechanisms are analogous to those discussed for bulk $CuInS_2$, and invoke lattice vacancies or interstitial defects to generate DAP or free-to-bound recombination processes similar to in bulk.[17,22–25] A recent study has proposed the existence of substitutional Cu^{2+} in $CuInS_2$ NCs as the source of the broad PL.[26] Alternatively, a theoretical study based on the multi-band effective-mass approximation proposes the existence of large Stokes shifts and long PL lifetimes in quantum-confined $CuInS_2$ NCs stemming from the first-order forbid-

denness of the lowest-energy inter-band electronic transition, which becomes partially allowed through low-symmetry effects.[27] In this interpretation, absorption is dominated by higher-energy excitonic states, but PL occurs *via* this low-energy forbidden state, generating a large Stokes shift. Yet another proposal is that $CuInE_2$ NC PL involves exciton self-trapping.[15] This mechanism accounts for both the large Stokes shifts and the broad bandshapes by invoking strong excited-state electron-phonon coupling that leads to partial localization of photogenerated charge carriers. This interpretation has been proposed based on similarities in PL bandwidths, lifetimes, Stokes shifts, and magnetic-field dependence between $CuInS_2$ and Cu^+-doped semiconductor NCs.[15,16] In the latter NCs, photogenerated holes localize around individual Cu^+ dopants, causing large lattice distortion at this localization site. Single-particle spectroscopy can provide new insights into the mechanism of PL in $CuInS_2$ NCs by evaluating ensemble particle-size heterogeneity as a source of spectral inhomogeneous broadening. Inhomogeneous particle sizes account for only a small portion of the ensemble PL bandwidths of Cu^+ doped NCs,[28–30] but to date, there have been no reports of any single-particle spectra for any $CuInE_2$ NCs. PL blinking has been reported for single Zn-Cu-In-S alloyed NCs,[31] but single-particle PL spectra were not reported. In addition to resolving uncertainties about homogeneous PL bandwidths, single-nanocrystal studies of PL blinking can provide insights into carrier trapping and detrapping dynamics. Recent experiments have drawn attention to the possibility that single-NC PL blinking may be linked mechanistically to the phenomenon of delayed luminescence observed in CdSe, Cu^+:CdSe, and related NCs.[30,32–34] Shallow charge trapping can form metastable charge-separated states that de-trap only on very long timescales, leading to extremely slow luminescence decay. Here, we present the first single-particle spectra of colloidal $CuInS_2$ NCs. We show that the PL from single $CuInS_2$/CdS NCs is narrower than the ensemble PL but broader than typical excitonic PL, with fwhm values ranging from $190 - 270$ meV. Intermittency (blinking) is observed in the $CuInS_2$/CdS single-NC PL time-traces that display distributed ki-

netics similar to those of other semiconductor NCs. We also report the first delayed PL measurements for $CuInS_2$ NCs. Delayed PL is observed in ensemble measurements on the same $CuInS_2$/CdS NCs and shows very similar distributed decay kinetics as seen in the blinking experiments. The blinking and delayed PL dynamics are shown to overlap over a broad experimental time window. Both phenomena are attributed to the same reversible carrier-trapping processes. Excitation power-dependence data, measured for both prompt and delayed PL in the same experiment, are consistent with the proposed relationship between blinking and delayed PL, showing a linear power dependence for the prompt PL but facile power saturation of the delayed PL. These results illustrate the major role that excitation rate plays in determining the ratio of delayed to prompt PL intensities. We propose that this PL power dependence has important consequences at the single-particle level.

3.3 Results and Analysis

3.3.1 Photoluminescence Spectra and Blinking

Figure 3.1 summarizes the absorption and PL spectra of $CuInS_2$/CdS NCs. Figure 3.1A shows absorption and PL spectra of an ensemble of $d = 3.8$ nm $CuInS_2$/CdS NCs suspended in toluene. X-ray diffraction measurements show these NCs possess the chalcopyrite structure (Supporting Information). The absorption spectrum of the ensemble shows a broad feature centered at ~ 2.2 eV as the first detectable absorbance, followed by rising absorbance to higher energy. The ensemble PL spectrum shows a broad (fwhm ~ 300 meV) band centered at ~ 1.65 eV. These ensemble data are very similar to those reported previously for various $CuInE_2$ NCs.[15–19,21,25]

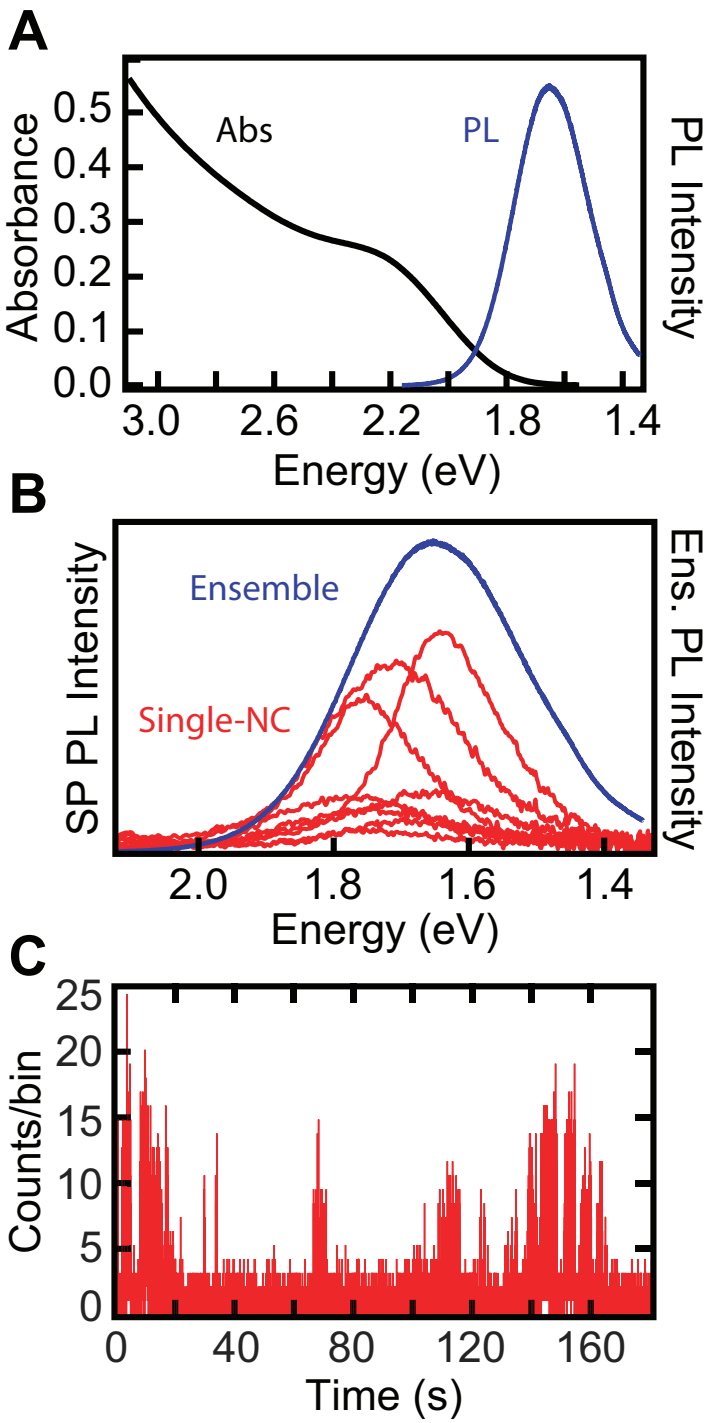

Figure 3.1: (A) Ensemble absorption and photoluminescence spectra of $d = 3.8$ nm $CuInS_2/CdS$ core/shell NCs in toluene, PL QY = 87%. (B) Single-particle and ensemble PL spectra of $CuInS_2/CdS$ NCs from the same sample. (C) A representative blinking trace from a $CuInS_2/CdS$ NC from this same batch (bin size of 7.5 ms). All data were collected at room temperature.

Figure 3.1B plots the PL spectra of several single nanocrystals from the same ensemble sample as used for Figure 3.1A, overlaid with the ensemble PL spectrum. The 140 ns PL decay of the $CuInS_2$ NCs requires working at relatively low excitation rates to avoid multiple excitation events. The PL QY appears to drop substantially upon film preparation, making acquisition of these single-NC PL spectra challenging, and optimization of the nanocrystal preparation conditions was necessary to achieve reasonable photon counts at the single-particle level (see Methods and Supporting Information). The single-NC spectra in Figure 3.1B each show a fairly broad PL band, but the fwhm of this band is not the same for all NCs. Individual fwhm values range from 190 meV up to 270 meV, with no apparent correlation between the PL peak energy and its fwhm (see Supporting Information). These single-NC fwhm values are all narrower than the ensemble fwhm (300 meV, Figure 3.1A), indicating some amount of ensemble inhomogeneous broadening, but they are also quite broad in comparison to single-NC excitonic luminescence in II-VI, IV-VI, or related NCs, where room-temperature bandwidths of $\sim$ 50 meV are typical.[35–38] Overall, these single-NC data illustrate the existence of an effective PL broadening mechanism in individual $CuInS_2$ NCs. The single-NC PL bandshapes observed here are consistent with the proposal of exciton self-trapping in $CuInS_2$ NCs,[15] in which photogenerated holes localize around a single or small groups of lattice Cu^+ ions, stabilized by strong electron-phonon coupling. Rather than displaying band-like excitonic emission like in II-VI or III-V NCs, $CuInS_2$ NCs thus more closely resemble high-copper analogs of dilutely Cu^+-doped II-VI and III-V NCs.[15,16] In the Cu^+-doped NCs, single-particle PL bandshapes are broadened by Franck-Condon progressions reflecting vibronic displacement along a combination of lattice contraction and Jahn-Teller distortion coordinates centered at the copper.[39] These distortions are induced by photoexcitation when the copper oxidation state is formally increased from Cu(I) to Cu(II) upon hole localization.[39] Similar lattice distortions are proposed for $CuInS_2$ NCs, although the narrower single-NC PL bandwidths of the $CuInS_2$/CdS NCs compared to Cu^+:CdSe NCs containing

single copper dopants[30] (fwhm of 235 ± 40 vs 325 meV, respectively) imply shallower hole trapping in the former. These data alone do not eliminate other trap-based PL mechanisms. Figure 3.1C plots a representative PL time trace for one of the single NCs from Figure 3.1B. PL blinking is readily observed. Blinking data for a total of 88 NCs were analyzed following the Bayesian detection and change-point analysis method outlined by Riley, *et al.*[40] The results of this analysis are discussed below.

3.3.2 Delayed Photoluminescence

Figure 3.2A presents room-temperature PL decay data measured from the same ensemble of $CuInS_2/CdS$ nanocrystals used for Figure 3.1. The main figure shows a semi-log plot of the first 30 μs of PL decay data following photoexcitation. The inset shows a log-log plot of the same PL decay, now over 7 orders of magnitude in time. Two clearly separable time regimes are observed in these plots: (*i*) the first ca. microsecond following photoexcitation, in which the majority of the PL decays, and (*ii*) the following period spanning from a few microseconds to over 160 ms (Figure 3.2A, inset), in which persistent low-level delayed luminescence is observed. The first regime is dominated by "prompt" PL decay with a time constant of $\tau \approx 140$ ns. In contrast, the delayed PL decays non-exponentially, showing broadly distributed kinetics. From these data, we estimate a steady-state ratio of delayed to total luminescence intensities of only $I_{\text{Delayed}}/[I_{\text{Delayed}} + I_{\text{Prompt}}](\text{steady state}) \approx 5\text{x}10^{-3}$. The ratio of delayed to total PL intensities measured *after* the excitation pulse is terminated is much greater. Delayed PL intensities are difficult to determine accurately in the time regime where the prompt PL is dominant. We therefore report a lower limit for this ratio determined by only counting photons emitted at times longer than 10x τ as delayed PL, where τ is the prompt PL lifetime (140 ns). From this conservative approach, the ratio of delayed to total PL occurring during the PL decay after termination of the excitation pulse is $I_{\text{Delayed}}/[I_{\text{Delayed}} + I_{\text{Prompt}}](\text{decay}) \geq 10^{-1}$. This ratio indicates that the steady-state population of NCs able to eventually emit a delayed

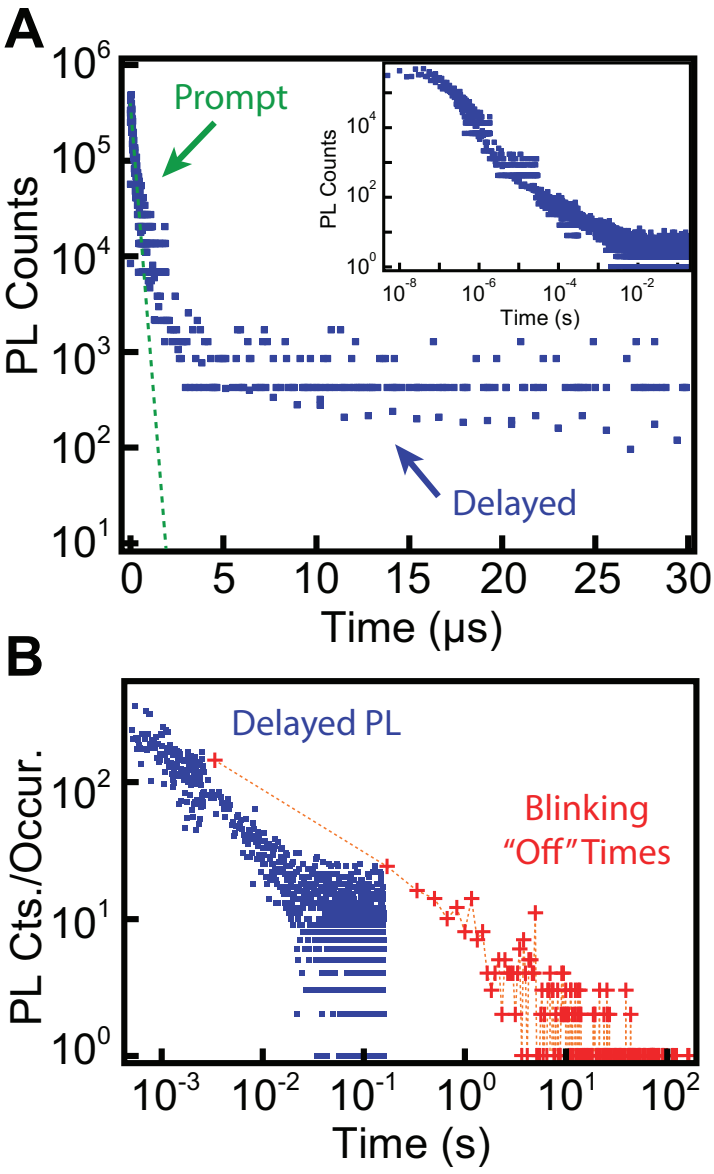

Figure 3.2: (A) Semi-log plot of PL intensity decay for the same $CuInS_2/CdS$ NCs from Figure 3.1, showing two distinct time regimes. Prompt luminescence is observed that decays approximately exponentially with a a time constant of $\tau \sim 140$ ns (green dashed curve). Delayed PL is also observed, decaying with distributed kinetics. (Inset) Double-log plot of the same PL decay data, now showing over 7 orders of magnitude in time. Plots were obtained by stitching together multiple time windows with time bins ranging from 5 ns to 10 μs. (B) Delayed PL of $CuInS_2/CdS$ NCs (blue squares) and histogram of blinking "off" statistics (red crosses). The blinking data were binned at 1.6 ms for determination of "off" statistics by a Bayesian detection method.[40] The dashed line is a guide to the eye. All data were collected at room temperature.

photon is quite large, even though the delayed luminescence does not constitute a large fraction of the emission measured under the steady-state excitation conditions used here.

Figure 3.2B presents the non-emissive ("off") blinking statistics collected on many single nanocrystals from the same ensemble as used for the delayed luminescence shown in Figure 3.2A. The red crosses in Figure 3.2B plot the "off" times for data binned to 1.6 ms and histogrammed with 1000 bins. For comparison, the long-time portion of the delayed PL data from Figure 3.2A (inset) is also reproduced in Figure 3.2B. The quantitative intensity scaling for the two experiments is arbitrary because they were performed using different optical systems. Nevertheless, the comparison in Figure 3.2B illustrates that both the blinking and delayed PL data exhibit similar distributed kinetics that extend over many orders of magnitude in time, and moreover experimentally demonstrates overlapping timescales of the blinking "off" dynamics and the delayed PL decay dynamics. These striking similarities support the hypothesis that these two phenomena are linked mechanistically.[30,32–34]

3.3.3 Photoluminescence Excitation Power Dependence

A key difference between the experimental conditions used for the single-NC blinking and ensemble delayed luminescence measurements shown in Figure 3.2B is the NC excitation rate. Single-NC PL measurements generally require excitation rates that are several orders of magnitude greater than those typically used for ensemble PL measurements. For example, the delayed PL data of Figure 3.2B were collected with an average excitation rate of 33 s^{-1}, whereas the blinking data of Figure 3.2B were collected with an averate excitation rate of $1.7x10^5$ s^{-1} (see Methods). An investigation of the ensemble PL excitation power dependence would therefore be informative. Figure 3.3 summarizes the excitation power dependence of the prompt and delayed PL intensities for the same $CuInS_2$ NCs used in Figures 3.1 and 3.2. As illustrated in Figure 3.3A, NCs were excited using square-wave pulses, allowing collection of prompt

and delayed PL during the "pulse on" and "pulse off" durations of the same experiment, respectively. As discussed above, when the excitation pulse is on, the steady-state PL intensity is dominated by the prompt PL, allowing the prompt PL power dependence to be measured directly at steady state. Following termination of the excitation pulse, the total PL intensity decays with the kinetics shown in Figure 3.2A. The relative power dependence of the delayed PL was measured by integrating from 10 – 500 μs following the end of the excitation pulse at various excitation powers. The excitation power during the "pulse on" period was tuned to generate average NC excitation rates ranging from $k_{exc} = 5$ to 80,000 s^{-1}. The lowest excitation rates in this range represent those typical of our ensemble PL measurements, and the highest excitation rates are very similar to those used in our single-NC measurements.

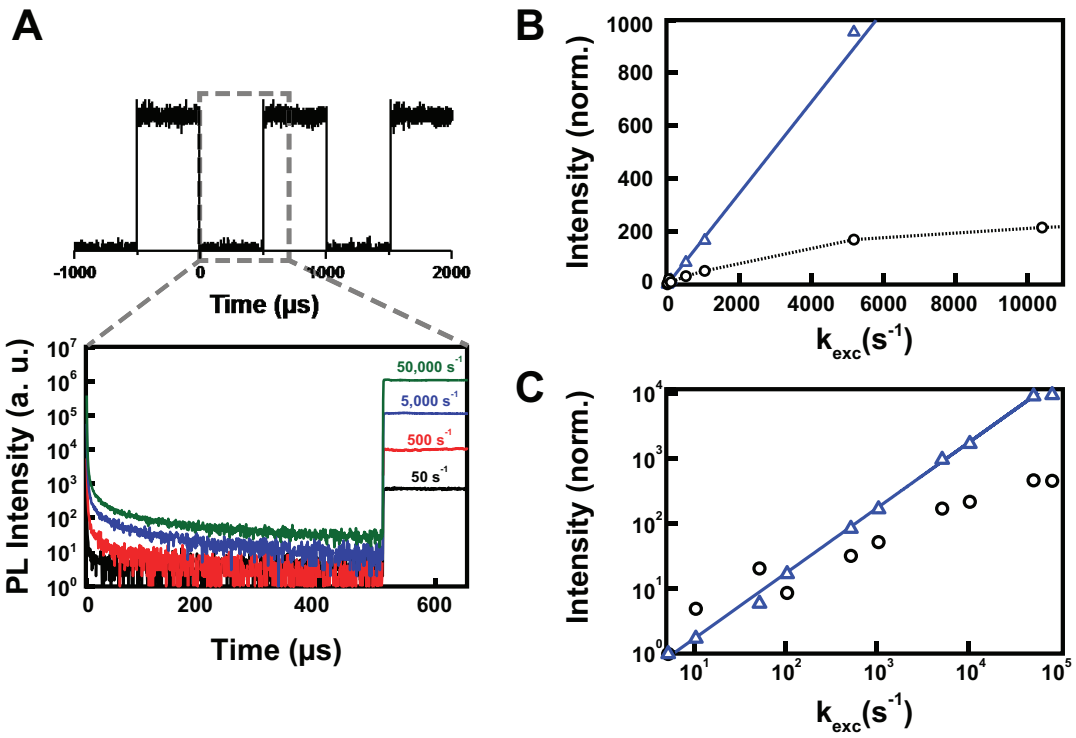

Figure 3.3: Photoluminescence power dependence measured for the same $CuInS_2/CdS$ NCs used for Figures 3.1 and 3.2. (A) Top: Excitation pulses transmitted through the sample and measured on a silicon photodiode. The dashed gray box illustrates the time within the pulse train for which PL data were collected. Bottom: PL decay traces measured at 750 nm for selected excitation powers (corresponding to the indicated values of k_{exc}), showing a complete "pulse off" period and the beginning of the next "pulse on" period. (B) Plot of the delayed PL intensity measured during a "pulse off" period (black circles) and the prompt PL intensity measured during a "pulse on" period (blue triangles) versus the excitation rate constant (k_{exc}), normalized at $k_{\text{exc}} = 5$ s^{-1}. The delayed PL intensities were obtained by integrating from 10 – 500 μs after termination of the excitation pulse. The prompt PL intensities were obtained by integrating during the "pulse on" period. The solid blue line represents a linear fit of the prompt PL intensities with the y-intercept fixed to the origin. The dashed line is a guide to the eye. (C) Double-log plot of the full power-dependence data set (some of which is shown in B), demonstrating linear power dependence of the prompt PL over the entire power range. All data were collected at room temperature.

Figure 3.3B plots the prompt and delayed PL intensities versus excitation power obtained from these measurements, normalized in the low-power limit, *i.e.*, where $I_{\text{Delayed}}/[I_{\text{Delayed}} + I_{\text{Prompt}}]$(steady state) $\sim 10^{-3}$. The prompt PL intensity increases linearly with increasing excitation rate over the entire range explored here. The shorter ($\sim$ 140 ns) lifetime of the prompt PL allows the $CuInS_2$ NCs to cycle between ground and luminescent excited states without saturating, even at the high excitation rates of our single-NC PL measurements. In contrast, the delayed PL intensity saturates quickly with increasing excitation rate, showing sub-linear power dependence starting even in the low-power regime ($k_{\text{exc}} \sim 5 - 500$ s^{-1}). Sub-linearity of the delayed PL vs excitation rate implies that recovery following photoexcitation takes longer than the time between two successive excitation events. The sub-linear delayed-luminescence power dependence evolves over several orders of magnitudes of excitation rates. Figure 3.3C plots the full excitation power range in a log-log representation, which highlights the observation that the delayed PL intensity does not fully saturate but instead continues to grow with increasing excitation powers in all power regimes. This continued evolution is a manifestation of distributed relaxation kinetics for the metastable charge-separated state responsible for delayed PL, with delayed luminescence involving the longest-lived metastable states saturating at the lowest excitation powers. Figure 3.3C shows that the delayed PL is reduced by $\sim 10^2$ relative to linearity at the highest excitation powers. $I_{\text{Delayed}}/[I_{\text{Delayed}} + I_{\text{Prompt}}]$(steady state) is therefore only $\sim 10^{-5}$ at $k_{\text{exc}} = 10^5$ s^{-1}, which is close to the excitation rate used in our single-NC blinking measurements. These power-dependence measurements thus predict that formation of the metastable state responsible for delayed luminescence darkens the NC PL by a factor of $\sim 10^5$ in the single-NC measurements of Figure 3.1, *i.e.*, NCs in the metastable state are "off". This PL excitation-power dependence is consistent with the proposed link between delayed luminescence and PL blinking. Figure 3.4 summarizes the proposed relationship between delayed luminescence and PL blinking. In the "on" state, NC photoexcitation is followed by

radiative recombination to regenerate the NC ground state. For delayed PL, one such photoexcitation event is followed by carrier trapping to generate a metastable charge-separated state. Slow spontaneous de-trapping from this metastable state reforms the emissive NC excited state and generates delayed luminescence. The long lifetime of the metastable charge-separated state allows subsequent photoexcitation of the same nanocrystal to generate a multiply excited NC. A multiply excited NC is more likely to undergo rapid non-radiative decay, *e.g.*, *via* Auger or Shockley-Read-Hall-type recombination mechanisms,[41–44] rendering it non-emissive. In other words, the metastable charge-separated state responsible for delayed PL is an "off" state. Based on our recent studies of Cu^{+}-doped CdSe NCs,[30] we propose that the trapped carrier in the metastable charge-separated state of $CuInS_2$ NCs is an electron, but this mechanistic scheme would be equally viable in the case of a trapped hole. Similarly, for convenience, one generic Auger recombination process is illustrated in Figure 3.4, but other nonradiative processes are not excluded. Because of this rapid non-radiative decay, the NC PL remains "off" until these charges recombine, at which point a delayed photon is emitted. For this reason, the delayed PL dynamics are associated specifically with the NC PL blinking "off" dynamics, as illustrated in Figure 3.4. Because very similar results are observed for undoped NCs, this general relationship is expected to also apply to excitonic emitters or doped NCs such as Cu^{+}:CdSe.

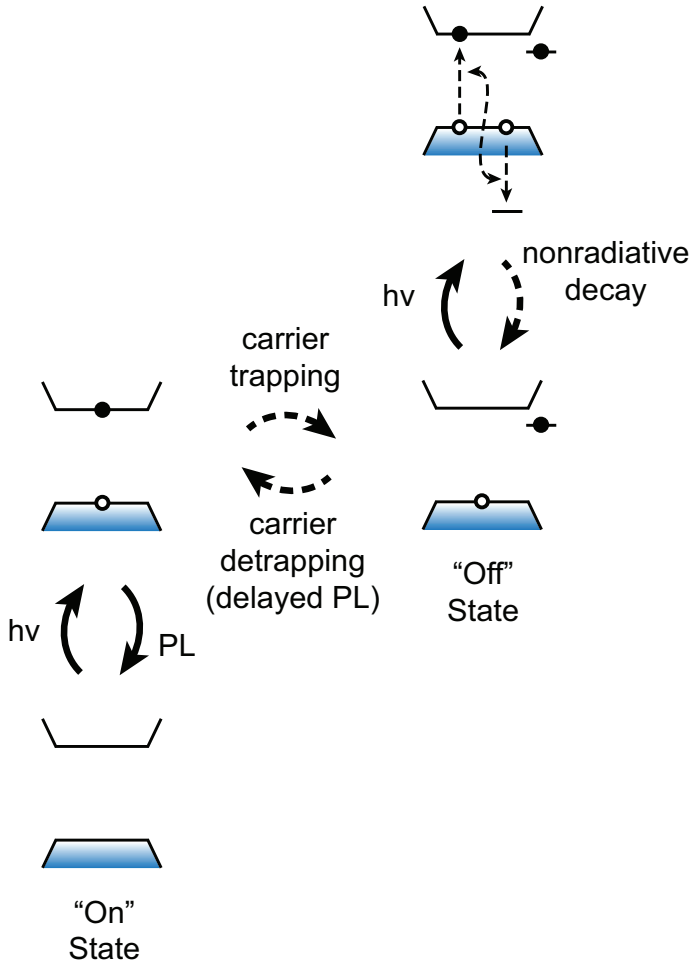

Figure 3.4: Generalized scheme illustrating the proposed mechanistic link between PL blinking and delayed luminescence in colloidal semiconductor NCs. The dashed arrows denote nonradiative processes and the solid arrows denote radiative processes. Various processes could possibly contribute to nonradiative decay in the photoexcited "off" state, but for the purposes of illustration here, only one generic Auger recombination process is depicted.

3.4 Summary

In summary, single-nanocrystal PL spectra are reported that demonstrate broadened PL bandshapes in individual $CuInS_2$ NCs. These bandshapes are consistent with strong electron-phonon coupling in the emissive excited state of these NCs. In addition to spectral information, single-NC measurements demonstrate luminescence blinking in individual $CuInS_2$ NCs. Ensemble measurements reveal long-lived delayed luminescence from the same NCs. A comparison is made between these single-NC blinking statistics and the decay dynamics of this delayed luminescence. The strong similarity between the data from these two measurements supports the hypothesis that the "off" state of the blinking phenomenon is identical to the metastable charge-separated state of the delayed luminescence phenomenon. Excitation power-dependence measurements provide additional support for a link between delayed luminescence and blinking by showing saturation of the delayed PL at the high excitation rates used for the blinking measurements, which at the single-NC level corresponds to the NC being "off" for multiple excitation events. A general scheme is presented that illustrates the relationship between these two phenomena in $CuInS_2$ and related colloidal semiconductor NCs.

3.5 Methods

3.5.1 Synthesis of $CuInS_2$/CdS Nanocrystals

Indium acetate, copper (I) iodide, cadmium nitrate tetrahydrate, myristic acid, sulfur powder, 1-dodecanethiol, and 1-octadecene were purchased from Sigma Aldrich; n-trioctylphosphine was purchased from Strem; sodium hydroxide was purchased from JT Baker. All reagents were used without further purification. $CuInS_2$/CdS nanocrystals were synthesized by a method adapted from the literature.[18] Briefly, a mixture of indium acetate (0.292 g, 1 mmol), copper iodide (0.190 g, 1 mmol), and dodecanethiol (5 mL) in a 50 mL three-neck round-bottom flask was degassed with three pump-purge

cycles at room temperature. The reaction was then heated to 110 °C under nitrogen and held for 10 min until the solution turned transparent and pale yellow. The reaction was then heated to 230 °C. The solution turned dark orange at $\sim$ 220 °C, and was very dark red by 230 °C. The reaction was held for 10 min at 230 °C, after which the vessel was cooled rapidly to $<$ 60 °C. For CdS shelling, cadmium myristate was prepared by dripping 5 mL of a 0.2 M solution of cadmium nitrate in anhydrous methanol into 30 mL of a 0.1 M solution of myristic acid and sodium hydroxide (0.113 g) in anhydrous methanol. The resulting white precipitate was collected and dried. A shell precursor solution was prepared by heating and sonicating cadmium myristate (0.272 g), sulfur (0.013 g), 1-octadecene (4 mL), and n-trioctylphosphine (0.4 mL) under a nitrogen atmosphere to form a uniform white dispersion. A portion of the crude reaction solution (1.0 mL) was added to 1-octadecene (4.0 mL) in a clean 50 mL three-neck round-bottom flask. The cores were degassed with three pump-purge cycles using nitrogen at room temperature and were then heated to 210 °C. The shell precursor solution was injected into the reaction at 0.2 mL/min. After addition of the precursor solution, the reaction was cooled gradually to $<$ 60 °C. Oleic acid (1 mL) and toluene (1 mL) were then added, and the mixture was stirred for 10 min. The resulting $CuInS_2$/CdS core/shell nanocrystals were purified with several cycles of precipitation with ethanol and centrifugation followed by resuspension in toluene. Samples were characterized by UV-Vis absorption spectroscopy, transmission electron microscopy (see Supporting Information), ensemble photoluminescence, and fluorescence microscopy.

3.5.2 Photoluminescence

Nanocrystals suspended in toluene were excited using a 405 nm diode laser. Photoluminescence was collected perpendicular to the excitation field. A long-pass filter was used to reject any scattered excitation photons, and a monochromator equipped with a LN_2 cooled CCD was used for detection.

3.5.3 Delayed Luminescence

Samples were prepared by sandwiching drop-coated films of nanocrystals between quartz disks. Samples were excited using a 405 nm diode laser at a power density of $\sim$ 80 mW/cm^2 ($k_{\text{exc}} \sim 33$ s^{-1}) modulated with a pulse waveform output from a function generator. Excitation pulse durations were 50 ms and cycle periods were varied from 55 to 250 ms depending on the time window of interest. PL decay traces were measured at 750 nm using a monochromator equipped with a PMT. Decay traces were collected over multiple time windows from 10 μs to 160 ms. The PMT signal was processed using a multichannel analyzer and collected with a custom LabView program.

3.5.4 Luminescence Excitation Power Dependence

Samples were prepared by sandwiching drop-coated films of nanocrystals between quartz disks. A brass foil with a 230-μm pinhole was mounted on the outsides of the disks, and the samples were placed under vacuum. Excitation was performed through the pinhole to ensure a uniform excitation density. Approximately 60% of the laser Gaussian beam profile (measured by the knife edge technique) was used for excitation. Laser powers were measured prior to the sample and calibrated to account for the $\sim$ 60% beam transmission. Samples were excited using a 405 nm diode laser with power densities ranging from 12 mW/cm^2 to 190 W/cm^2, corresponding to per-nanocrystal excitation rates of $k_{\text{exc}} = 5 - 80{,}000$ s^{-1}. Laser excitation was modulated with a square waveform output from a function generator, with a 1 kHz duty cycle. Emission was measured at 750 nm using a monochromator equipped with a PMT. The PMT signal was processed using a multichannel analyzer and collected using a custom LabView program. Spectra were collected under the same excitation conditions using the same monochromator and a LN_2 cooled CCD.

3.5.5 Single-Particle Luminescence

Extensive optimization of the conditions for single particle measurements was necessary to minimize the apparent decrease in PL QY of the $CuInS_2$/CdS NCs upon deposition onto the substate. This optimization process included many attempts to embed NCs in various polymers, and finally resulted in the elimination of polymer and addition of decanethiol upon dilution to (presumably) provide a suitable ligand environment for the NCs at the very small concentrations required for single-particle measurements. $CuInS_2$/CdS nanocrystals ($\sim$ 100 μM) were diluted by a factor of 200 into a solution of 9 parts toluene to 1 part dodecanethiol and then sonicated. The resulting solutions were then diluted in chloroform by a factor of 20,000 to give a final dilution factor of 400,000. The solutions were then spin coated onto cleaned zinc titania glass cover slips at 2000 rpm. The samples were mounted on an xy-piezoelectric nano-positioning stage (PI, P-545.2R7) in an inverted confocal microscope (Nikon, TE2000U). Single-particle experiments were performed under flowing N_2. Photoexcitation was accomplished using a 470 nm pulsed picosecond diode laser (PicoQuant, PDL 800-B with LDH-P-C-405B laser head) with a pulse width of 63 ps (full-width at half-maximum), repetition rate of 5 MHz, and an average power of 90 nW (measured at the focal point of the objective). Assuming a diffraction-limited focal point, this excitation power gives an upper bound photon absorption cross section of 0.037 photons per pulse, corresponding to an excitation rate of $1.7\text{x}10^5$ s^{-1}. A 562 nm dichroic long-pass mirror directed the excitation field to the back of a 100x oil-immersion objective (1.4 NA) where it was focused through the glass coverslip to a diffraction-limited spot. Luminescence was collected in an epi-geometry, passed through the 562 nm dichroic long-pass mirror and then passed through a second long-pass filter to reject scatter from the photoexcitation field. Luminescence was then split by a 50/50 beam splitter, with the transmitted and reflected fields focused onto two separate avalanche photodiode detectors (APD) with 50 μm active areas providing con-

focal resolution. Observation of single-step photobleaching events, diffraction-limited spot sizes, and a dependence of emission spots per area on nanocrystal concentration confirm measurement of single nanocrystals. Microscope and collection-electronics were controlled using a custom LabView program. Luminescence spectra of single $CuInS_2$/CdS nanocrystals were measured on the same spin coated films used for the luminescence blinking studies and using the same microscope. The luminescence was focused onto a 100 μm pinhole to achieve confocal resolution and then delivered to a monochromator equipped with a LN_2 cooled CCD. Spectra were collected with 300 sec exposures, 5 MHz rep rate, and 90 nW average excitation power.

3.6 Supporting Information

The supporting information includes TEM, XRD, additional power dependence measurements, and additional single particle data. This material is available free of charge *via* the Internet at http://pubs.acs.org.

Transmission Electron Microscopy

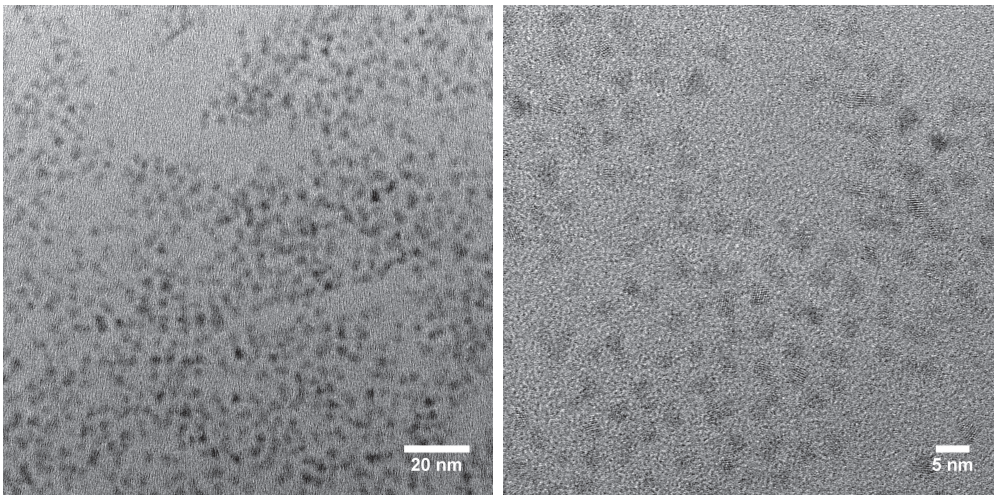

Figure 3.5: TEM images of the $CuInS_2/CdS$ nanocrystals used in this study. The diameters of 100 nanocrystals were measured, yielding a mean diameter of 3.8 ± 0.4 nm.

X-ray Diffraction

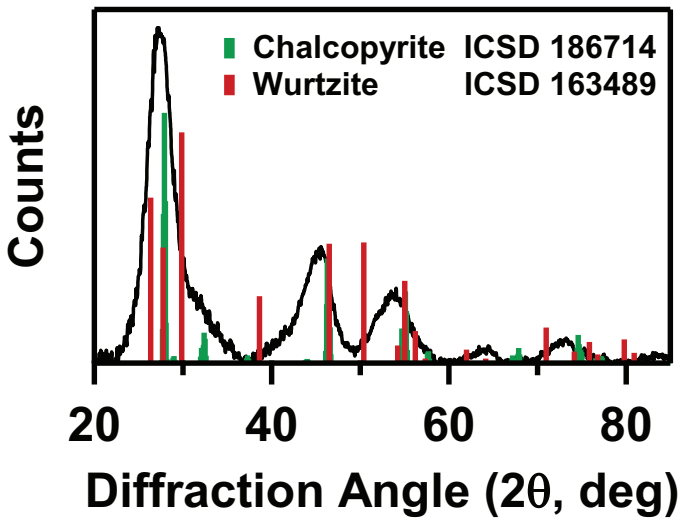

Figure 3.6: XRD data for the CuInS2/CdS nanocrystals used in this study, showing the chalcopyrite phase.

Single-Particle Peak Energy and Bandwidths

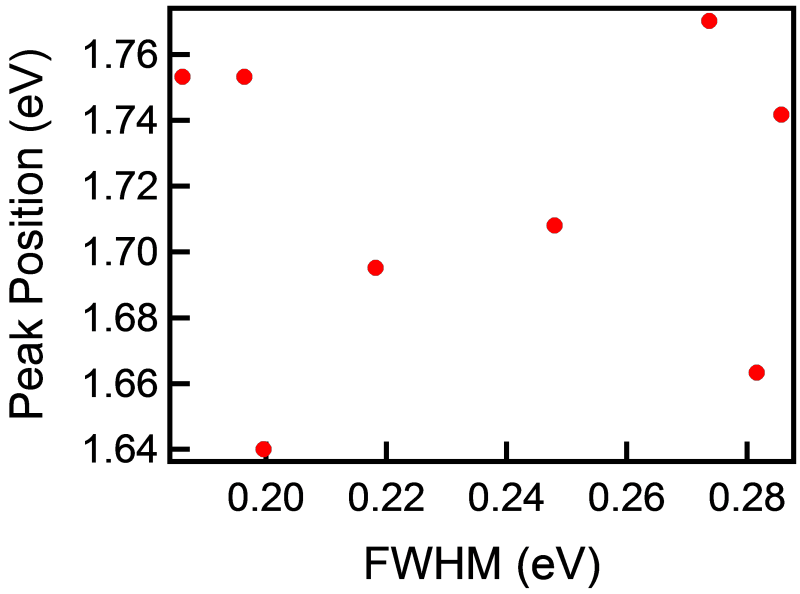

Figure 3.7: No correlation is seen between single-particle band widths and peak energies.

Single Particle PL Background Spectrum

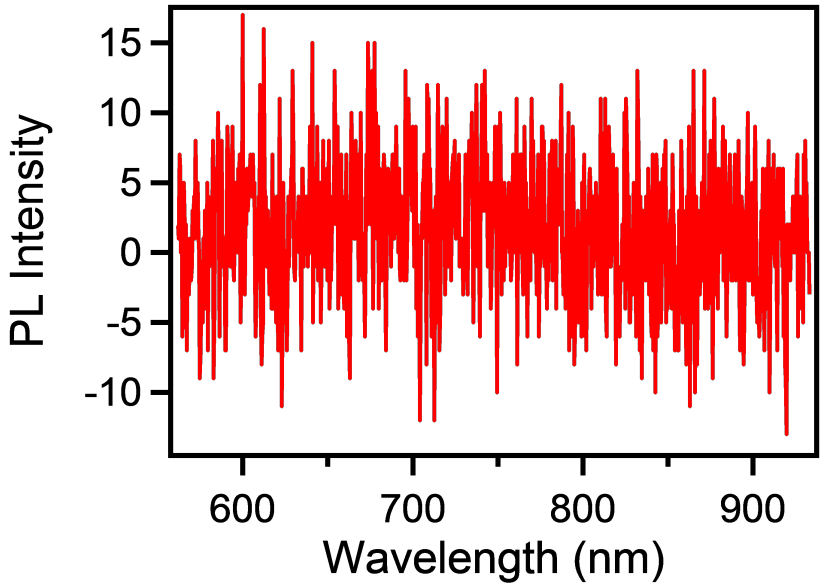

Figure 3.8: Background spectrum of cleaned zinc titania cover slip collected under laser illumination. The measurement was performed under the same experimental conditions as all of the single-particle measurements reported in the main text. Dark counts were subtracted from the above spectrum. Additional control experiments were performed by measuring under laser illumination zinc titania cover slip spin-coated with chloroform and zinc titania cover slip spin-coated with the ligand dilution. No signal is observed in the spectral region of interest (560 - 950 nm). Ligand emission occurs at shorter wavelengths (below 500 nm) and was blocked with a 562 nm long-pass filter.

Power-dependent Photoluminescence Spectra

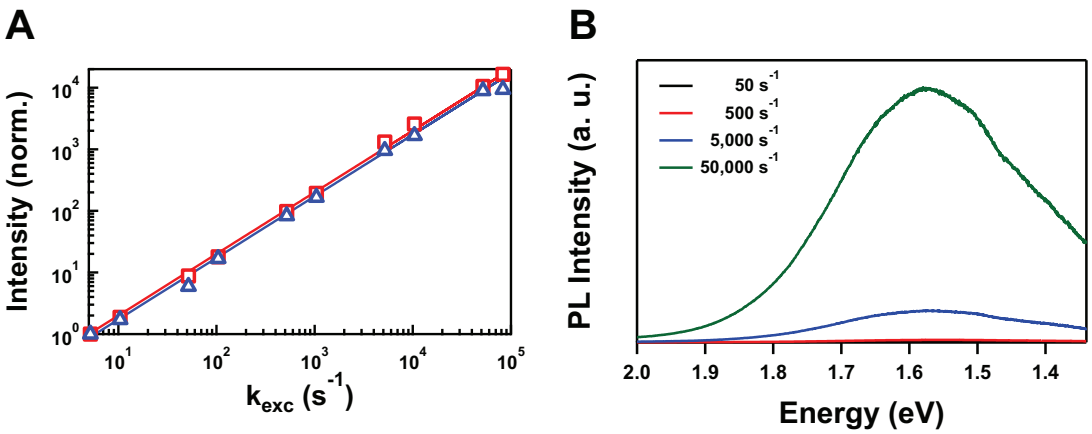

Figure 3.9: (A) Power-dependence of ensemble spectra (red squares) overlaid with prompt PL intensity data (blue triangles) shown previously in Figure 3.3 of the manuscript. The power-dependent PL agrees well with the prompt decay data collected in the square wave excitation experiment. (B) Sampling of the power-dependent spectra shown in A.

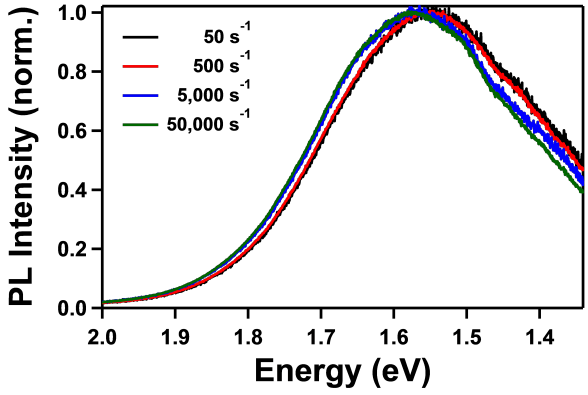

Figure 3.10: Normalized power-dependent photoluminescence peak shapes remain consistent with increasing excitation power. A small blue shift in the spectra is observed with increasing power—likely due to NC size inhomogeneity.

"On" Blinking Statistics

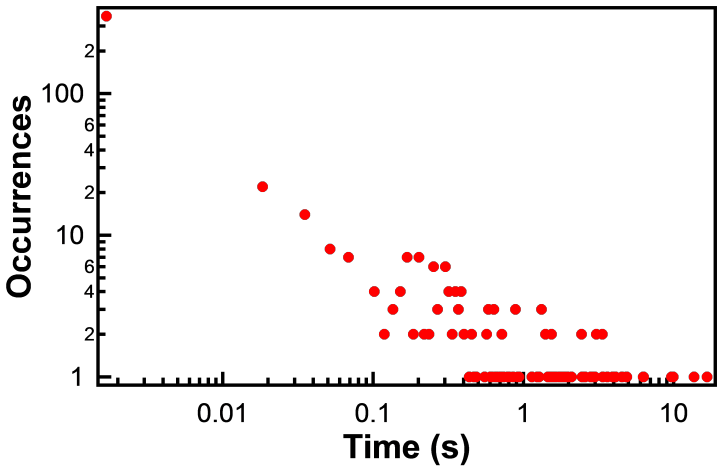

Figure 3.11: Histogram of blinking "on" statistics. Blinking data were binned at 1.6 ms for determination of "on" statistics by a Bayesian detection method.[40] All data were collected at room temperature. Histogram has 1000 bins.

Effect of Time Binning and Histogramming

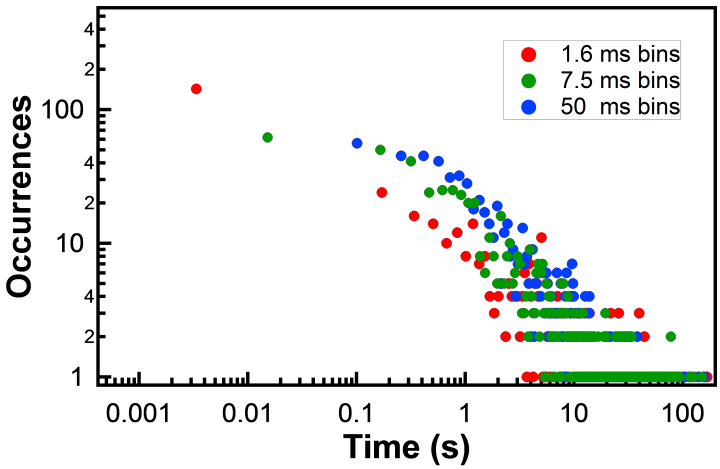

Figure 3.12: "Off" blinking events with different time bins of 1.6 ms (red), 7.5 ms (green), and 50 ms (blue). The effect of increasing the time bins reduces the number of short events observed and shifts the data towards longer time events. The curvature of short time events is also affected, long time events remain largely unaffected. These effects have previously been noted in the literature, please refer to SI reference[45]

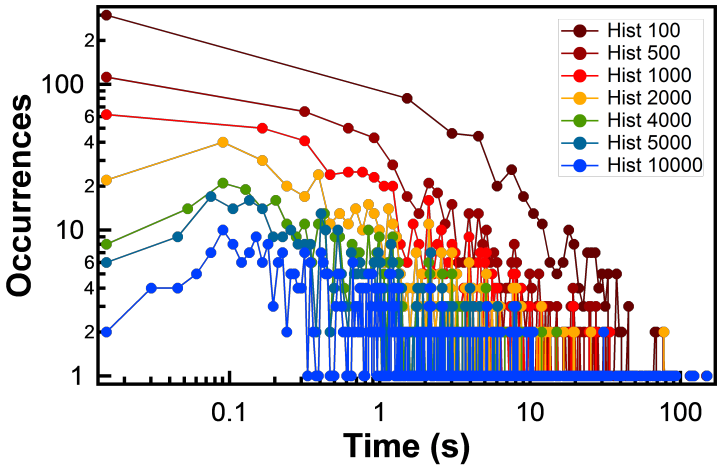

Figure 3.13: Changing the number of points used in histogramming the blinking data changes the curvature by changing the point of greatest occurrences. This effect does not change the length of time events just where they are observed on the histogram.

3.7 Author Information

Corresponding Authors

**E-mail: gamelin@chem.washington.edu.*

**E-mail: pjreid@uw.edu.*

Notes

The authors declare no competing financial interest.

3.8 Acknowledgments

Financial support from the National Science Foundation (CHE-1404674 to P.J.R. and DMR-1505901 to D.R.G.) is gratefully acknowledged. K.E.K. thanks the Department of Energy for support through an Energy Efficiency and Renewable Energy (EERE) postdoctoral research award. A. M. acknowledges the support of an Early Postdoc Mobility Fellowship from the Swiss National Science Foundation.

3.9 Bibliography

[1] Aldakov, D., Lefrançois, A., & Reiss, P. (2013). *Journal of Materials Chemistry C* **1**, 3756–3776.

[2] Leach, A.D. & Macdonald, J.E. (2016). *The Journal of Physical Chemistry Letters* **7**, 572–583.

[3] Yu, K., Ng, P., Ouyang, J., Zaman, M.B., Abulrob, A., Baral, T.N., Fatehi, D., Jakubek, Z.J., Kingston, D., & Wu, X.a. (2013). *ACS Applied Materials & Interfaces* **5**, 2870–2880.

[4] Chen, C.W., Wu, D.Y., Chan, Y.C., Lin, C.C., Chung, P.H., Hsiao, M., & Liu, R.S. (2015). *The Journal of Physical Chemistry C* **119**, 2852–2860.

[5] Chuang, P.H., Lin, C.C., & Liu, R.S. (2014). *ACS Applied Materials & Interfaces* **6**, 15379–15387.

[6] Knowles, K.E., Kilburn, T.B., Alzate, D.G., McDowall, S., & Gamelin, D.R. (2015). *Chemical Communications* **51**, 9129–9132.

[7] Li, C., Chen, W., Wu, D., Quan, D., Zhou, Z., Hao, J., Qin, J., Li, Y., He, Z., & Wang, K. (2015). *Scientific Reports* **5**, 17777.

[8] Meinardi, F., McDaniel, H., Carulli, F., Colombo, A., Velizhanin, K.A., Makarov, N.S., Simonutti, R., Klimov, V.I., & Brovelli, S. (2015). *Nature Nanotechnology* **10**, 878–885.

[9] Binsma, J.J.M., Giling, L.J., & Bloem, J. (1982). *Journal of Luminescence* **27**, 35–53.

[10] Tell, B., Shay, J.L., & Kasper, H.M. (1971). *Physical Review B* **4**, 2463–2471.

[11] Yakushev, M.V., Mudryi, A.V., Victorov, I.V., Krustok, J., & Mellikov, E. (2006). *Applied Physics Letters* **88**, 011922.

[12] Yoshino, K., Ikari, T., Shirakata, S., Miyake, H., & Hiramatsu, K. (2001). *Applied Physics Letters* **78**, 742–744.

[13] Ueng, H.Y. & Hwang, H.L. (1989). *The Journal of Physical Chemistry of Solids* **50**, 1297–1305.

[14] Ueng, H.Y. & Hwang, H.L. (1990). *The Journal of Physical Chemistry of Solids* **51**, 1–10.

[15] Knowles, K.E., Nelson, H.D., Kilburn, T.B., & Gamelin, D.R. (2015). *Journal of the American Chemical Society* **137**, 13138–13147.

[16] Knowles, K.E., Hartstein, K.H., Kilburn, T.B., Marchioro, A., Nelson, H.D., Whitham, P.J., & Gamelin, D.R. (2016). *Chemical Reviews*, Article ASAP.

[17] Castro, S.L., Bailey, S.G., Raffaelle, R.P., Banger, K.K., & Hepp, A.F. (2004). *The Journal of Physical Chemistry B* **108**, 12429–12435.

[18] Li, L., Pandey, A., Werder, D.J., Khanal, B.P., Pietryga, J.M., & Klimov, V.I. (2011). *Journal of the American Chemical Society* **133**, 1176–1179.

[19] Nakamura, H., Kato, W., Uehara, M., Nose, K., Omata, T., Otsuka-Yao-Matsuo, S., Miyazaki, M., & Maeda, H. (2006). *Chemistry of Materials* **18**, 3330–3335.

[20] Omata, T., Tani, Y., Kobayashi, S., & Otsuka-Yao-Matsuo, S. (2012). *Thin Solid Films* **520**, 3829–3834.

[21] Xie, R., Rutherford, M., & Peng, X. (2009). *Journal of the American Chemical Society* **131**, 5691–5697.

[22] Zhong, H., Zhou, Y., Ye, M., He, Y., Ye, J., He, C., Yang, C., & Li, Y. (2008). *Chemistry of Materials* **20**, 6434–6443.

[23] Chen, B., Zhong, H., Zhang, W., Tan, Z., Li, Y., Yu, C., Zhai, T., Bando, Y., Yang, S., & Zou, B. (2012). *Advanced Functional Materials* **22**, 2081–2088.

[24] Liu, W., Zhang, Y., Zhao, J., Feng, Y., Wang, D., Zhang, T., Gao, W., Chu, H., Yin, J., & Wang, Y.a. (2015). *Journal of Luminescence* **162**, 191–196.

[25] Sun, J., Ikezawa, M., Wang, X., Jing, P., Li, H., Zhao, J., & Masumoto, Y. (2015). *Physical Chemistry Chemical Physics* **17**, 11981–11989.

[26] Rice, W.D., McDaniel, H., Klimov, V.I., & Crooker, S.A. (2014). *The Journal of Physical Chemistry Letters* **5**, 4105–4109.

[27] Shabaev, A., Mehl, M.J., & Efros, A.L. (2015). *Physical Review B* **92**, 035431.

[28] Brovelli, S., Galland, C., Viswanatha, R., & Klimov, V.I. (2012). *Nano Letters* **12**, 4372–4379.

[29] Ishizumi, A., White, C.W., & Kanemitsu, Y. (2004). *Applied Physics Letters* **84**, 2397–2399.

[30] Whitham, P.J., Knowles, K.E., Reid, P.J., & Gamelin, D.R. (2015). *Nano Letters* **15**, 4045–4051.

[31] Zhang, A., Dong, C., Li, L., Yin, J., Liu, H., Huang, X., & Ren, J. (2015). *Scientific Reports* **5**, 15227.

[32] Rabouw, F.T., Kamp, M., van Dijk-Moes, R.J., Gamelin, D.R., Koenderink, A.F., Meijerink, A., & Vanmaekelbergh, D. (2015). *Nano Letters* **15**, 7718–7725.

[33] Rabouw, F.T., van der Bok, J.C., Spinicelli, P., Mahler, B., Nasilowski, M., Pedetti, S., Dubertret, B., & Vanmaekelbergh, D. (2016). *Nano Letters* **16**, 2047–2053.

[34] Sher, P.H., Smith, J.M., Dalgarno, P.A., Warburton, R.J., Chen, X., Dobson, P.J., Daniels, S.M., Pickett, N.L., & O'Brien, P. (2008). *Applied Physics Letters* **92**, 101111.

[35] Mekis, I., Talapin, D.V., Kornowski, A., Haase, M., & Weller, H. (2003). *The Journal of Physical Chemistry B* **107**, 7454–7462.

[36] Reiss, P., Bleuse, J., & Pron, A. (2002). *Nano Letters* **2**, 781–784.

[37] Yu, W.W., Qu, L., Guo, W., & Peng, X. (2003). *Chemistry of Materials* **15**, 2854–2860.

[38] We note that the sum of the single particle spectra shown in Figure 1B is slightly blue-shifted from the ensemble spectrum, which could reflect the relatively small statistical sampling of Figure 1B, or may be an effect of the very different excitation rates used in the ensemble and single-NC measurements; The ensemble PL spectrum shows a small blueshift with increasing excitation rate (see Supporting Information).

[39] Nelson, H.D., Li, X., & Gamelin, D.R. (2016). *The Journal of Physical Chemistry C* **120**, 5714–5723.

[40] Riley, E.A., Hess, C.M., Whitham, P.J., & Reid, P.J. (2012). *Journal of Chemical Physics* **136**, 184508.

[41] Galland, C., Ghosh, Y., Steinbruck, A., Sykora, M., Hollingsworth, J.A., Klimov, V.I., & Htoon, H. (2011). *Nature* **479**, 203–207.

[42] Rinehart, J.D., Schimpf, A.M., Weaver, A.L., Cohn, A.W., & Gamelin, D.R. (2013). *Journal of the American Chemical Society* **135**, 18782–18785.

[43] Rosen, S., Schwartz, O., & Oron, D. (2010). *Physical Review Letters* **104**, 157404.

[44] Zhao, J., Nair, G., Fisher, B.R., & Bawendi, M.G. (2010). *Physical Review Letters* **104**, 157403.

[45] Kuno, M., Fromm, D.P., Hamann, H.F., Gallagher, A., & Nesbitt, D.J. (2001). *Journal of Chemical Physics* **115**, 1028–1040.

Chapter 4

TUNNELING IN THE DELAYED LUMINESCENCE OF COLLOIDAL CDSE, CU^{+}-DOPED CDSE, AND $CUINS_2$ SEMICONDUCTOR NANOCRYSTALS, AND RELATIONSHIP TO BLINKING

Arianna Marchioro‡, Patrick J. Whitham‡, Kathryn E. Knowles, Troy B. Kilburn, Philip J. Reid, and Daniel R. Gamelin*

Department of Chemistry, University of Washington, Seattle, WA 98195-1700, USA

‡ These authors contributed equally

This chapter has been submitted to the Journal of Physical Chemistry C.

4.1 Abstract

The photoluminescence decay dynamics of colloidal CdSe, Cu^+:CdSe, and $CuInS_2$ nanocrystals have been examined as a function of temperature and magnetic field. All three materials show photoluminescence decay on timescales significantly longer than the intrinsic lifetimes of their luminescent excited states, *i.e.*, delayed luminescence. Gated photoluminescence and magneto-luminescence measurements demonstrate that the prompt and delayed luminescence signals both come from the same emissive excited state in each given sample, confirming that the delayed luminescence involves formation of a metastable trapped excited state followed by detrapping to reform the emissive excited state. Surprisingly, the delayed luminescence decay kinetics are remarkably similar for all three samples. Luminescence decay data spanning over 8 decades in time and 6 decades in intensity show a clear deviation from power-law dynamics in each case. Moreover, for all three materials, the delayed luminescence decay dynamics are nearly independent of temperature between 20 K and room temperature, showing thermal activation of nonradiative decay at elevated temperatures in some cases. This result reveals that tunneling is the dominant mechanism for detrapping from the metastable state in all three of these materials up to room temperature. A kinetic model invoking a log-normal distribution of tunneling rates reproduces the full range of delayed luminescence decay dynamics well. These findings are discussed in relation to photoluminescence blinking, with which delayed luminescence appears closely associated.

4.2 Introduction

Delayed luminescence, or the observation of photoluminescence (PL) on timescales much longer than the material's intrinsic luminescence lifetime, has recently been recognized as an integral and possibly universal feature of colloidal semiconductor nanocrystal photophysics, appearing in various CdSe,[1–5] Cu^+-doped CdSe (Cu^+:CdSe),[3] and ternary copper indium sulfide ($CuInS_2$)[6] nanocrystals (NCs) with and without additional shell layers. Delayed luminescence has been attributed to formation of a metastable charge-separated state, in which one or both of the charge carriers are trapped, followed by slow detrapping to repopulate the intrinsic emissive state. Delayed luminescence decay does not follow simple exponential kinetics, but instead displays distributed kinetics spanning from sub-microsecond to seconds.[1–6] Although the delayed luminescence amplitude is small relative to the total PL amplitude during photoexcitation ($\sim 1\%$),[6] delayed luminescence can account for a large fraction of the total emission after an excitation pulse (from $\sim 10\%$[4,6] to as much as $\sim 50\%$[5]). This reversible charge-carrier trapping is thus not necessarily detrimental to quantum yield (QY). Indeed, QYs as large as 50% have been recorded in CdSe platelets for which $\sim 50\%$ of the emission following a short laser pulse comes from delayed luminescence.[5] Photoexcitation power-dependence measurements show facile saturation of the delayed luminescence intensities,[6] indicating that photoexcitation of NCs already in the metastable state is followed by efficient nonradiative decay. Elongation of the prompt PL decay time through either hole localization[3] or NC photonic cavity effects[4] increases the fraction of PL coming from delayed luminescence, indicating that the metastable state is populated directly from the relaxed emissive state. Comparisons between Cu^+-doped and undoped CdSe NCs suggest specifically that electron trapping and detrapping are the rate-determining steps in the delayed luminescence of these NCs.[3]

A link between delayed luminescence and single-NC PL blinking was proposed as

early as 2008,[1] when similar power-law coefficients were observed in sub-microsecond delayed luminescence and blinking data collected on a timescale of seconds for the same CdSe-based single NCs.[1] The "on"- and "off"-state statistics from PL blinking measurements generally display distributed kinetics and are most commonly fitted using power-law functions.[7,8] Several models have been proposed to explain these dynamics,[9–14] most of which invoke charge-carrier localization in the "off" state.[15,16] To account for the large integrated delayed luminescence intensities following short excitation pulses, it has been proposed that blinking "on" periods are characterized by rapid carrier trapping and detrapping that cycles faster than successive photoexcitation events.[4]

Although many complementary approaches have been applied to characterize NC blinking, delayed luminescence has not yet been thoroughly explored, and a great deal remains to be learned from such measurements. Here, we describe new observations pertaining to the delayed luminescence of CdSe, Cu^{+}:CdSe, and $CuInS_2$ NCs. Despite their very different chemical compositions and spectroscopic characteristics, all three materials show remarkably similar delayed luminescence, but with key differences related to their different electronic structures. In particular, all three samples show delayed luminescence dynamics that are nearly temperature independent from 20 K to room temperature. This observation indicates a similar tunneling mechanism for detrapping from the metastable states of all three materials. Moreover, in all three materials, the delayed luminescence decay clearly deviates from power-law behavior. Quantitative analysis shows that these dynamics can be accounted for by a Gaussian distribution of tunnel barriers, which results in a log-normal distribution in tunneling (detrapping) rates. The implications of these results and analysis are discussed and related to existing blinking models.

4.3 Experimental

4.3.1 Synthesis of $CuInS_2$ nanocrystals

$CuInS_2$ NCs were synthesized by a method adapted from the literature.[17] A mixture of indium acetate (0.292 g, 1 mmol), copper iodide (0.190 g, 1 mmol), and dodecanethiol (5 mL) in a 50 mL three-neck round-bottom flask was degassed with three pump-purge cycles using nitrogen at room temperature. The reaction mixture was heated to 110 °C under nitrogen and held for 10 minutes until the solution turned optically clear and pale yellow. The reaction mixture was then heated to 230 °C. The solution turned dark orange at $\sim$ 220 °C, and was very dark red by 230 °C. The reaction was held for 10 min. at 230 °C, after which the vessel was cooled rapidly to <60 °C. NCs were purified with several cycles of precipitation with ethanol and centrifugation followed by resuspension in toluene.

4.3.2 Synthesis of CdSe and Cu^+:CdSe nanocrystals

CdSe and Cu^+:CdSe NCs were synthesized by a heat-up method adapted from recent literature.[18] Briefly, $Cd(oleate)_2$ was synthesized *via* adaptation of a cadmium myristate synthesis in the above reference. Sodium hydroxide (0.40 g, 10 mmol) and oleic acid (2.82 g, 10 mmol) were dissolved in 100 mL of methanol at 60 °C in ambient atmosphere. Cadmium nitrate tetrahydrate (6.16 g, 20 mmol) was dissolved in 16 mL methanol and added dropwise to the sodium oleate solution at 60 °C in ambient atmosphere under vigorous stirring. After addition, the reaction mixture was stored in a freezer overnight and then washed with cold methanol $\sim$ 5 times. The solid product was collected by filtration and dried under vacuum. The final product is a white powder, and is stored under inert atmosphere to slow oxidation. 0.2025 g of the prepared $Cd(oleate)_2$ solution, 0.0334 g SeO_2 and 13.22 g octadecene were degassed at 55 °C with three pump-purge cycles with N_2 in a separate reaction flask. The reaction mixture was heated to 235 °C under N_2. The mixture turned

pale yellow at $\sim$ 180 °C and was pale orange when the reaction reached 235 °C, after 5 min the solution was dark red. At this point a 5 mL aliquot of CdSe NCs was removed. In a separate reaction flask, 0.019 g CuCl and 2.40 g octadecene were degassed by bubbling with N_2. Then 0.1 mL tri-octylphosphine was added to the CuCl mixture. 1.5 mL of the CuCl mixture was injected into the CdSe NC reaction flask. 1 mL aliquots were removed from the Cu^+:CdSe NC reaction at 10, 20, and 25 min following injection. The remaining 1.5 mL of CuCl solution was injected after the 25 min aliquot, additional aliquots were taken 10 and 15 min after the second injection. Finally, 20 min after the second injection, the remaining reaction mixture was cooled to room temperature. The CdSe aliquot and final Cu^+:CdSe reaction mixtures were then purified by precipitation with ethanol and centrifugation, the NC pellet was washed with acetone followed by NC resuspension in toluene.

4.3.3 General Characterization

Samples were characterized by UV-Vis absorption spectroscopy, transmission electron microscopy, and ensemble photoluminescence. Cu^+:CdSe was also characterized by inductively coupled plasma atomic emission spectroscopy (ICP-AES), and $CuInS_2$ by powder X-ray diffraction (see Supporting Information (SI)).

4.3.4 Spectroscopic Characterization

Absorption spectra of CdSe, Cu^+:CdSe, and $CuInS_2$ NCs suspended in toluene were measured using a Varian Cary 5000 spectrometer. Solution-phase PL spectra were measured using an Ocean Optics USB-2000+ spectrometer with 405 nm excitation. PL spectra were corrected for the instrument response unless otherwise indicated.

4.3.5 Temperature-dependent PL Lifetimes

Temperature-dependent PL decay measurements were performed on drop-coated films of NCs sandwiched between quartz disks and mounted in a closed-cycle helium cryostat. Samples were excited using a 405 nm diode laser modulated with a square pulse waveform output from a function generator (SRS, DS345). Excitation pulse durations were kept constant at 50 ms and cycle periods were varied from 55 ms to 3.3 s depending on the time window of interest. PL decay traces were measured near the peak emission maximum for each sample. The PL was passed through a 420 nm long-pass filter and focused into a monochromator (0.5 m, 150 g/mm grating blazed at 500 nm, band pass of < 20 nm) equipped with a PMT. Decay traces were collected over multiple time windows from 10 μs to 2.6 s. The signal was processed using a multichannel scaler and collected with a custom LabView program. Temperatures were varied from 20 K to 295 K.

4.3.6 Magnetic Circularly Polarized Luminescence

For magnetic circularly polarized luminescence (MCPL) measurements, drop-coated films of NCs sandwiched between quartz disks were loaded into a superconducting magneto-optical cryostat with a variable-temperature sample compartment (Cryo-Industries SMC-1659 OVT). A 405 nm diode laser was used for photoexcitation at an incident angle of $\sim 20^{\circ}$ relative to the optical detection axis. Excitation was modulated at 500 Hz with the square wave output from a function generator. PL was collected along the magnetic field axis (Faraday geometry), passed through a liquid crystal variable retardation plate set to $\lambda/4$ at the emission maximum, followed by a linear polarizer used to separate left and right circularly polarized PL components. A 420 nm long-pass filter placed after the linear polarizer removed scattered excitation light before the PL was collected by an optical fiber and directed into a monochromator. Spectra were collected with a LN_2 cooled CCD. PL lifetimes were collected

with a PMT connected to a multichannel scaler. PL was measured at constant wavelengths, 760 nm for Cu^+:CdSe and 740 nm for $CuInS_2$, with bandwidths $\sim$ 10 nm. MCPL polarization ratios were calculated from the relative intensities of left and right circularly polarized PL at various applied magnetic field strengths, following the sign convention described in Piepho and Schatz.[19]

4.3.7 Time-Resolved PL Spectra

Temperature-dependent PL measurements were performed on films of NCs sandwiched between quartz plates. The films were measured in a flow cryostat cooled at liquid helium temperature. A 405 nm diode laser (2 mW, 4 mm spot) was used for photoexcitation at an incident angle of $\sim 90^\circ$ relative to the optical detection axis. Excitation was modulated at 100 Hz for Cu^+:CdSe and $CuInS_2$ NCs and at 5000 Hz for CdSe NCs, with a square pulse waveform output from a function generator (SRS, DS345). TRPL data containing both the ON and OFF pulse periods were recorded using a streak camera (Hamamatsu, C10627) combined with a monochromator and synchronized with the square-wave generator.

4.4 Results and Analysis

4.4.1 Absorption and Photoluminescence Spectra

Figure 4.1 summarizes the absorption and PL spectra of the colloidal CdSe, Cu^+:CdSe, and $CuInS_2$ NCs investigated here. Unless otherwise noted, these samples were used for all subsequent experiments, but very similar results are obtained for other samples of the same materials. Figure 4.1A shows absorption and PL spectra of CdSe NCs suspended in toluene. The first excitonic absorption feature is centered at 2.25 eV. A sharp excitonic PL band is observed centered at 2.19 eV, with a small and broad trap PL feature observable centered at $\sim$ 1.5 eV. The PL of the

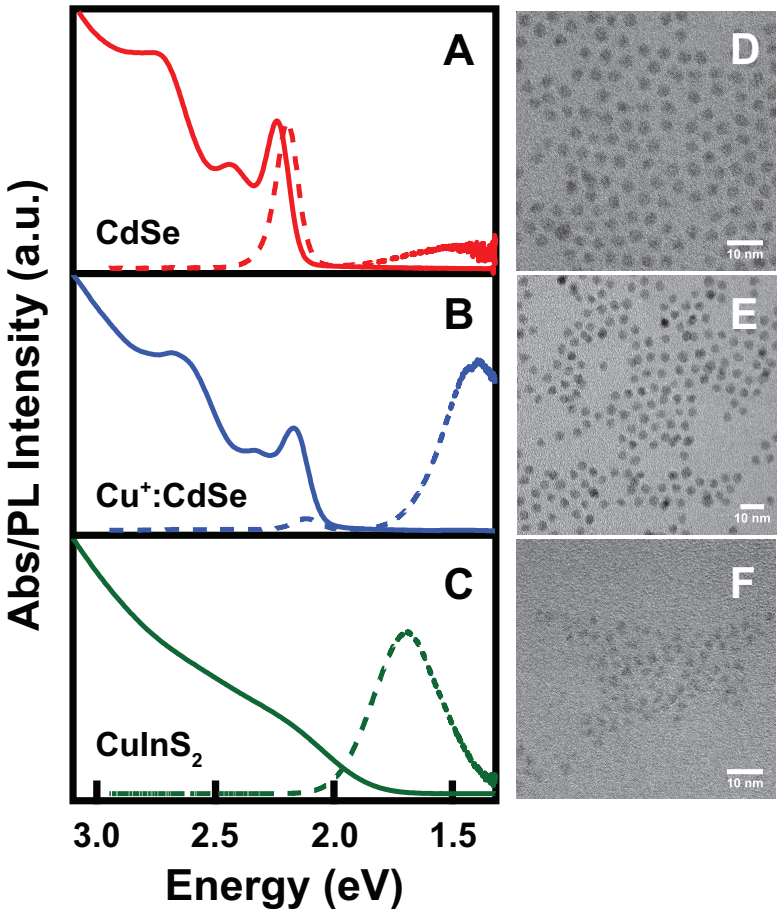

Figure 4.1: Room-temperature electronic absorption and photoluminescence spectra of (A) CdSe, (B) Cu^{+}:CdSe ($\sim$ 0.7 % copper), and (C) $CuInS_2$ NCs suspended in toluene. TEM images of these (D) CdSe, (E) Cu^{+}:CdSe, and (F) $CuInS_2$ NCs. The scale bars represent 10 nm. The diameters of 100 NCs were measured for each sample, yielding mean values of (D) 4.3 $\pm$ 0.4 nm, (E) 5.1 $\pm$ 0.5 nm, and (F) 3.9 $\pm$ 0.7 nm, respectively.

Cu^+:CdSe NCs shown in Figure 4.1B is dominated by a broad PL band centered at 1.38 eV associated with recombination of a delocalized conduction-band electron and a copper-localized hole.[20] A small amount of residual excitonic PL is observed at 2.12 eV, attributable to the presence of some undoped CdSe NCs within the NC ensemble. Figure 4.1C shows the absorption and PL spectra of $CuInS_2$ NCs. This PL spectrum consists of a broad band centered at 1.7 eV, commonly associated with recombination involving one or more deeply trapped carriers.[20] TEM images are provided for each sample, showing pseudo-spherical NCs in each case.

4.4.2 Luminescence Decay

Figure 4.2 plots 20 K PL decay traces for the same undoped CdSe, Cu^+:CdSe, and $CuInS_2$ NCs of Figure 4.1using a double-log representation. All three traces show distributed decay kinetics spanning many orders of magnitude in time. Two clearly separable time regimes can be identified. The first regime corresponds to prompt decay of the luminescent excited state and accounts for the majority of the luminescence amplitude. Fitting this prompt luminescence to a single exponential in each case yields lifetimes of *ca.* 40 ns (CdSe), 1 μs (Cu^+:CdSe), and 2 μs ($CuInS_2$). The second regime consists of PL decay that persists long after the prompt decay is complete. This component is referred to as delayed luminescence. The CdSe NCs exhibit substantially less delayed luminescence than displayed by either the Cu^+:CdSe or $CuInS_2$ NCs under otherwise essentially identical conditions. We interpret this difference as indicating that the shorter lifetime of the CdSe NC emitting state allows less time for trapping into the metastable state.[3] Surprisingly, all three materials show remarkably similar dispersed kinetics in their delayed luminescence extending over several orders of magnitude in time. In each case, these kinetics show a distinct deviation from power-law behavior, which would be linear in the double-log representation of Figure 4.2. Deviation of delayed luminescence decay from power-law dynamics has not been reported previously for any sample, but has important mechanistic implications.

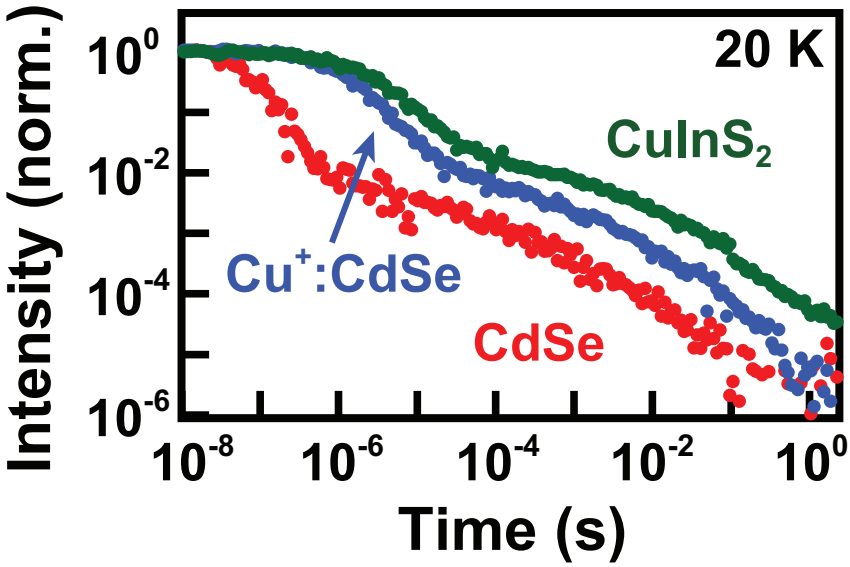

Figure 4.2: Double-log plot of 20 K PL intensity decay for $CuInS_2$, Cu^+:CdSe, and CdSe NCs, showing prompt and delayed luminescence regimes at short and long times, respectively. The CdSe NCs exhibit faster prompt decay and less delayed luminescence than either the $CuInS_2$ or Cu^+:CdSe NCs. The delayed luminescence for all three materials decays with remarkably similar dispersed kinetics extending over several orders of magnitude in time.

4.4.3 Prompt and Delayed Luminescence Spectra and Magneto-Luminescence

Figure 4.3 plots PL spectra of the Cu^+:CdSe and $CuInS_2$ NCs measured during photoexcitation (prompt luminescence) and integrated between 25 μs and 1.2 ms after the end of the excitation pulse (delayed luminescence), when all prompt luminescence has decayed. The delayed luminescence spectra are very similar to the prompt luminescence spectra, consistent with the hypothesis that the emitted photons come from the same excited state in both prompt and delayed time regimes. We note that both samples show a small (< 40 meV) red shift of the delayed luminescence relative to the prompt luminescence. Such a shift could conceivably be due to donor-acceptor pair recombination in the $CuInS_2$ NCs,[21,22] but this explanation is considered unlikely here because both samples in Figure 4.11 show essentially the same red shift even though the Cu^+:CdSe NCs decay *via* a free-to-bound ($ML_{CB}CT$) recombination mechanism.[20] Instead, this small redshift in both samples more likely arises from particle size inhomogeneity, in which smaller NCs show higher-energy emission, shorter prompt decay times,[23] and slightly less delayed luminescence (see below). Overall, these data support the interpretation that delayed luminescence involves slow detrapping to reform the intrinsic emissive excited state, rather than carrier recombination directly from the metastable state.

To test this interpretation in a more discriminating experiment, time-resolved magneto-PL measurements were performed. As reported previously,[24] Cu^+:CdSe and $CuInS_2$ NCs both display singlet-triplet excited-state exchange splittings, with the low-temperature luminescence originating from the lower-energy triplet state. Application of a magnetic field induces a Zeeman splitting of this triplet state, and at low temperatures the emission becomes partially circularly polarized. As the temperature is raised, the higher-energy singlet state is populated, but this singlet state is not split in a magnetic field and thus does not contribute to the magnetic circularly polarized photoluminescence (MCPL) signal in first order. Consequently, the prompt MCPL

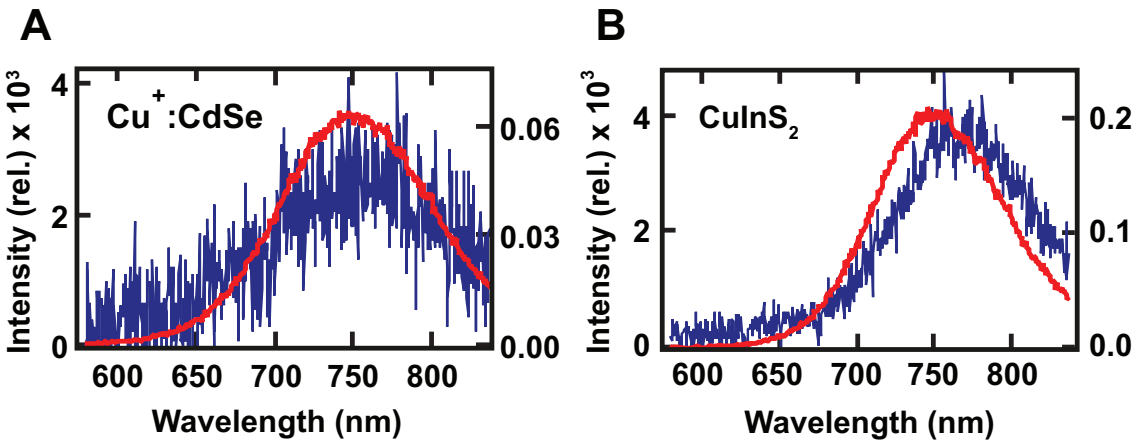

Figure 4.3: Prompt (red) and delayed (blue) photoluminescence spectra of (A) Cu^+:CdSe NCs and (B) $CuInS_2$ NCs, collected at 5 K. Spectra were not corrected for the instrument response. A constant baseline was subtracted from each delayed luminescence spectrum. The Cu^+:CdSe NCs are from a different synthetic batch but are spectroscopically nearly identical to those shown in Figures 4.10, 4.2, and 4.5 (see SI).

intensities of Cu^+:CdSe and $CuInS_2$ NCs both decrease with increasing temperature in a characteristic temperature range defined by their singlet-triplet splitting energies. Here, we show that the delayed luminescence from these two materials shows the same MCPL and temperature dependence as their prompt luminescence.

Figures 4.4A,B show MCPL spectra of Cu^+:CdSe and $CuInS_2$ NCs collected at 1.6 K and 6 T. The intensity of right (σ^+) circularly polarized luminescence has increased and that of left (σ^-) circularly polarized luminescence has decreased in response to the magnetic field. These MCPL signals are quantified using the polarization ratio ($\Delta I/I$), defined as shown in eq 4.1.

$$\frac{\Delta I}{I} = \frac{\sigma^- - \sigma^+}{\sigma^- + \sigma^+} \tag{4.1}$$

Figures 4.4C,D plot $\Delta I/I$ measured from 0 to 20 μs following the end of a photoexcitation pulse for the same Cu^+:CdSe and $CuInS_2$ NC samples, measured at 6 T and three different temperatures (1.6, 10, and 20 K). The full decay traces for σ^+ and σ^- polarized light are provided as Supporting Information. Similar behavior is observed for both samples. In accordance with our previous steady-state measurements,[24] the magnitude of $\Delta I/I$ is greatest at the lowest temperature and decreases with increasing temperature at all measurement times, with the same signs and similar values of $\Delta I/I$ observed in both the prompt and delayed luminescence regimes at each temperature. We note that for both samples, $\Delta I/I$ does change slightly during the full PL decay period. These changes are consistent with the small red-shift in PL energy, and are again attributed to NC inhomogeneity. Figures 4.4E,F summarize these data, plotting $\Delta I/I$ for the prompt and delayed luminescence components *vs* temperature for these two samples. Both prompt and delayed MCPL show very similar values of $\Delta I/I$ and identical trends with temperature, consistent with the delayed luminescence originating from the same electronic state that gives rise to the prompt luminescence in each sample. In particular, these results conclusively eliminate the possibility that delayed luminescence in either sample comes from

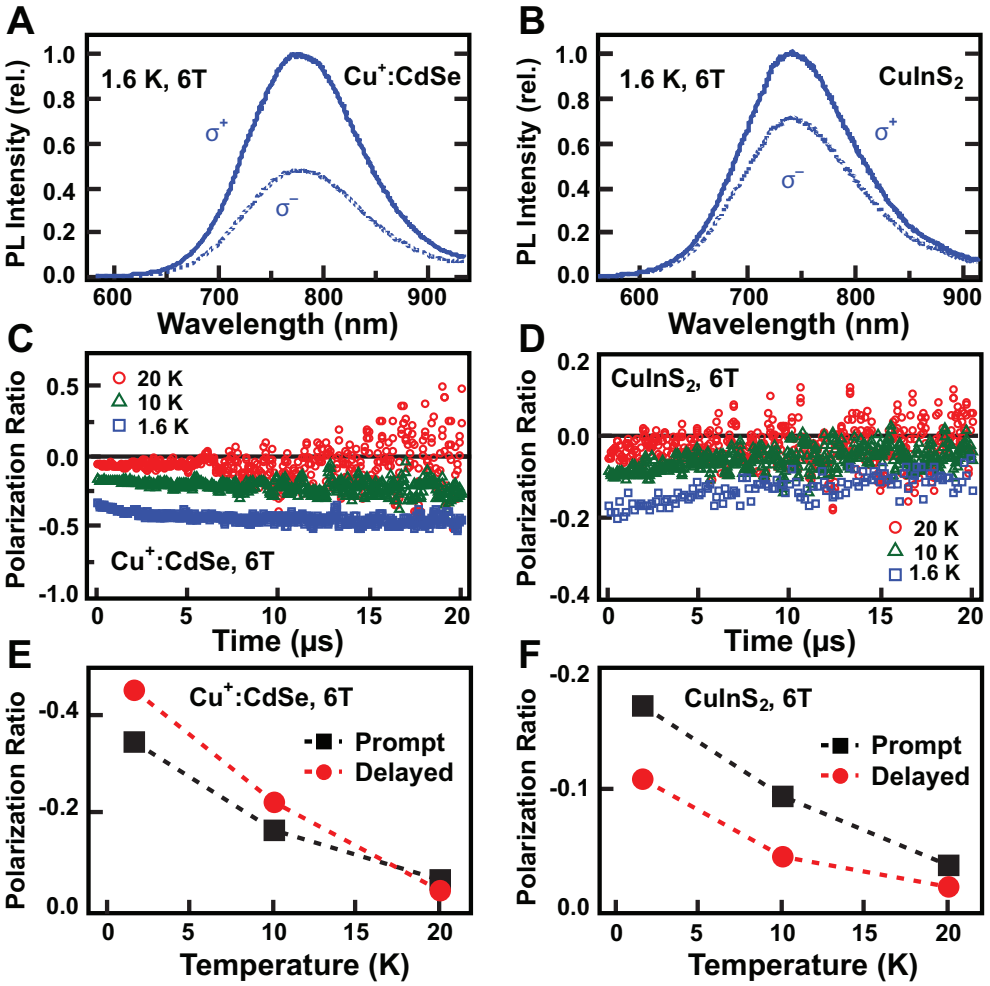

Figure 4.4: Magnetic circularly polarized photoluminescence (MCPL) spectra of (A) Cu^{+}:CdSe and (B) $CuInS_2$ NCs measured at 1.6 K, with an applied magnetic field of 6 T. Solid line: right circularly polarized, σ^{+}. Dashed line: left circularly polarized, σ^{-}. (C,D) MCPL polarization ratio ($\Delta I/I$) plotted *vs* luminescence decay time measured at 1.6 K (blue squares), 10 K (green triangles), and 20 K (red circles) for (C) Cu^{+}:CdSe and (D) $CuInS_2$ nanocrystals, all at 6 T. $\Delta I/I$ is measured at the prompt luminescence maximum. (E,F) $\Delta I/I$ plotted *vs* temperature for prompt (black) and delayed (red) luminescence. The delayed luminescence values represent $\Delta I/I$ averaged between 10 and 20 μs after the end of the excitation pulse, well after the decay of the prompt luminescence. The Cu^{+}:CdSe NCs are from the same sample as in Figure 4.3 (see SI).

donor-acceptor-pair recombination directly from the metastable charge-separated state: To achieve such long recombination times, this charge-separated state must have a substantially smaller electron-hole exchange coupling strength than the prompt emissive state, and hence should show substantially smaller MCPL and a significantly different MCPL temperature dependence from that observed in the prompt luminescence.

4.4.4 Temperature Dependence of Delayed Luminescence

Figure 4.5 summarizes the temperature dependence of the CdSe, Cu^+:CdSe, and $CuInS_2$ NC PL dynamics. Figures 4.5A-C plot PL decay curves for each sample, measured at various temperatures between 20 K and room temperature and from nanoseconds to seconds. The PL decay curves of the CdSe NCs (Figure 4.5A) are essentially temperature independent between 20 K and room temperature, showing only a small and gradual drop in both the prompt and delayed luminescence intensities with increasing temperature. The Cu^+:CdSe and $CuInS_2$ NCs show a stronger temperature dependence. With increasing temperature, the amplitude of the prompt luminescence of the Cu^+:CdSe NCs (Figure 4.5B) changes little but the delayed luminescence amplitude appears to decrease substantially, even though the long-time dynamics remain nearly parallel at all temperatures. This trend is even more pronounced in the data from the $CuInS_2$ NCs (Figure 4.5C). For this sample, the delayed luminescence intensity appears anomalously low at room temperature, attributed to the onset of a new thermally activated nonradiative decay channel.

The above description of these decay curves is quantified by analyzing I_{delayed}/I_0, which represents the ratio of the delayed PL intensity (I_{delayed}, measured 450 μs after termination of illumination) to the steady state PL intensity (I_0, measured under cw illumination). Because the delayed luminescence curves are nearly parallel, I_{delayed} is approximately proportional to the total delayed luminescence amplitude. Likewise, the small steady-state amplitude of the delayed luminescence means that I_0 is

very nearly equivalent to the prompt luminescence amplitude.[6] Figures 4.5D-F plot I_{delayed}/I_0 *vs* temperature for the CdSe, Cu^+:CdSe, and $CuInS_2$ NCs, respectively, all with absolute y-axis scaling. From these plots, it is evident that I_{delayed}/I_0 is an order of magnitude larger for the two copper-containing NCs than it is for the CdSe NCs. For the Cu^+:CdSe and $CuInS_2$ NCs, I_{delayed}/I_0 decreases with increasing temperature, whereas for the CdSe NCs I_{delayed}/I_0 shows a much smaller but more complicated temperature dependence. Specifically, the CdSe NC data are complicated by the presence of deep-trap luminescence (*e.g.*, Figure 4.10A). Both exciton and deep-trap delayed luminescence are observed from these CdSe NCs, but the trap luminescence carries much more relative intensity during delayed luminescence than under cw excitation (see SI), similar to data reported for CdSe and CdSe/CdS nanoplatelets.[5] These data demonstrate the existence of two qualitatively different types of trap states in CdSe NCs: (*i*) non-emissive metastable trap states that are essentially degenerate with the lowest excitonic states and that decay by detrapping to reform excitons, and (*ii*) deep trap states that can decay by emission of mid-gap photons. From comparison of CdSe and Cu^+:CdSe NCs, we have previously argued that the former involves reversible electron trapping.[3] The relative increase in CdSe NC mid-gap luminescence during delayed luminescence suggests that this deep trapping becomes more likely after the excited NC enters the metastable state, consistent with the emissive mid-gap trap state involving deep hole trapping. Understanding the relationship between this emissive mid-gap trap state and the non-emissive metastable state in CdSe and related NCs poses an interesting challenge for future studies that can perhaps be addressed *via* additional delayed luminescence measurements.

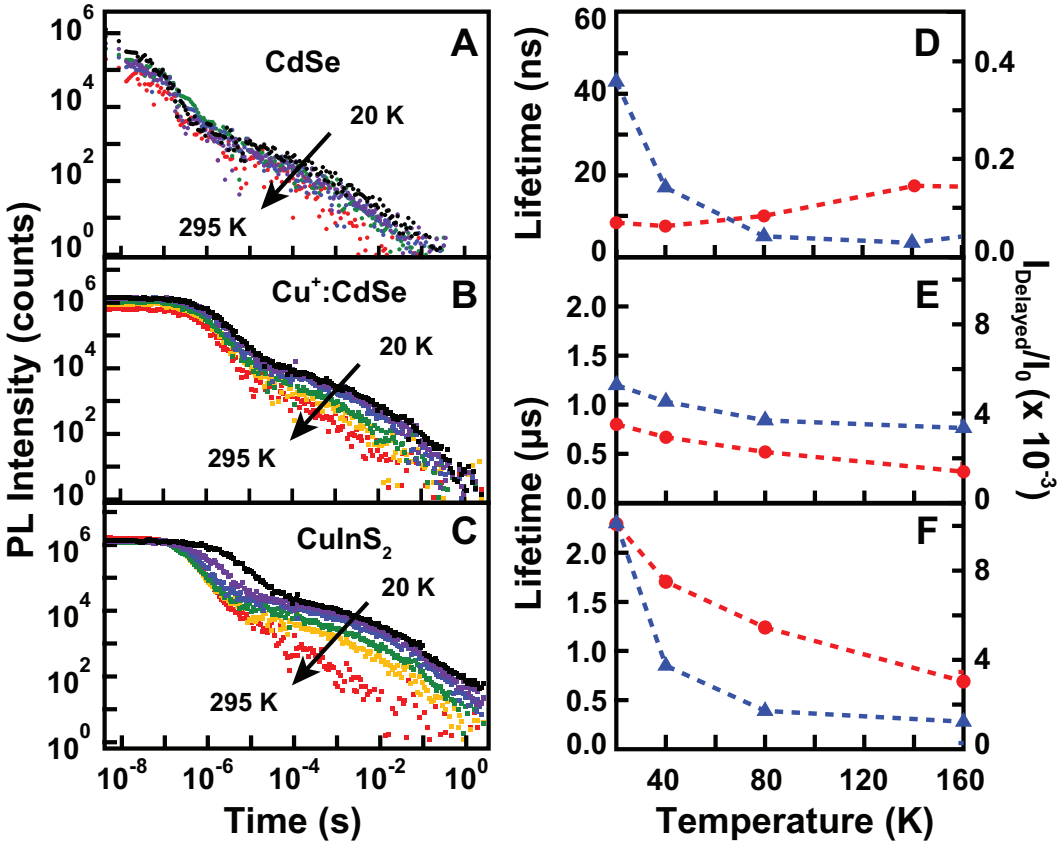

Figure 4.5: (A, B, C) Double-log plots of PL intensity decay for (A) CdSe, (B) Cu^+:CdSe NCs, and (C) $CuInS_2$ NCs collected from 20 to 295 K. Color code: black = 20 K, purple = 40 K, green = 80 K, blue = 140 K (CdSe) or 160 K (Cu^+:CdSe & $CuInS_2$), yellow = 200 K, red = 295 K. (D, E, F) Temperature dependence of prompt luminescence decay lifetimes from single-exponential fits (τ_{prompt}, blue triangles,) and the ratio of delayed to steady state luminescence intensities (I_{delayed}/I_0, red circles), where I_0 is the steady-state luminescence intensity measured during photoexcitation and I_{delayed} is the luminescence intensity measured 450 μs after termination of the photoexcitation. (D) CdSe NCs, (E) Cu^+:CdSe NCs, and (F) $CuInS_2$ NCs.

Figures 4.5D-F also plot the prompt luminescence lifetime (τ_{prompt}) *vs* temperature for the same three samples. The data for the Cu^+:CdSe and $CuInS_2$ NCs, which are not complicated by the competing deep-trap luminescence seen in the CdSe NCs, demonstrate a strong positive correlation between τ_{prompt} and I_{delayed}/I_0. The variations in I_{delayed}/I_0 are interpreted as reflecting variations in τ_{prompt} because the probability of populating the metastable state responsible for the delayed luminescence is proportional to the lifetime of the emissive excited state that feeds this metastable state. The smaller I_{delayed}/I_0 of the CdSe NCs is consistent with their shorter τ_{prompt}, bearing in mind the caveat of additional hole trapping discussed above.

4.4.5 Kinetic Model

Three important observations arise from inspection of the delayed luminescence dynamics (t $> \sim 10^{-4}$ s) shown in Figure 4.5: (*i*) The delayed luminescence decay is highly non-exponential, requiring a distribution of rate constants to account for these dynamics, (*ii*) log-log plots of the delayed luminescence decay data for all three samples show significant curvature, indicating that the underlying distributions of rate constants cannot be described by power-law expressions, as used to date,[1,4,5] and (*iii*) the dynamics of delayed luminescence are temperature independent, which implies that the rate-limiting detrapping step involves tunneling. Similar temperature-independent delayed luminescence has recently been reported for CdSe nanoplatelets over a shorter time window,[5] supporting the generality of this observation. Here, we demonstrate that all three of these key features can be accounted for simultaneously in a single kinetic model by invoking a log-normal distribution of tunneling rate constants.

The kinetic model used to describe the variable-temperature PL dynamics shown in Figure 4.5 combines prompt PL with a continuous distribution of tunneling rate

constants governing the delayed luminescence decay (eq 4.2).

$$I(t) = A_P \exp(-k_{\text{prompt}} t) + A_D \int_0^\infty p(a) \exp(-k_{\text{tunnel}}(a) \cdot t) da \tag{4.2}$$

The first term in eq 4.2describes the prompt luminescence decay and the second describes the delayed luminescence. The parameters A_P and A_D represent the amplitudes of prompt and delayed luminescence, respectively. $k_{\text{prompt}} = 1/\tau_{\text{prompt}}$ describes the prompt luminescence decay rate constant, as summarized in Figure 4.5. The tunneling rate constant, k_{tunnel}, depends exponentially on the tunneling barrier width a, as described by eq 4.3, where β is the tunneling decay constant.

$$k_{\text{tunnel}}(a) = k_0 \exp(-\beta a) \tag{4.3}$$

The term $p(a)$ in equation 4.2 represents the distribution of tunnel widths. Here we model $p(a)$ as a Gaussian distribution using eq 4.4.

$$p(a) = \frac{1}{\sigma\sqrt{2\pi}} \exp\left(\frac{-(a - \langle a \rangle)^2}{2\sigma^2}\right) \tag{4.4}$$

In equation 4.4, $\langle a \rangle$ is the average width tunnel width and σ is the standard deviation defining the Gaussian distribution. Equation (4.4) can be rewritten in terms of k_{tunnel} to give:

$$p(k_{\text{tunnel}}) = \frac{1}{\sigma\sqrt{2\pi}} \exp\left(\frac{-(\ln k_{\text{tunnel}} - \langle \ln k_{\text{tunnel}} \rangle)^2}{2(\beta\sigma)^2}\right) \tag{4.5}$$

Eq 4.5 illustrates that the tunneling rate constants emerging from a Gaussian distribution of tunnel barriers are log-normally distributed.

This model captures the key features of the experimental data remarkably well. Figure 6 plots the results of this model in comparison with the experimental data from the Cu^+:CdSe NCs. These data were chosen as representative of all three data sets in Figure 4.5 and are used here because they have better signal-to-noise ratios than the CdSe NC data and they show less nonradiative decay than the $CuInS_2$ NC data at room temperature. For modeling this data set, the prompt luminescence decay was fit at each temperature, and a single set of parameters was used

to describe the delayed luminescence at all temperatures, with the exception of A_D, which is temperature dependent as reflected in the data of Figure 4.5E (note that $A_D/(A_P + A_D) \propto I_{\text{delayed}}/I_0$). The good agreement between the simulated and experimental delayed luminescence data summarized in Figure 4.6 implies that the rate constants for delayed luminescence follow a temperature-independent log-normal distribution with an average value of $k_{\text{tunnel}} \approx 5\text{x}10^4$ s^{-1}. The full distribution in k_{tunnel} is derived from a $\sigma = 30\%$ standard deviation about the mean the tunnel barrier width, $\langle a \rangle$, with $\beta\langle a \rangle \gg 1$. Rate constants smaller than 10^3 s^{-1} account for $\sim 10\%$ of the delayed luminescence intensity. The prominence of such small rate constants accounts for the remarkable observation of PL even seconds after photoexcitation. The very similar delayed luminescence observed in all three data sets of Figure 4.5 indicates that the same log-normal distribution can be applied for all three NC samples investigated here, with different specific parameters to account for their different prompt luminescence dynamics and nonradiative decay at elevated temperatures.

We note that although this model can reproduce the salient features of the data very well, the simulated curves in Figure 6 do not represent optimized fits of the data. Given the number of unknown variables in the model, we are unable to identify a unique set of best-fit parameters by least-squares procedures. For this reason, we do not analyze the specific model parameters further. Instead, we highlight the general conclusions that can be drawn from this analysis, namely that a non-power-law distribution of tunneling rates is required to describe the delayed luminescence decay dynamics, and that the key features of this decay are reproduced well using a temperature-independent log-normal distribution of tunneling rates, as would arise from a tunneling process involving a Gaussian distribution of tunnel-barrier widths.

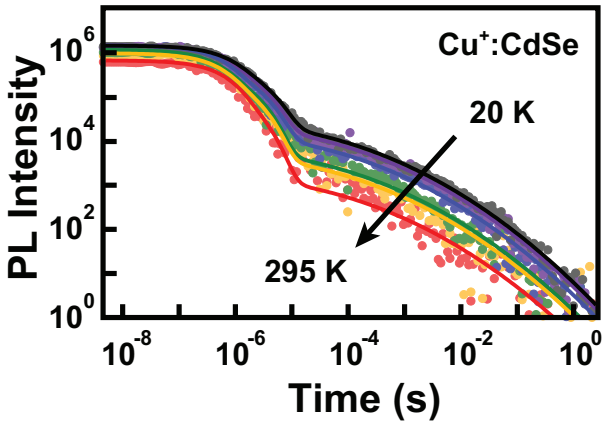

Figure 4.6: Simulated PL decay curves for Cu^+:CdSe NC data from Figure 4.5, calculated using eq 4.2. The first 160 μs of the prompt luminescence decay at each temperature was fitted to a sum of two exponentials, summarized by the average lifetime data shown in Figure 4.5E. The delayed luminescence was modeled as a tunneling process using $k_0 = 10^9$ s^{-1} and a Gaussian distribution in tunneling barrier widths defined by $\langle a \rangle = 1.0$ and $\sigma = 0.3$, with a tunnel decay constant of $\beta = 10$ (all given in reduced units). The same parameters were used for simulation of the delayed luminescence at all temperatures with the exception of A_D, which is temperature dependent. See main text and SI for additional details.

4.5 Discussion

The data presented here reveal surprisingly similar delayed luminescence phenomena in three qualitatively distinct types of colloidal semiconductor NCs, CdSe, Cu^{+}:CdSe, and $CuInS_2$. From these results, we hypothesize that delayed luminescence is a universal feature of the photophysics of colloidal chalcogenide-based semiconductor nanocrystals, and may perhaps be even more general among colloidal semiconductor nanocrystals. In each of the materials investigated here, delayed luminescence decay shows distributed kinetics that are not describable by a power law over the full 8 orders of magnitude in experimentally measured decay time. Such non-power-law dynamics are not evident from previous reports of NC delayed luminescence because data were not collected over sufficiently long time windows. Strikingly, for all three nanocrystal types examined here, the delayed luminescence kinetics are temperature independent between 20 K and at least 200 K. This distinctive temperature independence provides strong evidence that delayed luminescence involves detrapping from a metastable excited state *via* a tunneling mechanism as a general feature in various types of semiconductor NCs. At temperatures approaching room temperature, a thermally activated nonradiative decay channel emerges that appears to be material (and likely sample) dependent.

Figure 4.7 uses a single-configurational-coordinate diagram to illustrate schematically the process of carrier detrapping *via* tunneling implied by the data presented here. Analysis shows that the distributed decay kinetics displayed by the delayed luminescence are reproduced well over all 8 orders of magnitude in time when using a temperature-independent Gaussian distribution in tunnel widths (σ = 30%), corresponding to a log-normal distribution in tunneling rates. Such a distribution in tunnel widths could conceivably arise from a distribution in the displacement of the metastable state's potential energy surface relative to the emissive state's surface along the tunneling coordinate, or could arise from a distribution in tunneling driving

forces; our data do not speak to the microscopic origin of the distribution. In either scenario, such distributions are assumed to be generated by local chemical variations at the NC surfaces, such as inhomogeneous ligand, ion, or surface-dipole distributions.

Despite the temperature independence of the delayed luminescence kinetics, the delayed luminescence amplitude can change with temperature for a given sample. We propose that this observation reflects the temperature dependence of the prompt luminescence decay times and illustrates the competition within the emissive excited state between prompt luminescence and formation of the metastable state. For the same reason, materials with much longer prompt luminescence lifetimes (Cu^+:CdSe and $CuInS_2$ NCs, compared to CdSe NCs) show much greater delayed luminescence amplitudes relative to their prompt luminescence ($A_D/(A_P + A_D)$, or I_{delayed}/I_0). In CdSe NCs, an additional competition exists involving formation of a luminescent deep-trap state. The observation that delayed luminescence intensities are influenced by changes in prompt luminescence lifetimes from 10 ns to 10 μs illustrates that trapping into the metastable state must occur over at least 4 orders of magnitude in time. This finding is consistent with our previous conclusion of distributed trapping dynamics, inferred from the excitation-power dependence of room-temperature delayed luminescence intensities in $CuInS_2$ NCs.[6]

We note in passing that the similarity in delayed luminescence decay dynamics among these three very different NCs should not be construed as necessarily implying similar microscopic identities of their traps. Instead, this similarity is likely due in large part to the fact that the phenomenon itself is strongly biased toward the scenario of nearly degenerate emissive and metastable trapped excited states;[2] A trapped excited state too far above the emissive excited state is unlikely to form and unlikely to detrap slowly, while a trapped excited state too far below the emissive state may likely form but is unlikely to detrap to yield a delayed emission event.

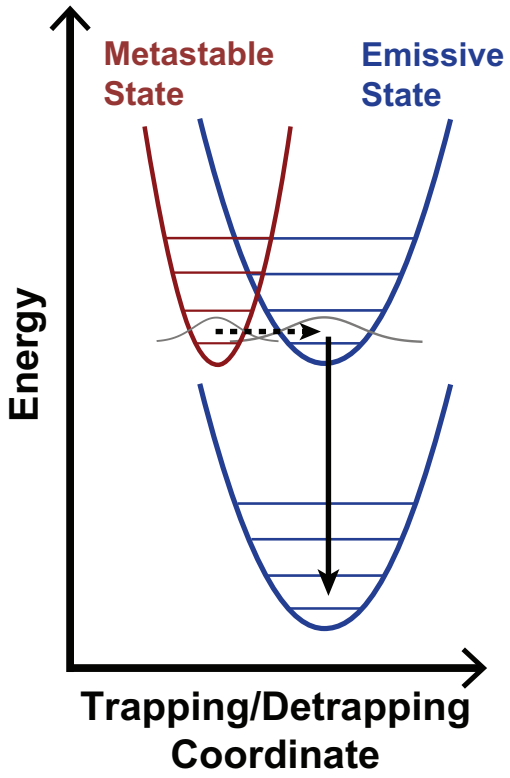

Figure 4.7: Single-configurational-coordinate diagram illustrating the generation of delayed luminescence by detrapping from a metastable charge-separated excited state. Detrapping occurs by tunneling from this metastable state to the emissive state (dashed arrow). Delayed luminescence is observed upon subsequent radiative decay to the ground state (solid arrow). The experimental decay dynamics indicate a Gaussian distribution in tunneling widths, corresponding to a log-normal distribution in tunneling rates.

As discussed in the Introduction, there is growing evidence of a mechanistic link between delayed luminescence and photoluminescence blinking in colloidal semiconductor nanocrystals.[1,3–6] The data and analysis presented here bolster proposals of such a link. Although power-law behavior is often reported in blinking studies[7,8,25] and has been reported for delayed luminescence as well,[1,4,5] deviations from power-law have been emphasized in recent blinking literature.[26–28] Deviations from power-law kinetics are clearly evident in the delayed luminescence kinetics reported here. For both delayed luminescence (this study) and blinking,[26–28] log-normal distributions reproduce the dynamics better than power-law distributions. Even more compelling is the observation in blinking measurements on CdSe NCs that the "off" statistics (which reflect detrapping dynamics analogous to the delayed luminescence decay dynamics described here) are also temperature independent,[7,8,25,29,30] implying a tunneling process for detrapping. The tunneling process illustrated in Figure 4.7 is thus directly analogous to the tunneling mechanism of carrier detrapping invoked in several PL blinking models.[7,9,10] As stressed previously,[7] a $\sim$ 25% variation in the mean trap distance can generate a 10^7-fold variation in tunneling times, and hence could account for the broadly distributed blinking "off" dynamics. Here, we find that a 30% variation in the mean tunnel width reproduces the distributed delayed luminescence dynamics well (Figure 4.6). Whereas stochastic trap-state fluctuations must be explicitly invoked to account for single-particle blinking dynamics,[7,10,13,25] ensemble delayed luminescence measurements average over all such fluctuations within the ensemble, allowing adequate description of the dynamics using a static distribution of tunnel widths. Overall, the evidence in support of a direct mechanistic link between delayed luminescence and luminescence blinking in colloidal semiconductor nanocrystals appears persuasive.

Blinking and delayed luminescence measurements also exhibit interesting contrasts. To assemble an adequate data set for analysis of blinking dynamics, measurements are typically performed for long times on individual NCs, and data from

multiple NCs are sometimes then collected together into a single data set that effectively reconstructs the behavior of the NC ensemble. Analogous to the advantages of applying photon-correlation methods at the ensemble level,[31] the delayed luminescence experiment is performed directly on the NC ensemble, and reflects the same (or an even broader) sampling of events without selection bias. Delayed luminescence measurements can be performed on free-standing colloidal NCs, eliminating the effects of NC interactions with substrates or host polymers, which may lead to potential intensity-modification or sample-orientation effects, or even to background luminescence artifacts.[32] Finally, ensemble delayed luminescence measurements allow data collection at much lower excitation rates than are typically used in blinking measurements, enabling traversal from a high-power regime in which the phenomenon is excitation-power independent (as found in blinking "off"-state dynamics[7]) to a low-power regime in which it becomes power dependent.[6] Delayed luminescence measurements thus offer a highly flexible experimental approach to exploring the underlying microscopic processes involved in metastable trapping and detrapping, complementing existing blinking techniques.

4.6 Summary

Surprisingly similar delayed luminescence dynamics are observed across a variety of colloidal semiconductor NC materials. CdSe, Cu^+:CdSe and $CuInS_2$ NCs all show distinctly non-power-law decay dynamics when measured over 8 decades in time, and these dynamics are independent of temperature from 20 K until at least 200 K, where thermally activated nonradiative decay begins to appear. A model is presented that reproduces the key observations in the delayed luminescence decay and its temperature dependence. This model invokes detrapping *via* tunneling from a degenerate charge-separated metastable state as the rate-determining process in delayed luminescence, and reproduces the data well using a log-normal distribution of tunneling rates, such as obtained from a Gaussian distribution of tunnel widths. Several of

the observations made in these delayed luminescence measurements are reminiscent of analogous observations from photoluminescence blinking measurements, and specific relationships between delayed luminescence and blinking are discussed. Delayed luminescence measurements are proposed as a flexible and complementary approach to blinking measurements for understanding the microscopic processes responsible for both phenomena.

4.7 Supporting Information

Additional sample characterization, spectroscopic data, and modeling parameters. This material is available free of charge *via* the Internet at http://pubs.acs.org.

X-ray diffraction (XRD) of $CuInS_2$ NCs

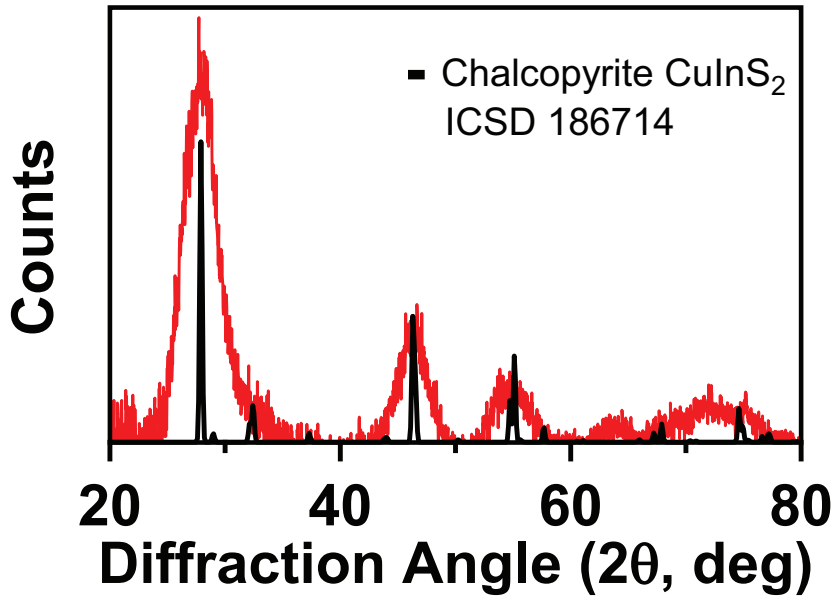

Figure 4.8: X-ray diffraction data for $CuInS_2$ nanocrystals used in this study, showing the chalcopyrite phase.

Magneto-photoluminescence decay traces

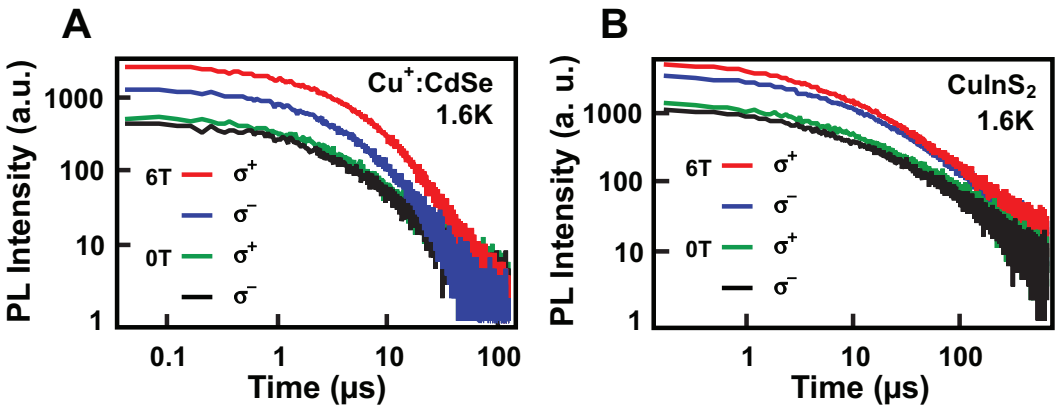

Figure 4.9: Magneto-photoluminescence decay traces for right (σ^+) and left (σ^-) circularly polarized light for (A) Cu^+:CdSe and (B) $CuInS_2$ NCs measured at 1.6 K, corresponding to the MCPL data presented in Figures 4.4C,D of the main text. Decay data were measured at the peaks of the PL spectra shown in Figures 4.4A,B.

Absorption and PL of Cu^+:CdSe NCs

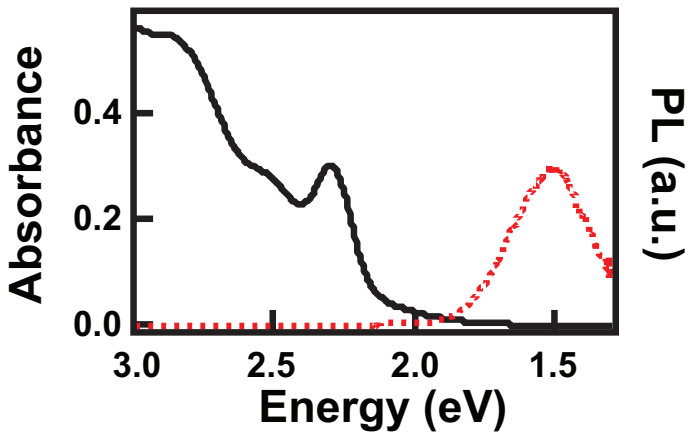

Figure 4.10: Electronic absorption and PL spectra of the Cu^+:CdSe nanocrystals used in MCPL measurements ($d \sim 3.2$ nm), taken at room temperature in toluene.

Gated spectra of CdSe NCs

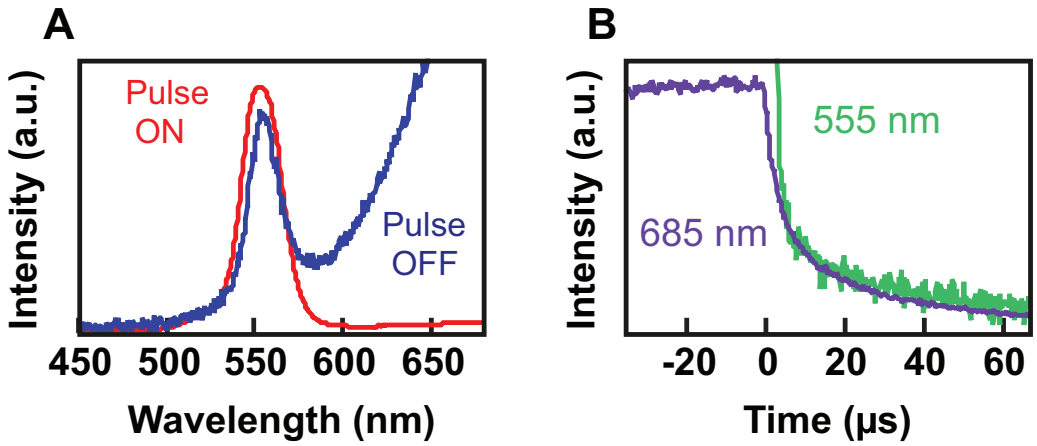

Figure 4.11: (A) Prompt (red curve, pulse ON) and delayed (blue curve, pulse OFF, integrated between 640 ns and 35 μs after the end of the excitation pulse) photoluminescence spectra of CdSe NCs. A constant baseline was subtracted from the delayed luminescence spectrum. (B) Luminescence decay curves measured for the same sample of CdSe NCs at wavelengths of exciton emission (green, 555 nm, 20 nm bandwidth) and trap emission (black, 685 nm, 20 nm bandwidth). A constant baseline was subtracted from the dynamics. All data collected at 5 K.

Table 4.1: Parameters used for modeling Cu^{+}:CdSe NC temperature-dependent luminescence decay data described in the main text. The results of this modeling are depicted in Figure 4.6. For all temperatures, Gaussian parameters of <a> = 1.0 and $\sigma = 0.3$ were used, and $\beta = 10$. These parameters are all given in reduced units, defined by $\langle a \rangle = \langle a_{\mathrm{dim}} \rangle / \langle a_{\mathrm{dim}} \rangle \equiv 1.0$, $\sigma = \sigma_{\mathrm{dim}} / \langle a_{\mathrm{dim}} \rangle$, and $\beta = \beta_{\mathrm{dim}} \langle a_{\mathrm{dim}} \rangle$. For all temperatures, $k_0 = 10^9$ s^{-1}.

T (K)	A_1(x10^3)	τ_1(x$10^{-7}s$)	A_2(x10^5)	τ_2(x$10^{-6}s$)	A_D	$\langle a \rangle$	σ	β	$k_0(10^9 s^{-1})$
20	9.99	7.89	4.20	3.40	35456	1	0.3	10	1
40	10.31	6.62	4.13	2.87	28327	1	0.3	10	1
80	11.23	5.75	3.24	2.82	18403	1	0.3	10	1
160	8.84	5.01	2.75	2.36	8056	1	0.3	10	1
200	7.56	5.56	2.14	2.36	6199	1	0.3	10	1
295	5.60	6.32	1.10	2.23	2005	1	0.3	10	1

4.8 Author Information

Corresponding Authors

**E-mail: gamelin@chem.washington.edu.*

Notes

The authors declare no competing financial interest.

4.9 Acknowledgments

Financial support from the National Science Foundation (CHE-1404674 to P.J.R. and DMR-1505901 to D.R.G.) is gratefully acknowledged. K.E.K. thanks the Department of Energy for support through an Energy Efficiency and Renewable Energy (EERE) postdoctoral research award. A. M. acknowledges the support of an Early Postdoc Mobility Fellowship from the Swiss National Science Foundation. We thank Mr. Luming Yang for synthesis of a Cu^{+}:CdSe sample used in these studies. The authors would like to thank Mr. Michael De Siena and Dr. Sidney Creutz for collecting TEM data. Part of this work was conducted at the Molecular Analysis Facility, which is supported in part by funds from the Molecular Engineering & Sciences Institute, the Clean Energy Institute, the National Science Foundation and the National Institutes of Health.

4.10 Bibliography

[1] Sher, P.H., Smith, J.M., Dalgarno, P.A., Warburton, R.J., Chen, X., Dobson, P.J., Daniels, S.M., Pickett, N.L., & O'Brien, P. (2008). *Applied Physics Letters* **92**, 101111.

[2] Jones, M., Lo, S.S., & Scholes, G.D. (2009). *Proc. Natl. Acad. Sci. USA* **106**, 3011–3016.

[3] Whitham, P.J., Knowles, K.E., Reid, P.J., & Gamelin, D.R. (2015). *Nano Letters* **15**, 4045–4051.

[4] Rabouw, F.T., Kamp, M., van Dijk-Moes, R.J., Gamelin, D.R., Koenderink, A.F., Meijerink, A., & Vanmaekelbergh, D. (2015). *Nano Letters* **15**, 7718–7725.

[5] Rabouw, F.T., van der Bok, J.C., Spinicelli, P., Mahler, B., Nasilowski, M., Pedetti, S., Dubertret, B., & Vanmaekelbergh, D. (2016). *Nano Letters* **16**, 2047–2053.

[6] Whitham, P.J., Marchioro, A., Knowles, K.E., Kilburn, T.B., Reid, P.J., & Gamelin, D.R. (2016). *The Journal of Physical Chemistry C* **120**, 17136–17142.

[7] Kuno, M., Fromm, D.P., Hamann, H.F., Gallagher, A., & Nesbitt, D.J. (2001). *The Journal of Chemical Physics* **115**, 1028–1040.

[8] Kuno, M., Fromm, D.P., Hamann, H.F., Gallagher, A., & Nesbitt, D.J. (2000). *The Journal of Chemical Physics* **112**, 3117–3120.

[9] Verberk, R., van Oijen, A.M., & Orrit, M. (2002). *Physical Review B* **66**, 233202.

[10] Kuno, M., Fromm, D.P., Johnson, S.T., Gallagher, A., & Nesbitt, D.J. (2003). *Physical Review B* **67**, 125304.

[11] Tang, J. & Marcus, R.A. (2005). *Physical Review Letters* **95**, 107401.

[12] Frantsuzov, P.A. & Marcus, R.A. (2005). *Physical Review B* **72**, 155321.

[13] Pelton, M., Smith, G., Scherer, N.F., & Marcus, R.A. (2007). *Proc. Natl. Acad. Sci. USA* **104**, 14249–14254.

[14] Frantsuzov, P.A., Volkan-Kacso, S., & Janko, B. (2009). *Physical Review Letters* **103**, 207402.

[15] Galland, C., Ghosh, Y., Steinbruck, A., Sykora, M., Hollingsworth, J.A., Klimov, V.I., & Htoon, H. (2011). *Nature* **479**, 203–207.

[16] Qin, W. & Guyot-Sionnest, P. (2012). *ACS Nano* **6**, 9125–9132.

[17] Li, L., Pandey, A., Werder, D.J., Khanal, B.P., Pietryga, J.M., & Klimov, V.I. (2011). *Journal of the American Chemical Society* **133**, 1176–1179.

[18] Chen, O., Chen, X., Yang, Y., Lynch, J., Wu, H., Zhuang, J., & Cao, Y.C. (2008). *Angewandte Chime International Edition* **47**, 8638–8641.

[19] Piepho, S.B. & Schatz, P.N. (1983). *Group Theory in Spectroscopy with Applications to Magnetic Circular Dichroism.* Monographs in Chemical Physics. John Wiley & Sons Inc.

[20] Knowles, K.E., Hartstein, K.H., Kilburn, T.B., Marchioro, A., Nelson, H.D., Whitham, P.J., & Gamelin, D.R. (2016). *Chemical Reviews*, Article ASAP (DOI: 10.1021/acs.chemrev.6b00048).

[21] Zhong, H., Zhou, Y., Ye, M., He, Y., Ye, J., He, C., Yang, C., & Li, Y. (2008). *Chemistry of Materials* **20**, 6434–6443.

[22] Tran, T.K.C., Le, Q.P., Nguyen, Q.L., Li, L., & Reiss, P. (2010). *Adv. Nat. Sci.: Nanosci. Nanotechnol.* **1**, 025007.

[23] Sun, J., Ikezawa, M., Wang, X., Jing, P., Li, H., Zhao, J., & Masumoto, Y. (2015). *Physical Chemistry Chemical Physics* **17**, 11981–11989.

[24] Knowles, K.E., Nelson, H.D., Kilburn, T.B., & Gamelin, D.R. (2015). *Journal of the American Chemical Society* **137**, 13138–13147.

[25] Shimizu, K.T., Neuhauser, R.G., Leatherdale, C.A., Empedocles, S.A., Woo, W.K., & Bawendi, M.G. (2001). *Physical Review B* **63**, 205316.

[26] Riley, E.A., Hess, C.M., Whitham, P.J., & Reid, P.J. (2012). *J. Chem. Phys.* **136**, 184508.

[27] Mitsui, M., Unno, A., & Azechi, S. (2016). *J. Phys. Chem. C* **120**, 15070–15081.

[28] Riley, E.A., Hess, C.M., Pioquinto, J.R., Kaminsky, W., Kahr, B., & Reid, P.J. (2013). *The Journal of Physical Chemistry B* **117**, 4313–4324.

[29] Nirmal, M., Dabbousi, B.O., Bawendi, M.G., Macklin, J.J., Trautman, J.K., Harris, T.D., & Brus, L.E. (1996). *Nature* **383**, 802–804.

[30] Banin, U., Bruchez, M., Alivisatos, A.P., Ha, T., Weiss, S., & Chemla, D.S. (1999). *The Journal of Chemical Physics* **110**, 1195–1201.

[31] Beyler, A.P., Bischof, T.S., Cui, J., Coropceanu, I., Harris, D.K., & Bawendi, M.G. (2014). *Nano Letters* **14**, 6792–6798.

[32] Rabouw, F.T., Cogan, N.M.B., Berends, A.C., van der Stam, W., Vanmaekelbergh, D., Koenderink, A.F., Krauss, T.D., & de Mello Donega, C. (2016). *Scientific Reports* **6**, 21187.

Appendices

Appendix A

ACRONYMS AND SYMBOLS

APD: Avalanche Photodiode Detector
CCD: Charged Coupled Device
cCDF: Complimentary Cumulative Distribution Function
CDF: Cumulative Distribution Function
DAP: Donor-Acceptor Pair
η_{PL}: Photoluminescence Quantum Yield
EPR: Electron Paramagnetic Resonance
FWHM: Full width at half maximum
hν: Photon energy
ICP-AES: Inductively Coupled Plasma Atomic Emission Spectroscopy
K: Kelvin
KS: Kolomogorov-Smirnov
λ: Wavelength
LED: Light Emitting Diode
LN_2: Liquid Nitrogen
MCD: Magnetic Circular Dichroism
NA: Numerical Aperture
NC: Nanocrystal
PL: Photoluminescence
PMT: Photomultiplier Tube
QY: Quantum Yield
SI: Supporting Information
σ: Standard Deviation
σ^-: Left Circularly Polarized Light
σ^+: Right Circularly Polarized Light
SP: Single Particle
XRD: X-Ray Diffraction

Appendix B

MICROSCOPE COMPONENTS FOR PL BLINKING

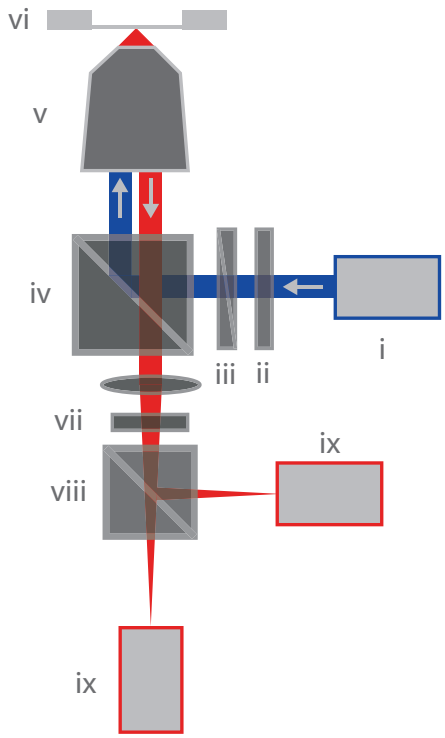

Figure B.1: Confocal fluorescence microscope in epi-geometry.
- i: Pulsed diode laser (Picoquant)
- ii: Excitation filter
- iii: Neutral Density Filter
- iv: Long-pass dichroic mirror
- v: 1.4 NA objective (Nikon, Plan-Fluor)
- vi: Piezoelectric nanopositioning stage (PI)
- vii: Long-pass emission filter (Chroma)
- viii: 50/50 beam splitter
- ix: Avalanche photodiode detector

Appendix C

MICROSCOPE COMPONENTS FOR SP SPECTRA

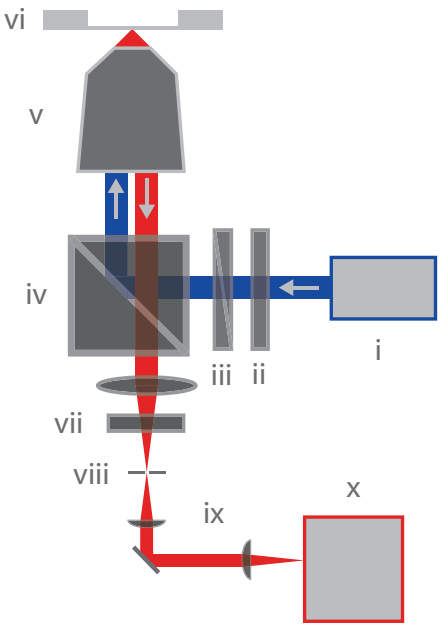

Figure C.1: Confocal fluorescence microscope in epi-geometry.

i: Pulsed diode laser (Picoquant)
ii: Excitation filter
iii: Neutral Density Filter
iv: Long-pass dichroic mirror
v: 1.4 NA objective (Nikon, Plan-Fluor)
vi: Piezoelectric nanopositioning stage (PI)
vii: Long-pass emission filter (Chroma)
viii: 100 μm pin hole
ix: Columnating and focusing lenses
x: Spectrograph and LN_2 cooled charged coupled device detector

VITA

Patrick James Whitham is the son of James and Vickie Whitham, born in Boise, Idaho in 1986. After receiving his high school diploma from Centennial High School in Boise, Idaho in 2004 he attended Idaho State University where he earned a Bachelor of Science in Chemistry in 2008 and a Master of Science in Chemistry in 2010 as part of a B.S./M.S. dual degree program. Following his masters work, he attended the University of Washington for graduate school where he obtained a Doctorate of Philosophy in 2016.